Thermal and non-thermal behavior of quantum systems: An open systems perspective

(Thermisches und nicht-thermisches Verhalten von Quantensystemen aus der Perspektive von offenen Systemen)

Dissertation

zur Erlangung des Doktorgrades der
Fakultät für Mathematik und Physik der
Albert-Ludwigs-Universität Freiburg

vorgelegt von

Sebastian Wenderoth

aus Göttingen

Dekan:	Prof. Dr. Michael Thoss
Erstgutachter/Betreuer:	Prof. Dr. Michael Thoss
Zweitgutachter:	Prof. Dr. Gerhard Stock
Tag der mündlichen Prüfung:	19.12.2022
Prüfer:	Prof. Dr. Michael Thoss Prof. Dr. Andreas Buchleitner Prof. Dr. Frank Stienkemeier

The most exciting phrase to hear in science,
the one that heralds new discoveries,
is not "Eureka!" (I found it!)
but "That's funny . . . ".
— Isaac Asimov

Abstract

Thermalization is one of the most prominent physical effects in our everyday experience of the world. It refers to the process of a system, which is in a non-equilibrium state, relaxing to a thermal equilibrium. The remarkable property of this process is that the thermal equilibrium state is determined by few macroscopic properties of the system, like the total energy of the system. The information about the precise initial configuration of the system is lost during this process: on a macroscopic scale, thermalization is an irreversible process. This is particularly surprising since the fundamental laws of motion, which describe how the microscopic particles move, is formally reversible at all times. Bridging this apparent contradiction between the fundamental laws of nature, prescribed by Newton's or Schrödinger's equation, and the emergence of thermalization on a macroscopic scale is a non-trivial question. Nowadays, the emergence of thermalization in a quantum mechanical system is understood in a local sense: subsystems are driven towards thermal equilibrium by the interaction with their remainder. The remainder acts as an effective environment and in the long-time limit the state of the subsystem becomes independent of the initial configuration. Over the last decade it was realized that thermalization can be decomposed into different aspects showing that systems can exhibit qualitatively different non-thermal behaviors depending on which aspects of thermalization is violated. Although the emergence of thermal behavior can be explained in this way and non-thermal behavior was found in a variety of different systems, there are still many open questions.

In this thesis we contribute to three of these open question: First, we analyze environment-induced effects and investigate in which situations an environment can thermalize a system. Second, we examine the local memory in thermal and non-thermal systems and how the information about the initial state distributes over the system. Third, we investigate the stability of a many-body localized system, one prominent example of a non-thermalizing systems, with respect to long-range interactions. To address these different issues, we consider three different model systems: the spin-boson model, the disordered XXZ Heisenberg spin chain, and a centrally coupled spin chain, respectively. Our analysis is based on a combination of analytic and numerical approaches. Based on the time-evolution of subsystems, we propose a measure to quantify the local memory in subsystems, which can be used as an indicator for thermal and non-thermal behavior in quantum systems. To simulate the dynamics of the different systems we employ exact diagonalization and the multilayer multiconfiguration time-dependent Hartree approach. While the first can be used to simulate the dynamics of small systems for arbitrary times, the later can be used to simulate the dynamcis of large systems at short and intermediate times.

Our findings demonstrate that all considered systems have a parameter regime in which they exhibit thermal behavior, i.e. subsystems approach a unique equilibrium state which is

determined only by macroscopic observables. The relaxation towards the equilibrium state, however, is qualitatively different for the different models and exhibit a rich and interesting dynamical behavior. In the weak coupling regime of the spin-boson model we find a transition from coherent to incoherent equilibration as well as a partial back flow of information, giving rise to non-Markovian dynamics. In the thermal phase of the disordered XXZ Heisenberg spin chain we identify different delocalization mechanisms, leading to different time scales in the relaxation. In the strong coupling regime of the centrally coupled spin chain we find that the spins of the chain are thermalized by the long-range interactions. On the other hand, all systems have a parameter regime in which they show non-thermal behavior. Depending on the spectrum of the environment, we find different non-thermal behaviors in the strong coupling regime of the spin-boson model. For a gapped spectrum we find a failure of *subsystem equilibration*, i.e. the state of the spin remains time-dependent at all times. For an Ohmic spectral density the spin localizes in its initial state, and thus retains information about the initial state in local observables. We find a similar effect in the disordered XXZ Heisenberg spin chain in the many-body localized phase and in the weak and intermediate coupling regime of the centrally coupled spin chain: some information about the initial state is stored in the asymptotic state of the spins. Furthermore, our results show that the initial state of a subsystem can influence the asymptotic state of the system if macroscopic observables, like the total energy, are influenced by the initial state. This can be seen in the asymptotic state of the central degree of freedom in the centrally coupled spin chain.

Zusammenfassung

Thermalisierung ist vermutlich der physikalische Effekte, den wir in unserem Alltag am häufigsten wahrnehmen. Dabei beschreibt Thermalisierung den Prozess, dass ein System, welches in einem Nichtgleichgewichtszustand ist, gegen einen Gleichgewichtszustand strebt. Eine der bemerkenswerten Eigenschaften dieses Prozesses ist es, dass der Gleichgewichtszustand nur von wenigen makroskopischen Eigenschaften des Systems, wie der Gesamtenergie, bestimmt wird. Die Information über den genauen Anfangszustand des Systems geht während der Zeitentwicklung verloren. Auf makroskopischer Skala ist Thermalisierung ein irreversibler Prozess. Das ist insbesondere überraschend, da die fundamentalen Gesetzte, welche die Dynamik der mikroskopischen Teilchen beschreiben, reversibel sind. Es ist nicht offensichtlich, wie Thermalisierung aus den fundamentalen Gesetzten der Natur, beschrieben durch Newtons oder Schrödingers Gleichung, hergeleitet werden kann. In quantenmechanischen Systemen, wird Thermalisierung heutzutage in einem lokalen Sinne verstanden: Kleine Teilsysteme werden durch die Wechselwirkung mit ihrer Umgebung gegen einen thermischen Gleichgewichtszustand getrieben. Ihrer Umgebung fungiert als ein effektives Bad und im langzeit Limes wird der Zustand des Teilsystems unabhängig von dem Anfangszustand des Systems. Um diesen komplexen Prozess besser untersuchen zu können, wird Thermalisierung in verschiedene Aspekte aufgeteilt, die separat untersucht werden können. Das bedeutet aber auch, dass es qualitativ verschiedenes nicht-thermisches Verhalten geben kann, je nachdem welcher der verschiedenen Aspekte verletzt ist. Obwohl das Auftreten von Thermalisierung auf diese Weise aus den fundamentalen Gesetzten erklärt werden kann, und nicht-thermisches Verhalten in verschiedenen Systemen beobachtet wurde, gibt es immer noch viele offene Fragestellungen in diesem Kontext.

Die vorliegende Arbeit stellt einen Betrag zu drei dieser offenen Fragen dar. Im ersten Teil untersuchen wir umgebungsinduzierte Effekte und analysieren unter welchen Voraussetzungen eine Umgebung Thermalisierung induzieren kann. Im zweiten Teil erforschen wir die Information in lokalen Observablen in thermischen und nicht-thermischen Systemen und wie sich diese Information von lokalen auf globale Observablen verteilt. Im letzten Teil untersuchen wir die Stabilität von einem vielteilchenlokalisiertem System, ein bekanntes Beispiel für ein nicht-thermalisierendes System, bezüglich langreichweitiger Wechselwirkungen. Um diese verschiedenen Aspekte zu adressieren, untersuchen wir drei verschiedene Modelsysteme: das Spin-boson Modell, die XXZ Heisenberg Spinkette mit lokaler Unordnung und eine zentral gekoppelte Spinkette. Dabei nutzen wir eine Kombination aus analytischen und numerischen Methoden. Ausgehend von der Zeitentwicklung von Teilsystemen, leiten wir ein Maß für das lokale Gedächtnis des Systems her, welches als Indikator für thermisches und nicht-thermisches Verhalten genutzt werden kann. Um die Dynamik der Systeme zu simulieren nutzen wir exakte Diagonalisierung, sowie die mehrlagige zeitabhängige Multikonfigurations-

Hartree-Methode. Erstere erlaubt es uns die Dynamik von kleinen Systemen auf beliebigen Zeitskalen zu beschreiben, wohingegen die zweite genutzt werden kann, um die Dynamik von großen Systemen auf kurzen und mittleren Zeitskalen zu simulieren.

Unsere Ergebnisse zeigen, dass in allen untersuchten Systemen ein Parameterregime existiert, in dem die Systeme thermisches Verhalten zeigen: Teilsysteme relaxieren zu eindeutigen Gleichgewichtszuständen, welche durch makroskopische Observablen des Systems bestimmt sind. Die Relaxation gegen den Gleichgewichtszustand ist dabei für die verschiedenen Systeme qualitativ unterschiedlich. Im Spin-boson Modell finden wir einen Übergang von kohärenter zu inkohärenter Relaxation, sowie einen teilweisen Rückfluss von Information, welcher zu nicht-Markovscher Dynamik führt. In der thermischen Phase der XXZ Heisenberg Spinkette identifizieren wir verschiedene Mechanismen, die zu Delokalisierung führen. Diese manifestieren sich in verschiedenen Zeitskalen in der Relaxation. In der zentral gekoppelten Spinkette finden wir Anzeichen für Thermalisierung der Spins für starke Kopplung. Gleichzeitig finden wir in allen Systemen Parameterbereiche, in denen diese nicht thermalisieren. Im Spin-boson Modell finden wir dieses Verhalten für starke Kopplungen, jedoch hängt das nicht-thermische Verhalten qualitativ von dem Spektrum der Umgebung ab. Für eine Umgebung mit einem gegapten Spektrum bleibt der Zustand des Spins auf allen Zeitskalen zeitabhängig. Für ein Bad mit Ohmscher Spektraler Dichte lokalisiert der Spin in seinem Anfangszustand und somit bleiben Informationen über den Anfangszustand in lokalen Observablen erhalten. Ein ähnliches Verhalten finden wir für die XXZ Heisenberg Spinkette in der Vielteilchenlokalisierten Phase und in der zentral gekoppelten Spinkette für schwache Kopplungen: Ein Teil der Information über den Anfangszustand bleibt in lokalen Observablen erhalten. Darüber hinaus kann der Anfangszustand eines kleinen Teilsystems die Langzeitdynamik des Systems beeinflussen, wenn dieser einen Einfluss auf makroskopische Observablen des Systems hat. Dieses Verhalten finden wir im asymptotischen Zustand des zentralen Freiheitsgrades der zentral gekoppelten Spinkette.

Publications

The following publications are based on parts of this work:

- S. Wenderoth, H.-P. Breuer, and M. Thoss, "Non-Markovian effects in the spin-boson model at zero temperature", *Phys. Rev. A* **104**, 012213 (2021)
- N. Ng, S. Wenderoth, R. R. Seelam, E. Rabani, H.-D. Meyer, M. Thoss, and M. Kolodrubetz, "Localization dynamics in a centrally coupled system", *Phys. Rev. B* **103**, 134201 (2021)

Danksagung

Die letzten viereinhalb Jahre, waren vermutlich die spannendsten und lehrreichsten Jahre meines bisherigen Lebens. Das Ergebnis dieser vier Jahre ist die vorliegende Arbeit. Dabei wäre es vermessen zu sagen, dass diese Arbeit mein alleiniger Verdienst ist. An dieser Stelle möchte allen Leuten zu danken, die in der ein oder anderen Art zum erfolgreichen Abschluss meiner Promotion beigetragen haben. Ich bitte jeden vergessen Namen zu entschuldigen. Es handelt sich definitiv nicht um böse Absicht.

Die vermutlich entscheidendste Person ist mein Betreuer Michael Thoss, der es mir ermöglicht hat meine Promotion in seiner Arbeitsgruppe zu machen. Während der letzten vier Jahre hat er mir sehr viele Freiheiten gegeben, sodass ich die Möglichkeit hatte eigene Ideen zu entwickeln und diese voranzutreiben. Durch unsere Diskussionen, in denen er immer wieder kritisch nachhakte, hat er meine Arbeit maßgeblich geprägt und zum erfolgreichen Abschluss meiner Promotion beigetragen.

Ein besonderer Dank gilt meiner Familie, die mich in den letzten 29 Jahren in allen Situationen begleitet hat und mich in guten wie in schlechten Zeiten unterstütz haben. Worte können nicht ausdrücken, wie dankbar ich für diese Stütze in meinem Leben bin. Neben der allgemeinen Unterstützung möchte ich mich insbesondere bei meinem Vater für seine Hilfe in der letzten, und vermutlich stressigsten Phase der Promotion, dem Zusammenschreiben, fürs Korrekturlesen und einen energischen Schubser an der richten Stelle bedanken.

Darüber hinaus möchte ich mich bei allen Mitgliedern unserer Arbeitsgruppe für eine angenehme Atmosphäre bedanken. Insbesondere möchte ich mich bei Christoph, Jakob, Samuel, und Sebastian bedanken, die ich während meiner Promotion unzählige Male mit Fragen genervt habe und die immer Zeit gefunden haben mit mir zu diskutieren. Auch möchte ich mich bei David und Luis bedanken, die ich während ihrer Abschlussarbeiten betreut habe. Ihr habt mich mit euren Fragen herausgefordert anders über Dinge nachzudenken und dadurch zu meinem Verständnis der Physik beigetragen. Neben der wissenschaftlichen Arbeit muss an der Uni eine Menge organisiert werden. Für die Hilfe bei all diesen Sachen möchte ich Helga und Simone danken, ohne die ich vermutlich im Dschungel der Bürokratie komplett aufgeschmissen gewesen wäre. Darüber bin ich sehr dankbar, dass ich meine Promotion als Teil des Graduiertenkollegs IRTG 2079 ‚Cold Controlled ensembles in Physics and Chemistry' durchführen konnte. Das internationale Umfeld und der Austausch mit Doktoranden verschiedenster Spezialisierung war sehr interesst und förderlich.

Als letztes möchte ich mich bei allen Leuten bedanken, mit denen ich während meiner Promotion zusammengearbeitet habe, die nicht Teil unserer Gruppe sind: Heinz-Peter Breuer, Mike Kolodrubetz, Hans-Dieter Meyer, Nathan Ng, Eran Rabani, Tobias Schätz, Rajagopala Seelam und Ulrich Warring.

Contents

1. Introduction

Thermalization describes the relaxation of a physical system to a thermal equilibrium state and is arguably one of the most present physical effects in our everyday experience of the world. A particular prominent example is a hot cup of coffee which eventually cools down to room temperature. The cup of coffee exchanges energy with its environment, the room, and thus approaches an equilibrium state which depends only on properties of the room, like the temperature or the pressure. In this picture the coffee is driven towards thermal equilibrium by interactions with its surrounding. To understand thermalization from first principles one has to describe the entire system, consisting of the cup of coffee and the room, as one joint system. From this perspective, thermalization describes the evolution from a non-equilibrium state of the joint system, in this case a non-uniform temperature distribution, to an equilibrium state. The fundamental principles which determine the dynamics out of equilibrium are the microscopic laws of motion. From this microscopic point of view, however, it is quite remarkable that the joint system approaches an equilibrium state which is only determined by some macroscopic properties of the room: A macroscopic system consists of $O(10^{23})$ particles, whose time-evolution is determined by the microscopic laws of motion prescribed by Newton's or Schrödinger's equation. In both cases, the state of the system at time t formally depends on the initial configuration of all constituents. If the state of the joint system in equilibrium depends only on a few macroscopic quantities, how can the information about the initial configuration get lost during the time-evolution?

In classical mechanics thermalization is explained by ergodicity, chaotic dynamics, and mixing [1, 2]. These concepts describe how the phase space is explored under Hamiltonian dynamics. In this context, thermalization originates from the basic postulate of statistical mechanics that all microstates compatible with the laws of physics are equally likely [3]. Different microstates of the system, characterized by the positions and momenta of all constituents, result in the same macrostate, characterized by macroscopic properties like the temperature, pressure, or the density. In an experiment we observe that macrostate which has the most microstates. This state is called the thermal equilibrium state [3]. An intuitive example of a classical system in which this can be demonstrated is given by hard spheres in a box. At time $t = 0$ all hard spheres are confined to a small region, which represents a

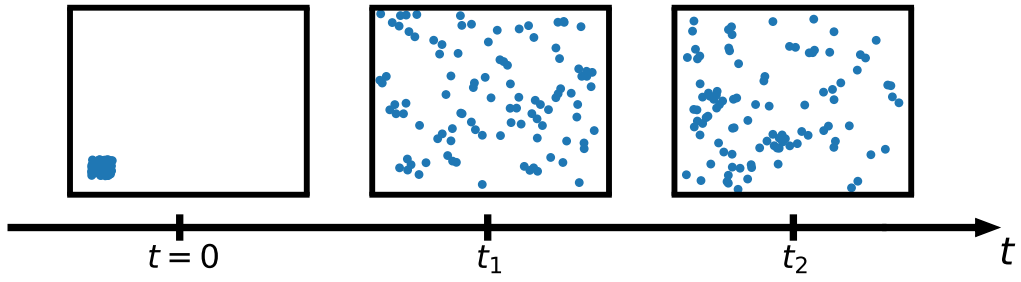

Figure 1.1: In the left plot the initial position of 100 hard spheres is shown, in the middle and right plot the positions at two later times t_1 and t_2 is shown. The initial configuration can be interpreted as a non-equilibrium situation, i.e. all particles are confined to a small region. At later times the hard spheres cover the box uniformly. Although the microstate is changing at all times, the macrostate remains constant after the transient dynamics.

non-equilibrium initial configuration. Over time, the hard spheres interact, exchange energy and eventually approach a uniform distribution, which is the macrostate compatible with the most microstates. Although the microstate is constantly changing, the macrostate of the system, given by a uniform distribution of the hard spheres, is constant for almost all times. This is demonstrated in Fig. 1.1 for 100 spheres. We note that for a system consisting of two hard spheres in a box, ergodicity was proven rigorously [4]. Since the microscopic laws of motion, i.e. Newton's equations of motion, are reversible, the information about the initial state is formally contained in the microstate of the system. However, if the macrostate of the system is compatible with different microstates, the information about the initial state is not accessible in experiments, which can only probe the macrostate, thus leading to the irreversibility of the dynamics.

Describing thermalization of a quantum mechanical system is more involved, since the concept of a phase space and chaotic motion cannot be transferred directly to quantum mechanics. Instead, it is nowadays believed that the emergence of statistical mechanics is related to properties of the spectrum and the eigenstates of the underlying Hamiltonian of the system. This idea, developed by Deutsch and Srednicki [5–7], is today known as the eigenstate thermalization hypothesis (ETH), and roughly states that in terms of physical observables each eigenstate looks thermal, i.e. a single eigenstate describes already a thermal equilibrium. Formally, this means that the expectation values of local obervables vary little between neighboring eigenstates, where the fluctuations decrease with increasing system size. In the thermodynamic limit expectation values of local observables in eigenstates are thus smooth functions of the eigenstate energy. The stationary value of an observable at long-times is determined by the expectation value in the contributing energy eigenstates, implying that for systems obeying the ETH the steady state can be described by a microcanonical ensemble [8]. Intuitively, this is understood as follows: a subsystem of a large quantum

system approaches thermal equilibrium by its interaction with its remainder. The remainder acts as an environment driving the subsystem towards thermal equilibrium. In Sec. 2.3 we discuss the interesting and non-trivial issue of thermalization in quantum systems in more detail. We note that to date it is an open question under which assumptions the ETH holds. Nevertheless, there are strong numerical evidences for its validity in a variety of example systems [9–12].

From a phenomenological point of view, thermalization is seemingly a straightforward process: a system which is in a non-equilibrium state relaxes to an equilibrium state. A closer analysis, however, reveals that this process can be decomposed into several different aspects [13, 14], which can be analyzed separately. On the one hand, it includes the relaxation of the system towards an equilibrium state. Second, it imposes certain properties on this equilibrium state i.e. the equilibrium state should only depend on macroscopic properties of the initial state, such as the total energy of the system and not on the precise initial configuration. The fact that thermalization can be decomposed into different aspects also implies the existence of different manifestations of non-thermal behavior, i.e. different aspects of thermalization can be violated. We discuss these rich and interesting physical phenomenons of non-thermal behavior in Sec. 2.4. At this point we emphasize that equilibration and thermalization have to be distinguished: while equilibration describes the relaxation to some stationary state, thermalization imposes additional properties on this stationary state.

It was recently shown by Linden and co-workers [13] that local equilibration is a general property of quantum many-body systems. Under mild assumptions on the spectrum of the Hamiltonian, they showed that the reduced state of a small subsystem approaches an equilibrium state and stays close to this state for almost all times. Similar results were also proven in Refs. [15–18]. Without further assumptions an interacting quantum system is thus expected to equilibrate.

The proof, however, does not guarantee that the equilbrium state is a thermal equilibrium state, i.e. a state which is characterized only by a few macroscopic observables of the system. One example of systems which equilibrate to a state which depends on extensively many parameters are so called integrable systems, i.e. systems with an extensive number of conserved quantities. In accordance with the results of Linden et al. [13] subsystems equilibrate, but are described by a so-called generalized Gibbs ensemble, which depends on the initial value of all conserved quantities [19–21]. A particular manifestation of this phenomenon can be found in localized systems, in which the conserved quantities are local in real space, thus making them particularly interesting. Localization, first described by Anderson in his seminal paper [22], describes the absence of transport in in non-interacting systems subject to strong disordered, a phenomenon nowadays known as Anderson localization. The absence

of transport was later extended to interacting systems [23, 24] and is known as many-body localization (MBL). The reason for the absence of transport is the emergence of quasi-local integrals of motion, so-called "l-bits". These conserved quantities, first conjectured in [25, 26] and later proven by Imbrie [27] give rise to a suppression of transport in the system, and thus, causing a failure of subsystem thermalization. Just recently, this effect was experimentally observed in trapped ion experiments [28, 29]. Furthermore, it was realized that MBL is not restricted to disordered systems but can also exist in systems subject to strong electric fields [30] or in quasi-periodic potentials [31].

The aim of this thesis is to investigate different aspects of thermal and non-thermal behavior of quantum systems. A quantum mechanical system is said to thermalize, if subsystems relax towards thermal equilibrium. Hence, thermal and non-thermal behavior of quantum systems can be investigated by considering the dynamics of subsystems. Formally, subsystems are described by open quantum system, whose time-evolution is not necessarily unitary. Throughout this thesis, we use this approach to investigate thermalization and to identify and analyze different non-thermal behavior in quantum systems. We address different aspects of thermal and non-thermal behavior, which can be grouped into three different topics.

1) Thermalization in a quantum system is usually understood as an environment-induced effect, i.e. a subsystem is driven towards thermal equilibrium by its remainder acting as an effective environment. We investigate such environment-induced effects and analyze in which situations an environment can equilibrate or even thermalize a subsystem.

2) One key property of thermalizing systems is that the long-time asymptotic state of subsystems is independent of its initial state, i.e. no information about the initial state is stored in local observables. We investigate the local memory in thermal and non-thermal systems, thus analyzing the process of thermalization and its failure.

3) Many-body localization was extensively studied in locally interacting systems, i.e. systems with nearest neighbor interactions. We discuss and analyze the stability of many-body localization in the presence of long-range interactions mediated by a central degree of freedom

To address these different questions we consider different model systems. This allows us to focus our analysis on particular aspects separately. Specifically, we consider three model systems. We consider the spin-boson model to investigate environment-induced effects, the disordered XXZ-Heisenberg spin chain to study local memory in thermal and non-thermal systems, and a centrally coupled spin chain to examine the effect of long-range interactions on many-body localization, respectively. We introduce the different models in the chapters 4, 5, and 6, respectively, in which we address the above introduced questions. Our analysis is based

on a combination of numerical, analytic, and perturbative methods. The naive numerical approach is usually limited to relatively small systems due to the exponential scaling of the Hilbert space. To circumvent this limitation we employ the multilayer multiconfiguration time-dependent Hartree (ML-MCTDH) approach, which was previously used to simulate the dynamics of large quantum systems [32–36] This approach allows us to simulate the dynamics of large systems at short and intermediate times. We complement the ML-MCTDH approach with results obtained from exact diagonalization, allowing us to simulate the dynamics of small systems at arbitrary times. To analyze the dynamics and to develop physical pictures we support the numerical data with analytic results.

This thesis is organized as follows: In Chap. 2 we introduce the general physical set up which we consider and discuss the theoretical concepts. This includes a review of the dynamics of closed and open quantum systems and a discussion of thermal and non-thermal behavior in quantum systems. Additionally, we give an overview over the most commonly used indicators for thermal and non-thermal behavior and propose a possibility to quantify the local memory in quantum system which can be used as a further indicator for thermalization or its failure. In Chap. 3 we summarize the methodology which we use to discuss and analyze the dynamics of the different systems. This includes a general overview of the numerical methods as well as a discussion of perturbative approaches which can be used to obtain analytic results. In the following three chapters we discuss different aspects of thermal and non-thermal behavior of closed quantum systems. Chapter 4 focuses on environment-induced effects, including the ability of an environment to equilibrate or thermalize a subsystem, memory effects, and non-Markovian behavior. To this end, we quantify the local memory in the dynamics of the spin-boson model and analyze memory effects using a recently proposed measure for non-Markovian behavior. In Chap. 5 we investigate the dynamics of the disordered XXZ Heisenberg spin chain, a paradigmatic model exhibiting a transition from thermal to non-thermal behavior. Based on the local memory we examine different mechanisms which potentially destabilize the localization and analyze in which regime the system exhibits thermal and localized behavior. In Chap. 6 we investigate the influence of a centrally coupled degree of freedom onto a many-body localized system. We investigate the interplay between the long-range interactions mediated by the central degree of freedom and the local interactions in the MBL system, and discuss in which regime the localization survives. Chapter 7 concludes this thesis with a summary and an outlook.

2. Dynamics of quantum systems, local thermalization, and atypical asymptotic states

Thermalization describes the process of a physical system relaxing to a thermal equilibrium state. In order to investigate this process, discuss non-thermal behavior of systems, and to analyze the underlying mechanisms leading to thermal and non-thermal behavior one first needs to define thermalization. The aim of this chapter is to introduce and discuss the theoretical concepts which are necessary to describe thermalization from a microscopical point of view. This includes the time-evolution of quantum systems, the emergence of statistical mechanics and effects, which can prevent a system from reaching thermal equilibrium. Furthermore, we examine different approaches how quantum systems can be classified into either thermal or non-thermal.

Section 2.1 is a short recap of the dynamics of quantum systems. We present the set up we consider, introduce the relevant notation, and discuss the theoretical issues arising from the microscopic description of thermalization. In Sec. 2.2 we review the time evolution of subsystems, i.e. the dynamics of open quantum systems, which is crucial to understand thermalization of quantum systems. In Sec. 2.3 we discuss the emergence of statistical mechanics from the microscopic description of a physical system and introduce our working definition of thermalization in quantum systems. In this context, we introduce the eigenstate thermalization hypothesis (ETH), a collection of concepts explaining in which situations a quantum system can be accurately described using equilibrium statistical mechanics, and discuss under which circumstances quantum systems thermalize. In Sec. 2.4, we discuss different effects which can prevent a system from reaching thermal equilibrium and introduce a class of systems which fail to thermalize: many-body localized systems. In the last section, 2.5, we present different approaches to classify a particular system into either thermal or non-thermal. This includes spectral properties of the underlying Hamiltonian, the time evolution of certain observables, and a measure to quantify the local memory in quantum systems.

2.1 Dynamics of closed quantum systems

Our goal is to investigate thermalization of a system which is prepared in a far-from equilibrium state, based on a complete quantum mechanical description of the system. In this section we introduce the necessary theoretical framework and discuss the set up we consider to study this question.

The systems we consider are composed of N degrees of freedom. Let $\mathcal{H}_n$ be the Hilbert space of the n-th degree of freedom. The degrees of freedom can be different, i.e. the $\mathcal{H}_n$ need not be equal. The Hilbert space of the joint system $\mathcal{H}$ is then given by $\mathcal{H} = \otimes_{n=1}^{N} \mathcal{H}_n$. Throughout this thesis we assume that the state of the system is pure. Consequently, the state of the joint system is represented by a vector $|\Psi\rangle \in \mathcal{H}$. To investigate thermalization in quantum systems we consider the following situation: At time $t = 0$ the system is initialized in some non-equilibrium state $|\Psi(0)\rangle$ of the form $|\Psi(0)\rangle = \bigotimes_{n=1}^{N} |\psi_n(0)\rangle_n$, where $|\psi_n(0)\rangle_n \in \mathcal{H}_n$. Physically this means that there is initially no entanglement between the different degrees of freedom. For times $t > 0$, the system evolves according to some Hamiltonian $\hat{H}$, which typically includes some kind of interactions between the different degrees of freedom, leading to entanglement between the different degrees of freedom. The time-evolution of the state is prescribed by the Schrödinger equation

$$i\hbar\partial_t |\Psi(t)\rangle = \hat{H} |\Psi(0)\rangle . \tag{2.1}$$

In the following we set $\hbar = 1$. The formal solution to Eq. (2.1) is given by

$$|\Psi(t)\rangle = \mathrm{e}^{-i\hat{H}t} |\Psi(0)\rangle , \tag{2.2}$$

which describes the state of the system at all times t.

In our discussion we distinguish two different dynamical regimes. The first are the transient dynamics, which take place on short and intermediate time scales. The other regime is the long-time limit, i.e. the state of the system as $t \to \infty$, also called the asymptotic state. The question whether the system thermalizes is related to the second regime and can be roughly phrased as: Can the asymptotic state of the system be described by a thermal equilibrium state?

There are some subtleties related to the unitary time-evolution of finite-dimensional quantum systems making this question non-trivial. To demonstrate these issues and to discuss how they can be resolved, the time dependent state $|\Psi(t)\rangle$ is expanded in the eigenbasis of the Hamiltonian $\hat{H}$. For finite-dimensional Hilbert spaces $\mathcal{H}$, the spectrum of

$\hat{H}$ is a pure point spectrum, yielding

$$|\Psi(t)\rangle = \sum_d \underbrace{\langle E_d|\Psi(0)\rangle}_{c_d} \mathrm{e}^{-iE_d t} |E_d\rangle \,. \tag{2.3}$$

Here $|E_d\rangle$ are the eigenstates and E_d are the corresponding eigenenergies of the Hamiltonian, i.e. $\hat{H}\,|E_d\rangle = E_d\,|E_d\rangle$. From this equation, (2.3), it is not obvious how a finite dimensional quantum system can thermalize or even equilibrate: $|\Psi(t)\rangle$ is a finite superposition of periodic functions, and is thus a periodic function itself. Consequently, the state of the system, $|\Psi(t)\rangle$, can never relax to a time-independent state. In Sec. 2.3 we introduce a generalized notion of equilibration and thermalization, which resolves these issues. We note that this apparent contradiction results from the unitary time-evolution and the spectrum of the Hamiltonian. If, for example, the underlying Hamiltonian has a continuous spectrum, which can occur for infinite dimensional Hilbert spaces, the wave function of the system can formally approach a time-independent state as $t \to \infty$.

2.2 Dynamics of open quantum systems

Equilibration and thermalization of quantum systems are usually understood in a local sense, i.e. subsystems of large quantum systems are driven towards equilibrium by the interaction with their remainder. To understand equilibration and thermalization it is thus inevitable to understand the dynamics of subsystems. In the following we introduce the theoretical framework necessary to describe the time evolution of subsystems.

We are interested in the time evolution of a subsystem S. The remainder of S acts as an environment and we assume that the joint system consisting of $S + E$ is a closed quantum system. Formally, the subsystem S can be understood as an open quantum system in contact with an environment E [37–39]. To discuss the time evolution of S, the Hilbert space of the joint system is separated as

$$\mathcal{H}_{SE} = \mathcal{H}_S \otimes \mathcal{H}_E, \tag{2.4}$$

where $\mathcal{H}_S$ and $\mathcal{H}_E$ denote the Hilbert spaces of S and E, respectively. Physical states of the joint system are represented by linear, self-adjoint, positive semidefinite operators of unit trace on $\mathcal{H}_{SE}$, also called density matrices. We denote the set of all physical states over a Hilbert space $\mathcal{H}$ with $\mathcal{S}(\mathcal{H})$. As mentioned above, we assume that the state of the joint system $S + E$ is pure. In this case the state of the joint system can always be written as $\hat{\rho}_{SE}(t) = |\Psi(t)\rangle_{SE}\langle\Psi(t)|_{SE}$. The state of the open system, also called the reduced state, is obtained by tracing out the environmental degrees of freedom of $\hat{\rho}_{SE} \in \mathcal{S}(\mathcal{H}_{SE})$, i.e. $\hat{\rho}_S = \mathrm{tr}_E\{\hat{\rho}_{SE}\}$, where $\mathrm{tr}_E\{\cdot\}$ denotes the partial trace over the environment. Note that

even if the joint system is in a pure state, the reduced state of S need not be pure. This is, for example, the case if there is some entanglement between S and E. Throughout this thesis we focus on the dynamics of finite dimensional subsystems S, and thus, the state of the reduced state of S can be represented as a Hermitian, positive semidefinite matrix with trace one.

To describe the time evolution of an open system S we start with the unitary time evolution of the joint system. We assume that the joint system is described by a Hamiltonian of the form

$$\hat{H} = \hat{H}_S + \hat{H}_E + \hat{H}_{SE}, \tag{2.5}$$

where $\hat{H}_S$ ($\hat{H}_E$) describes the Hamiltonian of the open system (environment), respectively, and $\hat{H}_{SE}$ describes the interaction between S and E. In the following we assume that at time $t = 0$ there are no correlations between the open system and the environment. In this case, the initial state can be written as

$$\hat{\rho}_{SE}(0) = \hat{\rho}_S(0) \otimes \hat{\rho}_E(0). \tag{2.6}$$

Since the joint system is closed, its time-evolution is described by a unitary time evolution operator $\hat{U}(t) = \mathrm{e}^{-i\hat{H}t}$. The state of the open system at time t is thus given by

$$\begin{aligned} \hat{\rho}_S(t) &= \mathrm{tr}_E\{\mathrm{e}^{-i\hat{H}t}\hat{\rho}_S(0) \otimes \hat{\rho}_E(0)\mathrm{e}^{i\hat{H}t}\} \\ &\coloneqq \Phi_t\hat{\rho}_S(0). \end{aligned} \tag{2.7}$$

For a fixed initial state of the environment $\hat{\rho}_E(0)$, Eq. (2.7) defines a linear map Φ_t on the set $\mathcal{S}(\mathcal{H}_S)$ as

$$\begin{aligned} \Phi_t : \mathcal{S}(\mathcal{H}_S) &\to \mathcal{S}(\mathcal{H}_S) \\ \hat{\rho}_S(0) &\mapsto \hat{\rho}_S(t) = \Phi_t\hat{\rho}_S(0). \end{aligned} \tag{2.8}$$

The map Φ_t, called the dynamical map, is a super operator mapping any initial state of the subsystem to the corresponding state at time t. Thus, it encodes the complete information on the time evolution of the reduced state of S. Using Eq. (2.7), one can show that the dynamical map preserves the Hermiticity and the trace of operators, and that it is a positive map, i.e. Φ_t maps positive operators to positive operators [38]. Thus, Φ_t maps physical states to physical states, implying that $\mathcal{S}(\mathcal{H}_S)$ is closed under the action of Φ_t. Note that the dynamical map is not only positive but also completely positive [37–39]

In the discussion of thermalization, the long-time limit of the reduced state, i.e. the state

of the subsystem S in the limit $t \to \infty$, is of particular importance. This state is called asymptotic state. For a given initial state $\hat{\rho}_S(0)$, the corresponding asymptotic state is defined as

$$\hat{\rho}_\infty\Big(\hat{\rho}_S(0)\Big) =: \lim_{t\to\infty} \Phi_t \hat{\rho}_S(0), \tag{2.9}$$

provided that the limit exists. In general, the asymptotic state can depend on the initial state. The dynamical map Φ_t is called relaxing if there exists a unique state $\tilde{\rho}_\infty \in \mathcal{S}(\mathcal{H}_S)$, such that

$$\tilde{\rho}_\infty = \lim_{t\to\infty} \Phi_t \hat{\rho}_S(0) \tag{2.10}$$

holds for all possible initial states $\hat{\rho}_S(0) \in \mathcal{S}(\mathcal{H}_S)$ [40, 41]. Note that there are situations, in which $\rho_S(t)$ does not become stationary as $t \to \infty$, and the limit in Eq. (2.9) does not exist. This happens, for example, if decoherence free subspaces in the Hilbert space of the open system exist [42].

The dynamical map Φ_t encodes the complete information about time evolution of the subsystem S in the presence of its environment E. Our goal is to analyze properties of the dynamical map, without referring to a particular initial state of S. To do this, we employ different representations of the dynamical map. Let $\rho_{S,ij}$ be the matrix representation of the reduced density matrix, i.e. $\rho_{S,ij} = \langle i|\hat{\rho}_S|j\rangle$, where $|i\rangle$ is some fixed basis of the Hilbert space of the open system. In the following D denotes the dimension of this basis. The action of the dynamical map on the reduced density matrix can be written as

$$\rho_{S,ij}(t) = \sum_{kl} \Phi_{t;ij,kl}(t) \rho_{S,kl}(0), \tag{2.11}$$

where $\Phi_{t;ij,kl} = \mathrm{tr}\Big\{(|i\rangle\langle j|)^\dagger \Phi_t |k\rangle\langle l|\Big\}$. In this representation the dynamical map is a rank-4 tensor with D^4 complex elements, which can in principle be studied by methods from linear algebra. For the analysis of the dynamical map, however, it is more convenient to use a representation of the density matrix in terms of the (D^2-1) dimensional Bloch vector. The reason for this is, that the elements of the density matrix are not independent of each other, since only matrices with trace one represent physical states, i.e. only $(D-1)$ diagonal elements are independent of each other. For finite dimensional open systems such a representation always exists.

Within the (D^2-1) dimensional Bloch representation [43, 44], sometimes also called the coherence vector representation [38, 45], the state $\hat{\rho}_S$ is expanded in terms of the (D^2-1)

Hermitian and traceless generators of $\mathrm{SU}(D)$ as

$$\hat{\rho}_S = \frac{1}{D}\hat{\mathbb{1}} + \frac{1}{2}\sum_{d=1}^{D^2-1} a_d \hat{T}_d, \tag{2.12}$$

where $\hat{\mathbb{1}}$ is the identity matrix, the matrices $\{\hat{T}_d\}$ are the (D^2-1) generators of $\mathrm{SU}(D)$, and $\{a_d\}$ constitutes the (D^2-1) dimensional Bloch vector, i.e. $a_d = \mathrm{tr}\{\hat{\rho}_S \hat{T}_d\}$. For a definition of the matrices $\hat{T}_d$ see, for example, [38, 46]. Thus, every state $\hat{\rho}_s$ is represented by a unique element of $\mathbb{R}^{D^2-1}$. This representation guarantees hermiticity and unity of the trace but not the positivity. Thus, not all elements of $\mathbb{R}^{D^2-1}$ represent physical states, and hence, the set of physical states is only a subset of $\mathbb{R}^{D^2-1}$, denoted with $B(\mathbb{R}^{D^2-1})$ which represents $\mathcal{S}(\mathcal{H}_S)$ and is sometimes called the Bloch-vector space [46, 47]. For $N = 2$, $B(\mathbb{R}^{D^2-1})$ is the well-known Bloch ball. For $D \geq 3$ only some general properties of $B(\mathbb{R}^{D^2-1})$ were proven [46–49]. For our discussion here, however, it is sufficient to know that $B(\mathbb{R}^{D^2-1})$ is closed under the dynamical map, which is guaranteed by the definition of the dynamical map.

To obtain the action of the dynamical map on the Bloch vector one can employ the fact that the dynamical map is completely positive and trace preserving. Thus, the action of the dynamical map can be represented in terms of a set of Kraus operators $\hat{B}_d$ as [38, 50]

$$\hat{\rho}_S(t) = \sum_{d=1}^{D^2} \hat{B}_d(t)\hat{\rho}_S(0)\hat{B}_d^\dagger(t), \tag{2.13}$$

with $\sum_{d=1}^{D^2} \hat{B}_d^\dagger(t)\hat{B}_d(t) = \mathbb{1}$. Using this representation and the expansion of the reduced density matrix in terms of the generalized Bloch vector given by Eq. (2.12) the action of the dynamical map on the generalized Bloch vector, denoted by ϕ_t, can be written as [38, 51]

$$\begin{aligned} \phi_t : B(\mathbb{R}^{D^2-1}) &\to B(\mathbb{R}^{D^2-1}) \\ \mathbf{a}(0) &\mapsto \phi\Big(\mathbf{a}(0)\Big) = \mathbf{a}(t) + \mathbf{M}(t)\mathbf{a}(0). \end{aligned} \tag{2.14}$$

Here $\mathbf{b}(t) \in \mathbb{R}^{D^2-1}$ and $\mathbf{M}(t) \in \mathbb{R}^{(D^2-1)\times(D^2-1)}$. The map ϕ_t defines an affine transformation on $B(\mathbb{R}^{D^2-1})$ relating the initial Bloch vector $\mathbf{a}(0)$ to the corresponding Bloch vector $\mathbf{a}(t)$ at time t.

In principle, the dynamical map encodes the complete information about the time evolution of the open system. In practice, it is usually not possible to calculate the dynamical map directly, since it involves the time evolution of the joint system. It is, however, possible to construct the dynamical map from the evolution of the open system S: The time evolution of D^2 different, linearly independent initial states of the open system can be used to invert Eq. (2.11), thus allowing to reconstruct the representation of the dynamical map in terms of

the rank-4 tensor. From this representation the quantities $\mathbf{M}(t)$ and $\mathbf{b}(t)$ can be calculated by inverting Eq. (2.14). This can be done, for example, by calculating the time evolution for the initial state $\mathbf{a}(0) = (0\ 0...0)^T$ and $(D^2 - 1)$ other linearly independent initial Bloch vectors.

2.3 Local equilibration and thermalization in quantum systems

From a phenomenological point of view, thermalization describes the process that the state of a physical system, which is initially in a non-equilibrium state, relaxes to a thermal equilibrium state as $t \to \infty$. As exemplified in the previous section, there is a problem with this intuitive picture: For any finite quantum system, the wave function is a periodic function, and thus, can never approach a stationary state. To bridge the microscopic description and our expectations from the macroscopic world a weaker notion of thermal equilibrium and thermalization was proposed, motivated by the following idea [5, 6, 13, 14].

In a typical experiment one measures expectation values of observables $\hat{A}$ which only probe a finite subsystem S, sometimes called local observables. Let S be this subsystem and E its remainder, which we denote as the environment of the subsystem. The expectation value of a local operator $\hat{A}$ is not determined by the wave function of the full system, but by the reduced state of the subsystem S, which is given by

$$\hat{\rho}_S(t) = \mathrm{tr}_E\{|\Psi(t)\rangle \langle\Psi(t)|\}, \tag{2.15}$$

where $\mathrm{tr}_E\{\cdot\}$ denotes the partial trace over the environment E. The reduce state $\hat{\rho}_S(t)$ can be mixed, and thus, expectation values of local observables can be similar to thermal expectation values even if the total system is in a pure state. Note that the reduced state is mixed, if the subsystem S is entangled with its remainder E, which is typically the case in interacting systems.

These considerations lead to the notion of local thermal equilibrium and local thermalization: For a subsystem S, its environment E can act as an environment, thus causing the subsystem to relax to a thermal equilibrium state, i.e. to thermalize. There are two aspects involved here. The first is the existence of a thermal equilibrium state, i.e. a pure state of the total system which leads to thermal expectation values of local observables. The second aspect is the relaxation of the non-equilibrium state to this thermal state.

The first aspect, i.e. the existence of a thermal equilibrium state, is subject of the eigenstate thermalization hypothesis (ETH). The ETH, developed by Deutsch and Srednicki [5, 6], explains the emergence of equilibrium statistical mechanics in terms of properties of the eigenstates of the underlying Hamiltonian $\hat{H}$. It states that expectation values of few-body observables in eigenstates of the Hamiltonian $\hat{H}$ vary little among neighboring eigenstates.

In the following, we briefly explain how this relates to the emergence of statistical mechanics. For a detailed review of this issue we refer the reader to Ref. [7]. In classical mechanics, the thermal equilibrium state is given by the microcanonical ensemble, i.e. all microstates with a given energy E are equally likely. The expectation value of an observable $\hat{O}$ in thermal equilibrium is thus given by averaging the expectation value uniformly over all microstates with energy E. For a quantum mechanical system, energy levels are quantized. The microcanoncial ensemble thus involves averaging over all eigenstates within a small energy window ΔE. For a quantum mechanical system, the microcanonical expectation value at the energy E is thus defined as [7]

$$\langle \hat{O} \rangle_{\mathrm{micro},E} = \frac{1}{\mathcal{N}} \sum_{E_d \in [E, E+\Delta E]} \langle E_d | \hat{O} | E_d \rangle \,, \tag{2.16}$$

where $\mathcal{N}$ are the number of levels being summed over. The width of the energy window ΔE has to be chosen smaller than any energy scale of the problem. We note that for large systems, the average nevertheless contains a large number of eigenstates. The ETH makes a statement about the expectation values of an observable $\hat{O}$ in eigenstates of the Hamiltonian. Specifically, it states that [5, 6]

$$\langle E_d | \hat{O} | E_d \rangle = \langle \hat{O} \rangle_{\mathrm{micro},E_d} + \Delta_d, \tag{2.17}$$

where Δ_d has zero mean and its amplitude vanishes as the system size increases. In a system obeying the ETH, every eigenstate already represents a thermal equilibrium state. Note that it is to date not known for which systems and observables the ETH holds. However, there is a variety of different numerical studies supporting the validity of the ETH [12, 52–54].

The other aspect of thermalization is the relaxation of a non-equilibrium state to an equilibrium state. As mentioned above, the reduced state $\hat{\rho}_S(t)$ of a subsystem can be mixed. For a finite dimensional system, however, the reduced state $\hat{\rho}_S(t)$ cannot become time-independent, i.e. cannot relax to a stationary thermal equilibrium state. In order to define a reasonable notion of thermalization one considers the fluctuations of the reduced state $\hat{\rho}_S(t)$ around the time-averaged state [13, 17, 18]. A subsystem is said to equilibrate, i.e. approach a time-independent state, if its state approaches some equilibrium state and stays close to this state for almost all times. To define this in a rigorous way, we need to define the time-average of a function and the distance between two density matrices. The time average of a function $f(t)$ is defined as

$$\langle f(t) \rangle_t = \lim_{T \to \infty} \frac{1}{T} \int_0^T f(\tau) \mathrm{d}\tau. \tag{2.18}$$

The distance between two density matrices $\hat{\rho}_1$ and $\hat{\rho}_2$ is defined as

$$\mathcal{D}(\hat{\rho}_1, \hat{\rho}_2) = \frac{1}{2}\mathrm{tr}\{|\hat{\rho}_1 - \hat{\rho}_2|\}, \tag{2.19}$$

where the modulus of an operator $\hat{A}$ is given by $|\hat{A}| = \sqrt{\hat{A}^\dagger \hat{A}}$. The state of a subsystem is said to equilibrate towards the time-averaged state $\hat{\omega}_S = \langle \hat{\rho}_S(t) \rangle_t$, i.e. towards an equilibrium state, if the fluctuations quantified by

$$\langle D(\hat{\rho}_s(t), \hat{\omega}_S) \rangle_t \tag{2.20}$$

are small. As the relative size of the environment E compared to the subsystem S is increased the fluctuations are expected to decrease and become unresolvable small in the thermodynamic limit.

Based on these concepts, thermalization in quantum systems can be defined as follows: a subsystem of a quantum system thermalizes if the reduced state of the subsystem relaxes to an equilibrium state, stays close to this state for almost all times, and if the equilibrium state fulfills properties of a thermal state listed and explained below. In order to investigate this complex process, modern approaches decompose thermalization into different aspects [13,14]. According to this, thermalization of a subsystem S consists of the following four properties:

1) *Subsystem equilibration*: A subsystem S equilibrates if its state evolves towards some particular state, called the equilibrium state, and remains close to this state for almost all times. Formally this means that the fluctuations defined by Eq. (2.20) are small. Note that this does not make any statement about the form of the equilibrium state. In particular, it need not be a thermal state and indeed may depend on the initial state of the system in an arbitrary way.

2) *Bath state independence*: The equilibrium state of the system should not depend on the precise initial state of the effective environment E. That is, the equilibrium state of S only depends on some macroscopic properties of the initial state of E, e.g. its energy.

3) *Subsystem state independence*: If the subsystem S is small compared to its environment E, the equilibrium state of the subsystem should be independent of its initial state.

4) *Gibbs state*: The equilibrium state is close to a Gibbs or thermal state. That means the equilibrium state $\hat{\omega}_S = \langle \hat{\rho}_S(t) \rangle_t$ is well described by [55]

$$\hat{\omega}_S = \mathrm{tr}_E\{\underbrace{Z^{-1}(\beta)\mathrm{e}^{-\beta \hat{H}}}_{\hat{\rho}^{th}(\beta)}\}. \tag{2.21}$$

Here $\hat{H}$ describes the Hamiltonian of the full system and $Z(\beta) = \mathrm{tr}\{\mathrm{e}^{-\beta\hat{H}}\}$ describes the partition function. Note that $\hat{\rho}^{th}(\beta)$ describes the equilibrium state of the joint system at inverse temperature β. The inverse temperature β is chosen such that $\mathrm{tr}\{\hat{\rho}^{th}(\beta)\hat{H}\} = \langle\Psi(0)|\hat{H}|\Psi(0)\rangle$, where $|\Psi(0)\rangle$ is the initial state of the joint system [56].

A subsystem S of a closed quantum system is thermalized by its environment if the reduced state of S fulfills the properties 1) to 4). If a subsystem S is thermalized by its environment, the expectation values of local operators acting on this subsystem S relax towards and remains close to a thermal equilibrium value, determined only by some macroscopic observables of the total system, like the total energy.

Recently, Linden and coworkers [13] showed that the first two properties, *subsystem equilibration* and *bath state independence*, are general properties of interacting quantum systems. Assuming that the Hamiltonian $\hat{H}$ has non-degenerate energy gaps, they showed that any small subsystem approaches and stays close to an equilibrium state, which only depends on some macroscopic properties of its environment, provided that the dimension of S is small compared to the number of eigenstates of the full system contributing to the dynamics [13]. A Hamiltonian has non-degenerate energy gaps if for any four eigenstates with energies E_k, E_l, E_m, and E_n, $E_k - E_l = E_m - E_n$ implies $k = l$ and $m = n$, or $k = m$ and $l = n$. More precisely, Linden et al. showed that the fluctuations around the equilibrium state defined by Eq. (2.20) are bounded by

$$\langle D(\hat{\rho}_s(t), \hat{\omega}_S)\rangle_t \leq \frac{1}{2}\sqrt{\frac{d_S^2}{d_{\mathrm{eff}}}}, \tag{2.22}$$

where d_S denotes the dimension of the subsystem and $d_{\mathrm{eff}} = (\sum_d |c_d|^4)^{-1}$ quantifies the number of contributing eigenstates, i.e. $c_d = \langle E_d|\Psi(0)\rangle$. Additionally, it was shown that the equilibrium state of the subsystem $\hat{\omega}_S$ is similar for most initial states of the total system, i.e. does not depend on the precise initial configuration of the joint system.

The third aspect of thermalization, the subsystem state independence, turns out to be more complicated. The main reason for this is that it is in fact not always true, as there are known examples in which the asymptotic state of an open system depends on its initial state [42,57–60]. It is, however, possible to connect the subsystem state independence of the equilibrium state with the ETH, which is typically used to explain the emergence of equilibrium statistical mechanics in isolated quantum systems. Assuming that the Hamiltonian has non-degenerate energy gaps, which guarantees that any small subsystem equilibrates, the

expectation value of a local observable $\hat{O}$ in equilibrium is given by

$$\langle\langle\Psi(t)|\hat{O}|\Psi(t)\rangle\rangle_t = \sum_d |c_d|^2 \langle E_d|\hat{A}|E_d\rangle \,. \tag{2.23}$$

The initial state influences this equilibrium value through the coefficients c_d. If the ETH holds, i.e. Eq. (2.17) holds, the expectation value $\langle E_m|\hat{D}|E_m\rangle$ can be replaced, within small corrections, by the microcanonical expectation value defined by Eq. (2.16). The equilibrium value of the expectation value of $\hat{O}$, given by

$$\langle\langle\Psi(t)|\hat{O}|\Psi(t)\rangle\rangle_t \approx \sum_d |c_d|^2 \langle\hat{O}\rangle_{\mathrm{micro},E_d} \,, \tag{2.24}$$

thus only depends on the energy distribution of the initial state, and not on the precise initial configuration. If this distribution is similar for all initial states of the subsystem, i.e. the influence of the initial state of the subsystem on the total energy is negligible, the expectation value does not depend on the initial state of the subsystem. If, on the other hand, the energy of the total system is changed significantly by changing the initial state of the subsystem, the equilibrium expectation value in general depends on the initial state.

We are particularly interested in the discussion and classification of the failure of thermalization. In this thesis, we consider only violations of the first three aspects, and will not consider the fourth aspect. We note, however, that a recent numerical study discusses whether the reduced states relaxes to a Gibbs state, and in fact shows that for particular systems the reduced state approaches a Gibbs state [56].

2.4 Non-thermal asymptotic behavior

A subsystem S of a quantum system fails to thermalize if at least one of the four aspects is violated. Thus, qualitatively different non-thermal behaviors are possible, depending on which of the four aspects is violated. In this section, we discuss two of these possible non-thermal behaviors in more detail. The first is that the reduced state of a subsystem S does not approach an equilibrium state, i.e. $\hat{\rho}_S(t)$ does not relax to some equilibrium state. We elaborate on this in 2.4.1. Second, the state of a subsystem S can relax to some equilibrium state, which depends on the initial state of the subsystem S, i.e. some information of the initial state is retained in local observables. A discussion of this is subject to 2.4.2, where we also mention some general properties of the equilibrium state provided that it exists. In Sec. 2.4.3 we introduce many-body localized systems, which represent a class of systems which fail to thermalize due to the existence of an extensive set of quasi-local conserved quantities.

2.4.1 Failure of subsystem equilibration

As already discussed in the previous section, the reduced state of a subsystem S of a finite dimensional system remains time-dependent at all times. For thermalizing systems, however, the fluctuations around the equilibrium state are expected to decrease with increasing size of its environment E. A violation of equilibration in this context thus means that the fluctuations around the equilibrium state remains finite in the thermodynamic limit, i.e. as the size of the environment goes to infinity.

A failure of subsystem equilibration can be explained as follows: According to the proof of Linden and coworkers [13], every subsystem equilibrates if the underlying Hamiltonian has non-degenerate energy gaps. A violation of equilibration thus means that the underlying Hamiltonian has degenerate energy gaps. This happens for example if there is a subsystem S such that the Hamiltonian assumes the form $\hat{H} = \hat{H}_S + \hat{H}_E$ [13]. For this particular subsystem S, its remainder cannot act as a bath, thus, preventing relaxation of the reduced state of the subsystem. We discuss an example of this in Sec. 4.2.3.

2.4.2 Failure of subsystem independence: The generalized Gibbs ensemble

Linden et al. proved that subsystem equilibration is a general property of interacting quantum system and that the equilibrium state does not depend on the precise initial state of the environment [13]. The initial state of the subsystem, however, can influence its equilibrium state. Thus, a natural question is whether there is a general concept which determines the equilibrium state when the subsystem does not thermalize.

If a subsystem thermalizes, the equilibrium state is described by a Gibbs state (see the fourth aspect of thermalization). Thus, the equilibrium state is determined by the temperature, or the total energy of the system. This dependence originates from the fact that the energy is a conserved quantity. The Gibbs form of the equilibrium state can in fact be derived from Jaynes' principle [61, 62] by maximizing the entropy under the constraint that the expectation value of the energy is known. The corresponding Lagrange multiplier is connected to the temperature. Following this line of reasoning, the equilibrium state of systems with more conserved quantities, is expected to depend on all of these conserved quantities.

A particular interesting class in this context are so called integrable systems, which posses an extensive number of conserved quantities. Note that there is up to date no clear definition of integrability in quantum systems [63]. However, one particular property implying integrability is the existence of an extensive set of local conserved quantities, i.e. operators which commute with the Hamiltonian and with each other, which are thus

conserved under the time evolution. The equilibrium state can be derived by applying Jaynes' principle with the constraint that the expectation value of every conserved quantity is known. The thus derived density matrix takes the form of a Gibbs ensemble with one Lagrange multiplier for each conserved quantity and is nowadays known as the generalized Gibbs ensemble (GGE) [19, 64]. The applicability of the GGE to describe the asymptotic behavior in integrable systems has been confirmed in many theoretical works [19–21, 64]. The experimental observation of a stationary state described by a GGE has been recently reported [65]. The long-time state of integrable systems depends on the initial value of all conserved quantities, and thus, the system fails to thermalize locally.

2.4.3 Many-body localization: Emergent integrability

A new kind of integrability that aroused a lot of interest in recent years emerges in systems exhibiting many-body localization. Localization, first introduced by Anderson in non-interacting lattice models [22], refers to the absence of transport in systems subject to static disorder. The absence of transport in Anderson localized systems originates from exponentially localized single-particle states. They give rise to an extensive set of local conserved quantities: the occupation number of the single particle states. First conjectured [24–26] and later shown by Imbrie [27], also interacting many-body systems can have an extensive number of quasi-local integrals of motion, thus leading to a strong suppression of transport in systems subject to strong enough disorder [23, 24]. This phenomenon is nowadays known as many-body localization (MBL). These quasi-local integrals of motion are associated with mutually commuting operators which are exponentially localized in real space and which commute with the Hamiltonian and among each other [25, 26].

The existence of these conserved quantities has an important consequence for the ability to thermalize, i.e. for the asymptotic state of subsystems of MBL systems. Subsystems of interacting systems are expected to relax to an equilibrium state which is determined by all conserved quantities of the system, i.e. they relax to the GGE [13]. For MBL systems, these conserved quantities are local in real space, and thus, the asymptotic state of subsystems is sensitive to local changes of the initial state of the system. This allows for the observation of non-thermal behavior in real space, like a dependence of the asymptotic state of subsystems on its initial state. Just recently, this dependence was observed in two experiments [28, 29]. To explain this non-thermal behavior and other properties of many-body localized systems a phenomenological model can be employed [25, 26]. For simplicity we consider a system of spins, which is sufficient to derive the phenomenology of MBL [66]. In spin systems which exhibit many-body localization there exist a set of pseudospins, also called "l-bits", whose z component are conserved quantities. Let $\{\hat{\tau}_n^z\}$ be the extensive set of conserved quantities. Since these operators are conserved quantities, the Hamiltonian of a many-body localized

system can be written as

$$\hat{H} = \sum_m h_m \hat{\tau}_n^z + \sum_{m,n} J_{m,n} \hat{\tau}_m^z \hat{\tau}_n^z + ..., \tag{2.25}$$

where the dots indicate interaction terms including three and more operators $\hat{\tau}_n$. A key property of MBL is that the conserved quantities are quasi-local, i.e. they are superpositions of spin operators with weights that fall off exponentially with the distance to the center of the conserved quantity [25, 26, 67]. The exponential tail of the l-bits mediate a long-range interactions between them. Since the l-bits are localized around a single lattice site, the interaction fall off exponentially with distance [26].

The form of the Hamiltonian given by Eq. (2.25) has some consequences for the dynamics: the z component of the l-bits is frozen, while their x and y components precess about the z axes of their Bloch spheres at a rate that is set by the interactions with the z components of all of the other l-bits. Thus, they are subject to dephasing and decoherence due to the interaction with this static spin bath. A second consequence is that the l-bits can get entangled only through their direct interaction. Since the effective l-bit interactions in the localized phase fall off exponentially with distance, after a time t, a given l-bit is entangled with all other l-bits within a volume $\ln t$. This gives rise to a characteristic logarithmic spreading of entanglement in many-body localized systems [68]. Besides other characteristics which we discuss in the next section, the logarithmic increase of the entanglement entropy serves as an indicator for many-body localization.

We finish with a short comment on the emergent integrability in MBL systems [69]. One characteristic feature of MBL systems is the existence of an extensive set of local conserved quantities. This seemingly places MBL systems in the same category as other integrable models. There are, however, some conceptual differences compared to other known kinds of integrability, like the integrability in non-interacting systems or Yang-Baxter integrable systems [70]. In contrast, if a non-interacting system, characterized by conserved occupations of single-particle eigenstates, is perturbed by introducing an arbitrarily weak two-body interaction, the integrability is immediately destroyed. A similar scenario is expected to hold for Yang-Baxter-integrable systems [54]. The robustness of the local integrals of motion reflects the fact that MBL is a dynamical phase of matter, while non-interacting systems and Yang-Baxter integrability represent isolated points or lines in the phase space.

2.5 Classification of thermal and non-thermal behavior in quantum systems

A subsystem S of a quantum mechanical system is said to thermalize if the reduced state of the subsystem fulfills all four aspects of thermalization introduced in section 2.3.

Consequently, non-thermal behavior is indicated by a violation of one of the four aspects. Deciding if a particular subsystem fulfills all four aspects of thermalization is, however, difficult. In particular the distinction between thermalizing and integrable systems can be challenging, as the reduced state of subsystems equilibrates in both situations: for thermalizing systems the equilibrium state is given by a Gibbs state, whereas for integrable systems it is given by a generalized Gibbs state. In both cases the asymptotic state of a subsystem is determined by all conserved quantities of the total system, i.e. by all operators which commute with the Hamiltonian and among each other. An obvious way to classify a system as thermalizing or integrable is to determine all operators which commute with the Hamiltonian. If an extensive set of operators commute with the Hamiltonian, the system is integrable. If, on the other hand, only a few global conserved quantities exist the system is not integrable. Based on the set of all conserved quantities it is thus possible to classify a system as either integrable or thermal. In practice, however, it is usually difficult to identify all conserved quantities.

In the following we discuss alternative indicators of integrability in quantum systems which can be used to classify systems as integrable or thermal without the need to identify all conserved quantities of the model. These indicators can be separated into two classes. The first are based on spectral properties of the underlying many-body Hamiltonian, i.e. properties of the eigenvalues and eigenstates. This approach is further discussed in Sec. 2.5.1. A second possibility is to study the dynamical evolution of a system which is initialized in some far-from equilibrium state. This includes, for example, the relaxation of observables towards some equilibrium value or the spreading of entanglement in the system. We elaborate on this in section 2.5.2. To exemplify the different approaches we discuss them for the XXZ Heisenberg spin chain with random local disorder. For weak disorder W this system is thermalizing, whereas for strong enough disorder the system is many-body localized. In this section, we only present the behavior of certain observables to demonstrate how they can be used to classify systems as thermalizing or integrable. A detailed discussion of the model is provided in Sec. 5.1. In the last section, 2.5.3, we employ the *subsystem state independence* in thermalizing system to identify non-thermal behavior. The existence of local conserved quantities in integrable systems imply that information about the initial state is stored in local observables at all times. This implies that the asymptotic state of a subsystem depends on its initial state. Based on the dynamical map describing the time evolution of subsystems, we propose a measure to quantify this dependence and discuss how it can be used to detect a violation of *subsystem state independence*, i.e. a failure of thermalization of S.

2.5.1 Spectral properties: Level spacing statistics and properties of eigenstates

Many of the commonly used methods to classify quantum mechanical systems as either integrable/non-thermal or thermal are based on spectral properties of the underlying Hamiltonian. Within this approach the fluctuations of the eigenvalues of the Hamiltonian, i.e. the energies E_d, are considered. To this end, the spectrum of the Hamiltonian is decomposed into a system-specific mean level density and a fluctuating part [71]. As we explain in the following, the fluctuating part can be used to classify a system into either thermal or integrable. To investigate the fluctuations of the energy levels, one first has to remove the system-specific mean level density. This procedure is called unfolding of the spectrum. This can only be done exactly if the system-specific mean level density is known, which is usually not the case. However, using approximations for the mean-level density, e.g. a least square fit for the mean-level density, it was shown that local properties, such as the local level fluctuations, can be extracted [72].

The central quantity of interest in this approach is the probability distribution of energy level spacings $p(s)$, where $s = \epsilon_n - \epsilon_{n-1}$ denotes the difference between neighboring energy levels of the unfolded spectrum. Originally, this approach dates back to works done by Wigner and Dyson aimed to understand the energy levels of large nuclei [73–76]. It was later discovered that the distribution of energy level spacings, i.e. the statistics of the difference between consecutive eigenenergies can also be used to distinguish between integrable and thermalizing systems. In this context two results are of particular importance: Berry and Tabor conjectured that the energy levels in integrable systems can be seen as independent random variables, meaning that the distribution of energy level spacings is Poissonian [77]. Later, Bohigas, Giannoni, and Schmit conjectured that in quantum systems whose classical counterpart is chaotic the energy level spacings are described according to a Wigner-Dyson distribution [78]. Both conjectures have been confirmed in different settings, e.g. [52, 53, 78–80] and can also be used to distinguish between integrable and thermalizing systems when there is no classical counterpart [52, 53, 81].

The distribution of energy level spacings can thus be used as an indicator for integrability in quantum systems. The qualitative difference between the distribution of the energy level spacings is demonstrated in Fig. 2.1 for a thermalizing (left plot) and an integrable (right plot) system. Classifying a system based on spectral statistics thus seems to be straightforward: calculate the spectrum of the Hamiltonian, unfold it, and investigate the distribution of energy level spacings. If the spacing follows a Wigner-Dyson distribution the system is expected to thermalize; if the spacing follows a Poissonian distribution the system is expected to be integrable. Based on this approach different models have been investigated and transitions between thermalizing and integrable dynamics were estimated [52, 82–84].

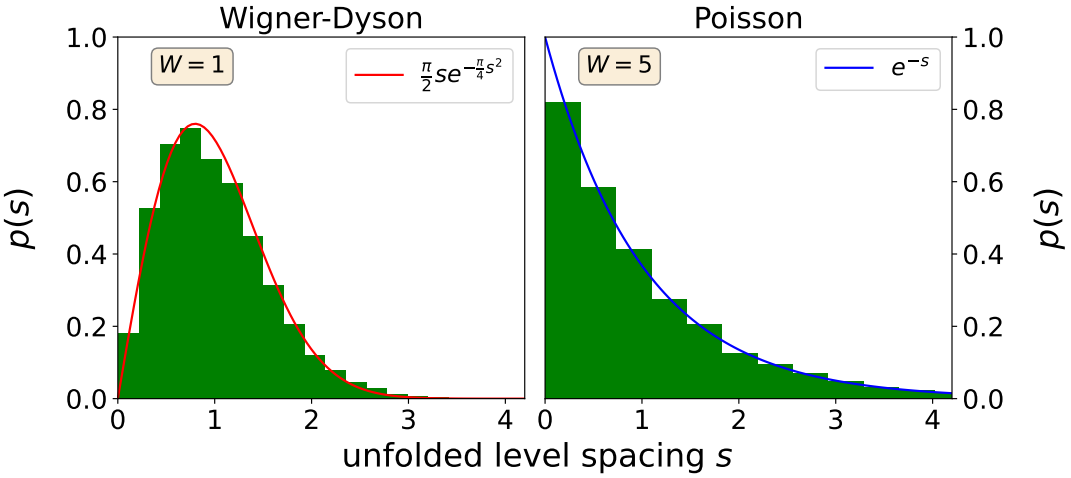

Figure 2.1: Histogram of the unfolded level spacings of an XXZ Heisenberg chain with random local disorder W for $L = 16$. In the weak disorder regime $(W = 1)$ the system thermalizes, and the level spacing distribution is described by a Wigner-Dyson distribution. In the integrable case $(W = 5)$ the distribution of the level spacings is Poissonian. The details of the model are given in Sec. 5.1.

Note that the unfolding of the spectrum can be avoided by considering the ratio of two consecutive energy gaps [82].

There are a few aspects we want to highlight and discuss in the following. Comparing the different distributions in Fig. 2.1, the most striking difference between them is their behavior as $s \to 0$. The Poissonian distribution has its maximum at $s = 0$, and thus, the spectrum of integrable systems is dominated by (near-) degeneracies. In contrast to this, the Wigner-Dyson distribution vanishes as $s \to 0$. Degeneracies are thus exceptional. In fact, it is possible to derive the Wigner-Dyson distribution by considering a non-integrable system as an integrable one subject to a random perturbation [85]. In first order perturbation theory the degenerate eigenstates of the integrable system are coupled leading to an avoided crossing of the perturbed eigenenergies. If the spectrum of the non-integrable system is dominated by such avoided crossings, i.e. if most of the eigenstates which are close in energy are coupled by the perturbation the statistics of energy level spacings is described by a Wigner-Dyson distribution.

Properties of the eigenstates provide alternative indications of thermal and non-thermal behavior. One can, for example, test if the eigenstates of the many-body Hamiltonian fulfill the eigenstate thermalization hypothesis. i.e. if expectation values of local observables vary little among neighboring eigenstates [54, 86]. The entanglement entropy can be used as further indicator: In thermalizing systems, the entanglement entropy is an extensive quantity, and thus, the von Neumann entropy of a subsystem scales with the volume of that subsystem [69]. In many-body localized systems, on the other hand, the existence of the set of local conserved quantities give rise to a von Neumann entropy which scales with the area

of the subsystem [25, 69, 87]. Other indicators are correlations between different degrees of freedom as a function of their distance [88] or the scaling of the mutual information [89].

Although spectral properties provide an easy way to classify quantum system into integrable or thermal, they have some problems. The first is rather obvious: all quantities which are based on the eigenvalues and eigenstates of the system require the diagonalization of the underlying many-body Hamiltonian, which limits this approach to relative small systems due to the exponential scaling of the many-body basis. The second issue is special to many-body localized systems and is related to the stability of the MBL phase with respect to the inclusion of thermal regions. Over the last years it was realized that a single thermal region embedded in a many-body localized system is capable of thermalizing the full system through an avalanche-like process [90–94]. In large systems with quenched local disorder, there are regions in which the random fields are small and the system locally thermalize. In the thermodynamic limit, such regions occur with probability one. This results in a finite local bath that then tends to thermalize the nearby localized regions, which ultimately results in an enlarged thermal region. The stability of the MBL phase in the thermodynamic limit is then connected to the question, whether this avalanche-like thermalization eventually stops. Recent numerical investigations in the XXZ Heisenberg chain with random local disorder indicate that the critical disorder at which the statistics of the energy level spacings change from Wigner-Dyson to Poissonian is in fact smaller than the critical value at which the avalanche-like thermalization eventually stops [88, 94]. This shows that the spectral statistics can be misleading.

2.5.2 Dynamical properties: Equilibration of observables and spreading of entanglement

Instead of considering spectral properties of the Hamiltonian one can alternatively investigate the time-evolution of certain observables. The idea behind this approach is the following: the system is initialized in some non-equilibrium state. One then considers the time-dependent expectation values of certain observables and investigates if these relax to expectation values compatible with thermal expectation values.

One example of such a quantity, which is used in the context of spin systems, is the averaged local autocorrelation function of the spins, sometimes also called Edwards-Anderson spin glass parameter [95],

$$q_{EA} = \frac{1}{L} \sum_n \langle \Psi | \hat{S}^z_n(t) \hat{S}^z_n(0) | \Psi \rangle \,, \tag{2.26}$$

where L is the length of the spin chain and $\hat{S}^z_n$ denote the z component of the n-th spin. As usual they are given by $\hat{S}^z = \frac{1}{2}\hat{\sigma}^z$, where $\hat{\sigma}^z$ denotes the Pauli matrix. $\hat{S}^z_n(t)$ denotes

the time-evolved operator, i.e. $\hat{S}_n^z(t) = \mathrm{e}^{i\hat{H}t}\hat{S}_n^z\mathrm{e}^{-i\hat{H}t}$. The quantity q_{EA} measures the averaged local correlation between the initial operator and the operator at a later time. If the system thermalizes these local correlations should vanish as $t \to \infty$ since the asymptotic value of subsystems is expected to be independent of their initial state. To exemplify the different behavior we show q_{EA} for the XXZ Heisenberg spin chain in Fig. 2.2a) for an initial state of the form $|\Psi\rangle = |\uparrow\downarrow ...\rangle$. For weak disorder (thermalizing regime) the spin glass parameter q_{EA} decays to a small value, showing that the average autocorrelation of the expectation value of $\hat{S}_n^z(t)$ with its initial value is small. For a many-body localized system (large disorder) the asymptotic value of q_{EA} is significantly larger than zero, showing that there is some correlation between the operator at time zero and at time t. We note that if the spin chain is initially in the Neel state, $|\Psi\rangle = |\uparrow\downarrow ...\rangle$, the spin glass order parameter is equal to the staggered magnetization or the imbalance, which was recently measured experimentally [28, 29].

Another indicator which can be used to distinguish between thermal and non-thermal behavior is the spreading of entanglement. Although experimentally hard to measure, it provides some physical insights into the dynamics of the system. In thermal systems entanglement spreads ballistically with a power law increase [96, 97]. In many-body localized systems the existence of the quasi-local integrals of motion, together with their interaction which decays exponentially with the distance, implies a logarithmic spreading of the entanglement entropy, special to these systems [68, 98]. To demonstrate this, the half chain entanglement entropy (HCEE), i.e. the entanglement entropy of the left half chain with the right half, of the XXZ Heisenberg spin model in the thermalizing regime ($W = 1J$) and in the many-body localized regime ($W = 5J$) is shown in Fig. 2.2b). In the thermalizing regime, the HCEE exhibits a fast increase after which it saturates. In the many-body localized regime a logarithmic increase is visible, which originates from the exponentially decaying interaction between the local integrals of motion.

2.5.3 Measuring the influence of the initial state on the dynamics of an open quantum system

Another key property of thermalizing systems is the *subsystem state independence*: the asymptotic state of a subsystem is independent of its initial state. A dependence of the asymptotic state of a subsystem on its initial state is thus an indication of non-thermal behavior. This can be investigated by considering the time evolution of a subsystem S for different initial states of the subsystem S while keeping the state of its environment fixed. To quantify the influence of the initial state of S different approaches are possible. The easiest way is to choose a particular observable $\hat{O}$, initialize the subsystem S in different initial states, and investigate the time dependent expectation value of $\hat{O}$. This approach,

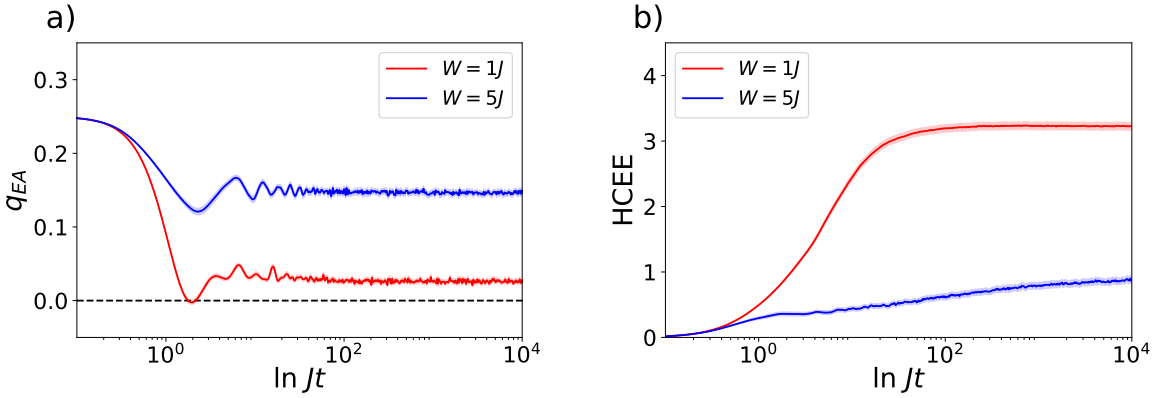

Figure 2.2: In the left panel the spin glass order parameter is shown, in the right panel the half chain entanglement entropy (HCEE) is shown. The red lines represent the results for a thermalizing system ($W = 1J$) the blue lines represent the results for a many-body localized spin chain ($W = 5J$). For a thermalizing spin chain, q_{EA} decays to a value close to zero and the HCEE quickly saturates. In the many-body localized phase, the spin glass order parameter approaches a value significantly larger than zero and the HCEE exhibits a characteristic logarithmic increase.

however, depends on the choice of the considered observable $\hat{O}$, as well as, the choice of the two initial states. Alternatively, one can consider the distance between the time dependent reduced state of S for two different initial conditions, given by Eq. (2.19). In thermalizing systems, this distance decays to zero as $t \to \infty$, for all pairs of initial states. In Fig. 2.3 this is shown for a single spin in the XXZ Heisenberg spin chain. As can be seen, the distance of the pair of initial states in the long-time limit is smaller for the thermalizing system ($W = 1J$) compared to the localized system ($W = 5J$). In principle, the time-dependent trace distance can be used as an indication of thermal behavior or non-thermal behavior. As can be seen from the results, however, the distance $\mathcal{D}$ depends on the choice of the two initial states. In the following we discuss a possibility to quantify the influence of the initial state of a subsystem on its dynamics without referring to a particular initial state. Based on these considerations it is possible to detect a failure of *subsystem state independence*. We note that the dependence of the equilibrium state on the initial state of a subsystem has been investigated in [99], employing the time average of the quantum dynamical map. Here, we consider the full time dependence of the quantum dynamical map. This not only allows us to discuss the influence of the initial state on the equilibrium state, but also to bound the impact of the initial state on expectation values. A further advantage of this approach is that, compared to the analysis based on spectral properties of the total Hamiltonian, an analysis of the dynamical map is much more feasible, as its dimension is determined by the subsystem. As we discuss in detail in chapter 5 this measure can also be used to investigate delocalization mechanisms and information loss in quantum systems, thus allowing us to analyze the underlying processes.

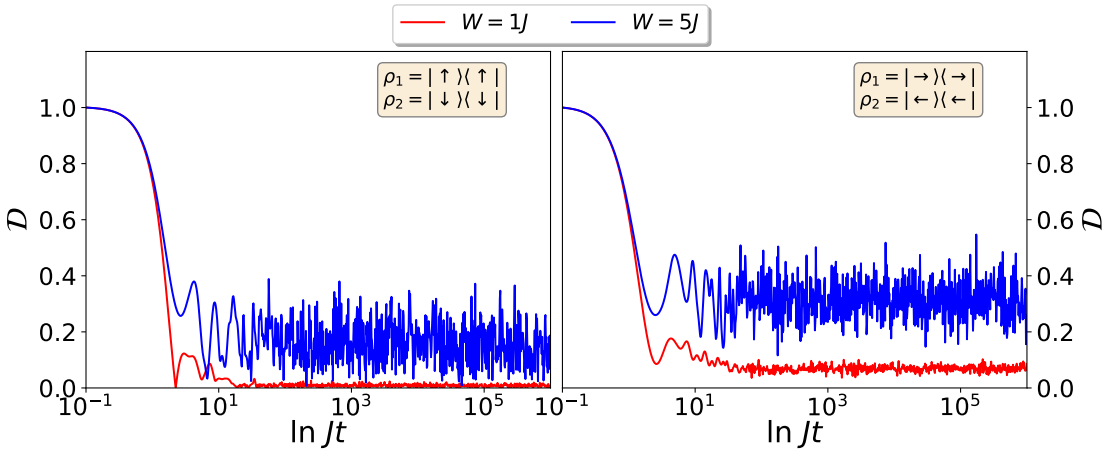

Figure 2.3: Shown is the time-dependent distance $\mathcal{D}$ between the reduced state for two different initial states for the XXZ-Heisenberg chain with random disorder for $L = 15$. The red curve ($W = 1$) represent the results for a thermalizing system, the blue curve ($W = 5$) represents results for a many-body localized system. The distance between the two different initial states is smaller for the thermalizing system compared to the localized system. The two plots show the influence of the chosen initial states: the pair of considered initial states in the left and in the right plot are different. We defined $|\rightleftarrows\rangle = \frac{1}{\sqrt{2}}(|\uparrow\rangle \pm |\downarrow\rangle)$

In order to quantify the influence of the initial state of a subsystem S on its dynamics, i.e. the local memory of S, we consider the following scenario. We separate the full system into the subsystem, of which we want to quantify the local memory, and its remainder, i.e. its environment E. The initial state of the subsystem is arbitrary, whereas the initial state of its remainder is kept fixed. From this viewpoint, the subsystem S is an open quantum system in contact with an environment E. Consequently, the time evolution of the subsystem is described by a dynamical map, as discussed in Sec. 2.2. The dynamical map encodes the full information of the time evolution of the open system, including the dependence of the asymptotic state on the initial state of the subsystem. In the following we discuss how the influence of the initial state of an open system, represented by the initial Bloch vector $\mathbf{a}(0)$, on its time evolution can be quantified by means of the dynamical map, i.e. by properties of the two quantities $\mathbf{M}(t)$ and $\mathbf{b}(t)$. Our starting point is the action of the dynamical map on a generalized Bloch vector, defined by Eq. (2.14). More precisely, we consider the action of the dynamical map on all possible initial states, i.e. the image of $B(\mathbb{R}^{N^2-1})$ under the dynamical map ϕ_t. To analyze and characterize this image we employ the singular value decomposition of $\mathbf{M}(t)$ given by

$$\mathbf{M}(t) = \mathbf{V}(t)\mathbf{S}(t)\mathbf{W}^T(t). \tag{2.27}$$

Since $\mathbf{M}(t)$ has real entries, $\mathbf{V}(t)$ and $\mathbf{W}(t)$ can be chosen to be real, orthogonal matrices and $\mathbf{S}(t)$ is a positive-semidefinite diagonal matrix.

Before discussing the influence of the initial state, we first note that if the time-evolution of the open system is unitary, e.g. for vanishing system-environment coupling, it directly follows that $\mathbf{b}(t) = \mathbf{0}$ and $\mathbf{M}^T(t)\mathbf{M}(t) = \mathbb{1}$, i.e. $\mathbf{M}(t)$ is an orthogonal matrix. The first can be shown by considering the action of the dynamical map on the Bloch vector $\mathbf{0} = (0\ 0\ ...)^T$. From Eq. (2.12) it follows that $\mathbf{0}$ is preserved under a unitary transformation. Thus, $\phi_t\mathbf{0} = \mathbf{0}$, which directly implies $\mathbf{b}(t) = 0$ for all times t. The orthogonality of $\mathbf{M}(t)$ can be shown by employing $\mathbf{b}(t) = \mathbf{0}$ and the fact that the euclidean norm of the Bloch vector under unitary time-evolution is preserved [38]. This implies that $||\mathbf{M}(t)\mathbf{a}(0)||_2 = ||\mathbf{a}(t)||_2$ holds for all times, where $||\mathbf{x}||_2 = \sqrt{\sum_n x_n^2}$ denotes the euclidean norm of a vector $\mathbf{x}$. This implies that $\mathbf{M}(t)$ is orthogonal for all times.

We start our analysis of the influence of the initial state by investigating its influence on the expectation value of an observable $\hat{O}$. To quantify this influence, we consider two different initial states of the open system, $\rho_S^1(0)$ and $\rho_S^2(0)$, and investigate the quantity

$$\delta_{1,2}(t;\hat{O}) = |\mathrm{tr}\Big\{\hat{O}\Big(\rho_S^2(t) - \rho_S^2(t)\Big)\Big\}|, \tag{2.28}$$

where $|\cdot|$ denotes the absolute value. The quantity $\delta_{1,2}(t;\hat{O})$ describes the difference of the expectation value of $\hat{O}$ at time t for two different initial states of the open system. Alternatively, $\delta_{1,2}(t;\hat{O})$ can be interpreted as the amount of information one can obtain about the initial state of the open system by measuring the observable $\hat{O}$. For $\delta_{1,2}(t;\hat{O}) = 0$ the outcome of a measurement is equal for the two initial states, thus no information about the initial state of the open system is obtained by measuring $\hat{O}$. If, on the other hand, $\delta_{1,2}(t;\hat{O}) \neq 0$ the outcome of the measurement depends on the initial state, and some information about the initial state of the open system can be obtained.

The quantity $\delta_{1,2}(t;\hat{O})$ relies on the choice of two initial states. Employing the singular value decomposition of the matrix $\mathbf{M}(t)$, a general upper bound can be derived yielding

$$\delta_{1,2}(t;\hat{O}) \leq \frac{N^{3/2}}{\sqrt{2}}|o_{\max}|\ s_{\max}(t)\ ||\mathbf{a}^1(0) - \mathbf{a}^2(0)||_2. \tag{2.29}$$

Here, $o_{\max}$ is the eigenvalue of O with the largest absolute value, $s_{\max}(t)$ is the largest singular value of $\mathbf{M}(t)$ at time t and $||\mathbf{x}||_2$ is the Euclidean norm of the vector $\mathbf{x}$. The proof of Eq. (2.29) is provided in appendix A.1. Equation (2.29) holds for any observable $\hat{O}$, and thus, we conclude that the largest singular value of $\mathbf{M}(t)$ is a measure for the influence of the initial state on the state at time t which is independent of the observable and the initial state. Alternatively, the largest singular value can also be interpreted as the local memory. If $s_{\max} = 0$ no information about the initial state is stored in local observables, for $s_{\max} \neq 0$ some information about the initial state can be obtained by measuring local observables.

As a second aspect, we discuss different long-time behaviors of an open system and how this can be classified by means of $\mathbf{M}(t)$. From Eq. (2.14) it directly follows that if the two limits

$$\mathbf{b}_\infty = \lim_{t\to\infty} \mathbf{b}(t) \tag{2.30}$$

$$\mathbf{M}_\infty = \lim_{t\to\infty} \mathbf{M}(t) \tag{2.31}$$

exist, every initial state has an asymptotic state, which is given by

$$\mathbf{a}_\infty = \mathbf{b}_\infty + \mathbf{M}_\infty \mathbf{a}(0). \tag{2.32}$$

The initial state $\mathbf{a}(0)$ has in general an influence on the asymptotic state. Equation (2.32) becomes independent of the initial state if all possible initial states are mapped to the same vector $\mathbf{b}_\infty \in \mathbb{R}^{N^2-1}$. This is exactly the case if the image of $\mathbf{M}_\infty$ is zero dimensional, i.e. if $\mathbf{M}_\infty = \mathbf{0}$. This follows from the fact that for any dimension of the open system the Bloch sphere $B(\mathbb{R}^{N^2-1})$ includes the (N^2-1) dimensional sphere with radius $r_s = \sqrt{\frac{2}{N(N-1)}}$ [100]. The image of this sphere is only zero dimensional if $\mathbf{M}_\infty = 0$. In this case, Eq. (2.32) becomes independent of the initial state and the unique asymptotic state is given by $\mathbf{b}_\infty$. Note that in this case $\delta_{1,2}(t;\hat{O}) \to 0$ as $t \to \infty$ independently of $\hat{O}$, implying that the expectation value of any observable becomes independent of the initial state $\mathbf{a}(0)$.

We conclude that the asymptotic state exists for all initial states if the limits (2.30) and (2.31) exist. The dynamical map is relaxing, i.e. the asymptotic state is unique, if and only if all singular values of $\mathbf{M}(t)$ decay to zero as $t \to \infty$. If the two limits (2.31) and (2.30) exists, but $\mathbf{M}_\infty \neq 0$, the asymptotic state exists for all initial states but depends on the initial state of the open system. If, on the other hand, one of the quantities $\mathbf{b}(t)$ or $\mathbf{M}(t)$ remain time-dependent for all times, there is at least one initial state for which the asymptotic state does not exist. Note that it is possible that the asymptotic state exists for some initial states, whereas for others the state of the open system remains time-dependent at all times. In such a situation, some singular values of $\mathbf{M}(t)$ become stationary and others remain time dependent.

Using the above derived concepts, a failure of *subsystem state independence* can be detected in the following way: consider a particular subsystem S of a quantum system and calculate the corresponding dynamical map ϕ_t. If the largest singular value of $\mathbf{M}(t)$ decays to a non-zero value as $t \to \infty$ some information about the initial state are stored in local observables, thus the asymptotic state is not independent of the initial state of S. If, on the other hand, $s_{\max} \to 0$ as $t \to \infty$ this is an indication that the subsystem under consideration is thermalized by its environment. Note that this is not a full proof of subsystem thermalization, as this only proves two of the four aspects of thermalization, i.e.

subsystem equilibration and *subsystem state independence*. In chapter 4 we demonstrate this approach of classifying the asymptotic behavior for the spin-boson model. In chapter 5 we then use this to investigate the local memory in different dynamical phases of the disordered XXZ-Heisenberg spin model.

3. Theoretical methodology

In order to investigate thermal and non-thermal behavior in quantum systems we consider the time-evolution of different observables. That is, we are interested in the expectation values of observables $\hat{O}$ defined by

$$\langle \hat{O} \rangle (t) = \langle \Psi(t) | \hat{O} | \Psi(t) \rangle \,, \tag{3.1}$$

where $|\Psi(t)\rangle$ is the wave function of the system at time t. The time-evolution of the wave function is prescribed by Schrödinger's equation defined by Eq. (2.1). To study time-dependent expectation values of the form (3.1) we thus need to calculate the time-dependent wave function, i.e. we need to solve the time-dependent Schrödinger equation.

In this chapter, we discuss various approaches which we use to calculate and analyze time-dependent expectation values. In the first section, 5.1, we introduce exact diagonalization (ED), which is based on an expansion of the wave function and the Hamiltonian in a complete basis of the Hilbert space. This method can be used to calculate the wave function at arbitrary times is, however, limited to relatively small system sizes due to the exponential scaling of the dimension of the Hilbert space. In order to simulate the dynamics of larger systems, more efficient representations of the wave function are necessary. In Sec. 5.2, we introduce one particular example of such a representation: the multilayer multiconfiguration time-dependent Hartree (ML-MCTDH) approach. These two methods allow us to cover two different regimes: ED can be used to investigate small systems at arbitrary times, while the ML-MCTDH approach allows us to simulate large systems at short and intermediate times. If one is interested in the expectation value of observables, which only probe a finite subsystem S, it is sufficient to know the reduced state of S. In the last section, 5.3, we discuss some aspects of the time-evolution of the reduced state of a subsystems. First, we present a formal proof that, in the thermodynamic limit, the dynamics of the reduced density matrix of a subsystem S coupled to a particular type of interacting environments can be described by an environment consisting of harmonic oscillators with an effective spectral density. By this, we extend an earlier result of Makri, who proved this for non-interacting environments [101]. Second, we discuss how the reduced system dynamics can be obtained

perturbatively. This approach can be used to derive some analytic results and to develop physical pictures for the numerical data.

3.1 Exact diagonalization

Exact diagonalization (ED) refers to the diagonalization of the Hamiltonian in a complete basis of the underlying Hilbert space. This means, that it can be used to treat finite dimensional systems. Within this approach one calculates the eigenenergies and eigenstates of the many-body Hamiltonian numerically. As discussed in Sec. 2.1 the solution to the time-dependent Schrödinger equation can be expressed in terms of the eigenstates $\{|E_d\rangle\}$ and eigenvalues $\{E_d\}$ of the Hamiltonian $\hat{H}$, i.e. the wave function at time t can be written as

$$|\Psi(t)\rangle = \sum_d \mathrm{e}^{-iE_d t} \langle E_d|\Psi(0)\rangle |E_d\rangle . \tag{3.2}$$

This means, that once the eigenvalues and eigenstates are known, the time-dependent wave function $|\Psi(t)\rangle$, and thereby any observable, can be calculated at arbitrary time. Since the only assumption is the Hermiticity of the Hamiltonian $\hat{H}$, this approach gives exact results for all parameter regimes at all times. To calculate the eigenvalues and eigenstates of the Hamiltonian, the operator $\hat{H}$ is expanded in a complete basis of the Hilbert space, i.e. is expressed as a matrix, which can be diagonalized numerically.

Exact diagonalization is an exact method which can be used to calculate the time-dependent wave function of the system. The numerical effort, however, increases exponentially with the system size as the dimension of the Hilbert space scales exponentially with the number of constituents of the system. Since the numerical diagonalization of a matrix scales with $\mathcal{O}(D^3)$, where D is the dimension of the matrix, this approach is limited to relatively small systems. On a usual computer, for example, only systems consisting of up to 16 to 18 two-level systems (spins) can be simulated.

3.2 Multilayer multiconfiguration time-dependent Hartree approach

The obvious limitation of ED is that only small systems can be simulated. The reason for this is that in the ED framework the wave function and the Hamiltonian are represented in a complete basis of the Hilbert space of the total system. This implies that the number of parameters of the wave function scale exponentially with the number of degrees of freedom. To demonstrate this the wave function can be expanded in the time-independent tensor product basis of the individual constituents yielding

$$|\Psi(t)\rangle = \sum_{j_1,\ldots,j_N} C_{j_1,\ldots,j_N}(t) \bigotimes_{n=1}^{N} |j_n\rangle , \tag{3.3}$$

where we assumed that the system consists of N degrees of freedom, labeled by n. The $\{|j_n\rangle\}_{i=1}^{f_n}$ constitute a basis for the Hilbert space of the n-th degree of freedom and f_n denotes the corresponding dimension. In this representation the wave function is determined by the N-dimensional tensor $C_{j_1,\ldots,j_N}(t)$, and is thus parametrized by $\prod_{n=1}^{N} f_n$ complex numbers. The number of parameters which are necessary to describe the wave function grows exponentially with the system size.

In many situations, however, a much smaller number of parameters is sufficient to accurately describe the wave function or specific observables. This is in particular true for systems exhibiting many-body localization for the following reason. Eigenstates of MBL systems obey the so-called area law for the entanglement entropy, i.e. the entanglement entropy of a region in space tends to scale as the size of the boundary of the region. Such states, however, only constitute a small subspace of the full Hilbert space. This follows from the following statement proven by Page [102]: a randomly picked state of a Hilbert space will most likely have an entanglement entropy between subregions that will scale like the volume of the subregion. Thus, eigenstates of MBL systems are strongly restricted to a small region of the Hilbert space, which can be parametrized by fewer parameters. A particular representation of the wave function which makes use of this observation is the representation in terms of a matrix product states (MPS) or, more generally, tensor networks [103]. Within these approaches the number of coefficients needed to accurately describe the wave function typically scales with the entanglement between the different degrees of freedom, i.e. the smaller the entanglement the fewer coefficients are needed. Using such representations, the ground state and the time-evolution of systems inaccessible for ED have been investigated [104, 105]. The representation of the wave function as a MPS turned out to be particularly efficient for one dimensional systems [106, 107].

In this thesis, however, we are interested in systems which are not necessarily one dimensional: The star-like geometry of the spin-boson model and the centrally coupled many-body localized system make the simulation based on matrix-product operator techniques like time-evolving block decimation inefficient [107]. To simulate the dynamics of these systems, we employ the multiconfiguration time-dependent Hartree (MCTDH) approach and its multilayer extension (ML-MCTDH) to simulate the dynamics of quantum systems. The ML-MCTDH [108–111] is a well-established, accurate (numerically exact) method to simulate the dynamics of quantum systems with many degrees of freedom. It represents a rigorous variational basis-set method, which uses a multiconfiguration expansion of the wave function, employing time-dependent basis functions and a hierarchical multilayer representation. In previous publications the ML-MCTDH was used to simulate the dynamics of different systems with a star-like geometry like the spin-boson model [32, 34, 36], a single spin coupled to a bath of spins [35], and a subsystem coupled to anharmonic environments [33]. For a

a)

$$|\Psi(t)\rangle = \sum_{\mathbf{J}} A_{\mathbf{J}}(t) \prod_{q=1}^{Q} |\phi^{q}_{j_q}(t)\rangle \,, \tag{3.4a}$$

$$|\phi^{q}_{j}(t)\rangle = \sum_{\mathbf{I}} B^{q,j}_{\mathbf{I}}(t) \prod_{r=1}^{R(q)} |\nu^{(q,r)}_{i_r}(t)\rangle \,, \tag{3.4b}$$

...

b)

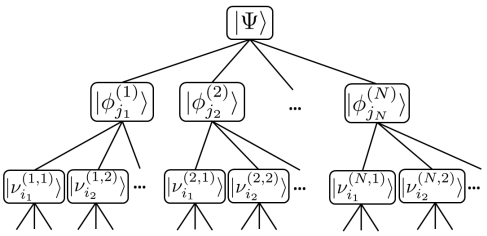

Figure 3.1: Expansion of the wave function used in the ML-MCTDH framework. In the left panel the formal expansion of the wave function $|\Psi(t)\rangle$ and the single particle functions of the first layer is shown. In the right panel the expansion as a tensor tree network is shown.

comprehensive overview of the method we refer to the reviews [108, 110, 111].

Within the ML-MCTDH approach the time-dependent wave function is recursively expanded as depicted in Fig. 3.1a). Here, $A_{\mathbf{J}}(t)$, $B^{q,j}_{\mathbf{I}}(t)$, and so on are the expansion coefficients for the first, second, etc., layers, respectively; $|\phi^{q}_{j_q}(t)\rangle$, $|\nu^{(q,r)}_{i_r}(t)\rangle$, etc., are the single particle functions (SPFs) for the first, second, etc. layers. In Eq. (3.4), Q denotes the number of single particle (SP) groups in the first layer and $R(q)$ denote the number of level two (L2) SP groups in the q-th level one (L1) SP group. Such a recursive expansion can be carried out to an arbitrary number of layers. Finally, the multilayer hierarchy is terminated at a particular level by expanding the SPFs in the deepest layer in terms of time-independent basis functions/configurations, each of which may contain several physical degrees of freedom. The recursive expansion of the wave function $|\Psi(t)\rangle$ over many layers in the ML-MCTDH framework is a representation which corresponds to a hierarchical tensor decomposition in the form of a tensor tree network, shown in Fig. 3.1b).

Following the Dirac-Frenkel variational principle [112], the equations of motion are obtained from a variation of the wave function $|\Psi(t)\rangle$ with respect to the expansion coefficients of each layer [108, 111], resulting in

$$i\frac{\partial}{\partial t} |\Psi(t)\rangle_{\text{L1 coefficients}} = \hat{H}(t) \, |\Psi(t)\rangle \,, \tag{3.5a}$$

$$i\frac{\partial}{\partial t} |\underline{\phi}^{(q)}(t)\rangle_{\text{L2 coefficients}} = \left[\mathbb{1} - \hat{P}^{(q)}\right] \left[\hat{\rho}^{(q)}(t)\right]^{-1} \langle \hat{H} \rangle^{(q)}(t) \, |\underline{\phi}^{(q)}(t)\rangle \,, \tag{3.5b}$$

$$i\frac{\partial}{\partial t} |\underline{\nu}^{(q,r)}(t)\rangle_{\text{L3 coefficients}} = \left[\mathbb{1} - \hat{P}^{(q,r)}_{\text{L2}}\right] \left[\hat{\varrho}^{(q,r)}_{\text{L2}}(t)\right]^{-1} \langle \hat{H} \rangle^{(q,r)}_{\text{L2}}(t) \, |\underline{\nu}^{(q,r)}(t)\rangle \,, \tag{3.5c}$$

...

where, the SPFs for each group are summarized in a symbolic vector as $|\underline{\phi}^{(n)}(t)\rangle = \{|\phi_1^{(n)}(t)\rangle, |\phi_2^{(n)}(t)\rangle, ...\}^T$ and analogously for the other SP groups. The time derivatives on the left hand side are only performed with respect to the expansion coefficients of a particular layer (denoted by the respective subscript). $\hat{H}(t)$ represents the Hamiltonian matrix in terms of the first layer configurations, i.e.,

$$\left(\hat{H}(t)\right)_{\mathbf{JL}} = \left(\prod_{n=1}^{N} \langle \phi_{j_n}^n(t)|\right) \hat{H} \left(\prod_{n=1}^{N} |\phi_{l_n}^n(t)\rangle\right). \tag{3.6}$$

In Eq. (3.5), $\hat{\rho}^{(q)}(t)$ and $\hat{\varrho}_{\mathrm{L2}}^{(q,r)}(t)$ are reduced density matrices for the first and second layers, respectively. The object $\langle \hat{H} \rangle^{(q)}(t)$ and $\langle \hat{H} \rangle_{\mathrm{L2}}^{(q,r)}(t)$ are mean-field operators for the first and second layer, respectively, and the $\hat{P}^{(q)}$ and $\hat{P}_{\mathrm{L2}}^{(q,r)}$ are SP-space projection operators for different layers. For the precise definition of these quantities we refer to Ref. [111].

To demonstrate the concept of the ML-MCTDH aproach and show its limitations, we discuss two limiting cases of the above described expansion of the wave function. To simplify the discussion we assume that each SP group contains one physical degree of freedom. We emphasize, however, that this is not necessary. If only one SPF for every degree of freedom is used, this results in a representation of the wave function as a single Hartree product of the form

$$|\Psi(t)\rangle = A(t) \prod_{q=1}^{Q} |\phi_{j_q}^q(t)\rangle . \tag{3.7}$$

This form of the wave function describes a state in which no entanglement between different degrees of freedom is present. It accurately describe the dynamics of a system consisting of non-interacting degrees of freedom. An interaction between different degrees of freedom typically lead to entanglement between the respective degrees of freedom which cannot be described with a single Hartree product of the form (3.7). The representation of the wave function in terms of a single Hartree product is insufficient. If, on the other hand, the number of SPFs for each degree of freedom is equal to the dimension of the underlying Hilbert space, the set of SPFs constitute a basis for this Hilbert space. Consequently, the projection operator on the SP-space $\hat{P}^{(n)} = \mathbb{1}$ and set of differential equations (3.5) reduces to the usual Schrödinger equation. Upon increasing the number of SPFs, the solution to Eqs. (3.5) converges to the solution of the Schrödinger equation.

The number of SPFs for each degree of freedom describes how much entanglement between this particular degree of freedom and the remainder can be accurately described by the ML-MCTDH wave function. If the system is many-body localized, i.e. the entanglement entropy of the state obeys an area law and is thus small, the ML-MCTDH approach allows for an accurate description of the dynamics using only a few SPFs for degree of freedom. In

such situations the ML-MCTDH approach allows for the simulation of much larger systems compared to ED. If, on the other hand, the system thermalizes, i.e. entanglement is an extensive quantity, many SPFs are needed to represent the wave function accurately and the benefits from using the ML-MCTDH approach compared to ED is expected to be small.

3.3 Time-evolution of the reduced density matrix

The two above introduced methods, exact diagonalization and the multilayer multiconfiguration time-dependent Hartree approach, can be used to calculate the time-dependent wave function of the total system, from which expectation values for any observable can be calculated. In order to study thermal and non-thermal behavior in quantum systems we are often interested in local observables, which only probe a small subsystem S. The expectation value of such observables can be calculated from the reduced state of the subsystem $\hat{\rho}_S$ as

$$\langle \hat{O} \rangle (t) = \mathrm{tr}_S\{\hat{O}\ \hat{\rho}_S(t)\}, \tag{3.8}$$

where $\hat{\rho}_S$ is defined by Eq. (2.15). Instead of calculating the time-evolution of the full system, i.e. the time-dependent wave function $|\Psi(t)\rangle$, one can calculate the time-evolution of the reduced state of the subsystem in the presence of its environment. Following this approach, one can derive an equation of motion for the reduced density matrix $\hat{\rho}_S(t)$ which includes the influence of the environment. Examples are given by the Nakajima-Zwanzig equation [113–115], the time-convolutionless master equation [116, 117], or the hierarchical equations of motion [118–121]. Alternatively, one can derive a path integral representation of the reduced density matrix, in which the influence of the environment is included in the influence functional [101, 122]. In this section we discuss different aspects of the time-evolution of the reduced density matrix which we use in our analysis.

If the environment consists of infinitely many non-interacting modes it is known that the influence of the environment on the subsystem S is completely determined by the first non-vanishing correlation function of the environment, provided that the coupling of the subsystem S is distributed uniformly over all environmental modes [101]. In the first part of this section, 3.3.1, we show that this still holds for a particular kind of interaction between the environmental degrees of freedom. In Sec. 3.3.2, we discuss a perturbative master equation for the reduced density matrix, which we use later to analyze different aspects from an analytic perspective and to develop physical pictures of the numerically observed results.

3.3.1 Linear response property for interacting environments

When considering the dynamics of the reduced state of the subsystem, the goal is to include the influence of the environment in some way into the equations of motion for the reduced density matrix $\hat{\rho}_S(t)$. Typically, the environment consists of many-degrees of freedom, and thus, the influence of the environment on the subsystem S depends, in general, on all of these degrees of freedom. Surprisingly, the influence of an environment consisting of infinitely many non-interacting modes is completely characterized by the first non-vanishing correlation function provided that the interaction between the subsystem S and the environment is distributed uniformly over all modes [101]. This fact can simplify the treatment of complex environments and was used, for example, to describe the dynamics of a two-level system coupled to a spin bath consisting of independent spins [101, 123] and to a bath of anharmonic vibrational degrees of freedom [33]. If the environmental modes are interacting, on the other hand, the influence of the environment is usually not that simple and correlation functions of all orders are needed to describe the effect of the environment on the subsystem S exactly. In a recent publication, for example, the effect of the interaction in Luttinger liquid leads was investigated by including the next-to-leading order correlation function in the hierarchical equation of motion approach [124]. This is, however, only a perturbative treatment of the effect of interactions in the environment on the subsystem S. In the following we show that for a specific type of interactions between the environmental modes, the influence of the environment on the subsystem S in the thermodynamic limit is still completely determined by the first non-vanishing correlation function. Our prove closely follows the one in Ref. [101], which is based on a cumulant expansion of the influence functional of a path integral representation of the reduced density matrix $\hat{\rho}_S(t)$. In particular, we show that under, certain assumptions about the interaction between the environmental modes, all terms in the cumulant expansion except the leading order term vanish in the thermodynamic limit. It is thus possible to construct an effective harmonic environment, which results in the same leading order term, and thus, in the same reduced system dynamics. By this we extend the result of Makri, who proved this for non-interacting environments [101].

In the following we consider an environment which consists of N degrees of freedom and assume that the Hamiltonian of the environment can be written as

$$\hat{H}_E = \sum_{n=1}^{N} \hat{H}_{E,n} + \sum_{n=1}^{N} \hat{B}_{E,n}\hat{B}_{E,n+1}, \tag{3.9}$$

where $\hat{H}_{E,n}$ and $\hat{B}_{E,n}$ act on the Hilbert space of the n-th environmental mode. We assume that the initial state of the environment, denoted by $\hat{\rho}_E$, factorizes between the different degrees of freedom and is an equilibirium state of the Hamiltonian of the environment, i.e. $[\hat{H}_E, \hat{\rho}_E] = 0$. The interaction between the subsystem S and the environment we consider

is of the form

$$H_{SE} = \hat{V}_S \sum_{n=1}^{N} c_n \hat{F}_n, \tag{3.10}$$

where $\hat{V}_S$ acts on the Hilbert space of the subsystem S and $\hat{F}_n$ acts on the Hilbert space of the n-th environmental mode. We assume that $[\hat{F}_m, \hat{F}_n] = 0$ for all m and n, i.e. the environmental modes are either spins or bosonic modes. To evaluate the different terms in the cumulant expansion, the time-dependent operator

$$\hat{f}(t) = \sum_{n=1}^{N} c_n \underbrace{\mathrm{e}^{i\hat{H}_E t} \hat{F}_n \mathrm{e}^{-i\hat{H}_E t}}_{:=\hat{F}_n(t)} \tag{3.11}$$

is required, which describes the force exerted on the subsystem S due to its interaction with the environment. Furthermore, we assume that

$$[\hat{H}_{E,n}, \hat{B}_{E,n}] = 0 \tag{3.12}$$

for all n. This assumption is crucial for our proof and guarantees that the time-evolved operators $\hat{F}_n(t)$ remain local at all times. This implies that the following holds

$$[\hat{F}_n(t), \hat{F}_m(t')] = 0 \quad \forall t, t' \geq 0 \quad \text{and} \quad \forall |m-n| \geq 2. \tag{3.13}$$

This follows from the fact that the operator

$$\hat{F}_m(t) = \mathrm{e}^{iH_E t} \hat{F}_m \mathrm{e}^{-iH_E t} \tag{3.14}$$

only acts on the Hilbert space of the modes $m-1$, m and $m+1$. This can be proven by using the fact that $[\hat{H}_{E,n}, \hat{B}_{E,n}] = 0$ and the resulting factorization of the operator

$$\mathrm{e}^{iH_E t} = \prod_n \mathrm{e}^{iH_{E,n} t} \mathrm{e}^{iB_{E,n} B_{E,n+1} t}. \tag{3.15}$$

In order to calculate the different terms in the cumulant expansion of the influence functional we need to calculate the k-point correlation functions defined as [101]

$$C^{(k)}(t_1, ..., t_K) = \langle \hat{f}(t_1) ... \hat{f}(t_K) \rangle_0 \,, \tag{3.16}$$

where $\langle ... \rangle_0$ denotes the expectation value with respect to the initial state of the environment.

In the following we assume that the average force exerted on the subsystem is zero, i.e.

$$\mathrm{tr}\{\hat{\rho}_E \hat{F}_n(t)\} = 0 \quad \forall n. \tag{3.17}$$

This holds, for example, if the $\hat{F}_n$ are linear in creation or annihilation operators. This also implies that only expectation values with an even number of $\hat{F}_n(t)$ with the same index n are non-vanishing. From this assumption, Eq. (3.17), it follows that the 1-point correlation function vanishes, i.e.

$$C^{(1)}(t) = 0. \tag{3.18}$$

In the following we show that in this situation the influence of the environment, in the thermodynamic limit, is completely determined by the force-force autocorrelation function

$$C^{(2)}(t_1, t_2) = \langle \hat{f}(t_1)\hat{f}(t_2)\rangle_0 \,. \tag{3.19}$$

We note, however, that if the 1-point correlation function is not equal to zero, i.e. if Eq. (3.17) does not hold, our arguments can be used to show that the influence of the environment is completely determined by the 1-point correlation function. Following the arguments of Makri [101], the higher order cumulants vanish if the higher order correlation functions either vanish or can be expressed in terms of 2-point correlation functions. Using Eq. (3.11) and the condition (3.17), the 2-point correlation function can be written as

$$C^{(2)}(t_1, t_2) = \sum_{m=1}^{N} c_n^2 \mathrm{tr}\{\hat{\rho}_E \hat{F}_m(t_1)\hat{F}_m(t_2)\}. \tag{3.20}$$

In the thermodynamic limit this expression diverges unless the couplings c_n scale as $\sim N^{-1/2}$ [101]. Thus, we consider this scaling of the coupling in the following. To finish the proof, we show that in the thermodynamic limit the k-point correlation functions factorize, i.e. can be expressed in terms of 1-point and 2-point correlation functions plus a correction of the order $\mathcal{O}(N^{-(k/2-1)})$. To demonstrate this we consider the 4-point correlation function defined as

$$C^{(4)}(t_1, t_2, t_3, t_4) = \sum_{m,n,o,p} \langle \hat{F}_m(t_1)\hat{F}_n(t_2)\hat{F}_o(t_3)\hat{F}_p(t_4)\rangle_0 \,. \tag{3.21}$$

We note that our arguments apply to all correlation functions for $k \geq 3$. As explained above there have to be an even number of $\hat{F}_n$ in the expectation value $\langle\cdot\rangle_0$ to be non-vanishing. Thus, two of the four indices have to be equal and the 4-time correlation function can be

decomposed as

$$C^{(4)}(t_1,t_2,t_3,t_4) = \sum_{m,n} c_m^2 c_n^2 \langle \hat{F}_m(t_1)\hat{F}_m(t_2)\hat{F}_n(t_3)\hat{F}_n(t_4)\rangle_0 + \sum_{\substack{m,n \\ m\neq n}} c_m^2 c_n^2 \langle \hat{F}_m(t_1)\hat{F}_n(t_2)\hat{F}_m(t_3)\hat{F}_n(t_4)\rangle_0 + \sum_{\substack{m,n \\ m\neq n}} c_m^2 c_n^2 \langle \hat{F}_m(t_1)\hat{F}_n(t_2)\hat{F}_n(t_3)\hat{F}_m(t_4)\rangle_0 . \tag{3.22}$$

To keep the equations simple, we only show how the first term on the right hand side can be written in terms of 2-point correlation functions plus a correction which vanishes like N^{-1} as $N \to \infty$. The double sum appearing in Eq. (3.22) can be decomposed as

$$\begin{aligned}\sum_{m,n} c_m^2 c_n^2 \langle \hat{F}_m(t_1)\hat{F}_m(t_2)\hat{F}_n(t_3)\hat{F}_n(t_4)\rangle_0 &= \sum_m c_m^4 \langle \hat{F}_m(t_1)\hat{F}_m(t_2)\hat{F}_m(t_3)\hat{F}_m(t_4)\rangle_0 \\ &+ \sum_m c_m^2 c_{m+1}^2 \langle \hat{F}_m(t_1)\hat{F}_m(t_2)\hat{F}_{m+1}(t_3)\hat{F}_{m+1}(t_4)\rangle_0 \\ &+ \sum_m c_m^2 c_{m+1}^2 \langle \hat{F}_{m+1}(t_1)\hat{F}_{m+1}(t_2)\hat{F}_m(t_3)\hat{F}_m(t_4)\rangle_0 \\ &+ \sum_{\substack{m,n \\ |m-n|\geq 2}}^{L} c_m^2 c_n^2 \langle \hat{F}_m(t_1)\hat{F}_m(t_2)\hat{F}_n(t_3)\hat{F}_n(t_4)\rangle_0 .\end{aligned} \tag{3.23}$$

For the chosen scaling of the coupling, i.e. $c_n \sim N^{-1/2}$ as $N \to \infty$, the first three terms vanish like N^{-1} as $N \to \infty$ [101]. Thus, we conclude that

$$\sum_{m,n}^{L} c_m^2 c_n^2 \langle \hat{F}_m(t_1)\hat{F}_m(t_2)\hat{F}_n(t_3)\hat{F}_n(t_4)\rangle_0 = \sum_{\substack{m,n \\ |m-n|\geq 2}}^{L} c_m^2 c_n^2 \langle \hat{F}_m(t_1)\hat{F}_m(t_2)\hat{F}_n(t_3)\hat{F}_n(t_4)\rangle_0 + \mathcal{O}\left(\frac{1}{N}\right). \tag{3.24}$$

Because the operators in the expectation value act on different Hilbert spaces, see Eq. (3.13), and the initial state factorizes, it follows that the expectation values can be factorized as

$$\sum_{\substack{m,n \\ |m-n|\geq 2}}^{L} c_m^2 c_n^2 \langle \hat{F}_m(t_1)\hat{F}_m(t_2)\hat{F}_n(t_3)\hat{F}_n(t_4)\rangle_0 = \sum_{\substack{m,n \\ |m-n|\geq 2}}^{L} c_m^2 c_n^2 \langle \hat{F}_m(t_1)\hat{F}_m(t_2)\rangle_0 \langle \hat{F}_n(t_3)\hat{F}_n(t_4)\rangle_0 \tag{3.25}$$

Adding the terms for $m = n$ and $|m - n| = 1$ to the double sum on the right hand side

gives an error of $\mathcal{O}(1/N)$, and thus, we can write

$$\sum_{m,n} c_m^2 c_n^2 \langle \hat{F}_m(t_1)\hat{F}_m(t_2)\hat{F}_n(t_3)\hat{F}_n(t_4)\rangle_0 = \sum_{m,n} c_m^2 c_n^2 \langle \hat{F}_m(t_1)\hat{F}_m(t_2)\rangle_0 \langle \hat{F}_n(t_3)\hat{F}_n(t_4)\rangle_0 + \mathcal{O}\left(\frac{1}{N}\right) \tag{3.26}$$

$$= C^{(2)}(t_1,t_2)C^{(2)}(t_3,t_4) + \mathcal{O}\left(\frac{1}{N}\right), \tag{3.27}$$

where we have identified the 2-time correlation functions. The other two terms in Eq. (3.22) can be treated similarly, resulting in the following expression for the 4-point correlation function for the thermodynamic limit

$$\lim_{N\to\infty} C^{(4)}(t_1,t_2,t_3,t_4) = \lim_{N\to\infty} C^{(2)}(t_1,t_2)C^{(2)}(t_3,t_4) + C^{(2)}(t_1,t_3)C^{(2)}(t_2,t_4) + C^{(2)}(t_1,t_4)C^{(2)}(t_2,t_3). \tag{3.28}$$

Using this one finds that the fourth order term in the cumulant expansion of the influence functional vanishes in the thermodynamic limit [101]. In a similar way one can show that all higher order terms in the expansion vanish, proving that in the thermodynamic limit the influence functional is completely characterized by the force-force autocorrelation function of the environment. This extends the result of Ref. [101] to interacting environments, in which the interaction operators between different environmental modes obey Eq. (3.12). One of the consequences of this is that for such an environment it is possible to construct an effective environment of harmonic oscillators which gives rise to the same dynamics of $\hat{\rho}_S(t)$ as the interacting environment.

3.3.2 Time-convolutionless master equation approach

Although it can be shown that the influence of the environment is completely characterized by the force-force autocorrelation function defined by Eq. (3.19), the exact equations of motion for the reduced density matrix $\hat{\rho}_S(t)$ are usually not solvable. They can, however, be used to derive approximative equations by employing perturbation theory in the coupling between the subsystem S and its environment [39]. These perturbative equations can be used to analyze different aspects from an analytic perspective and can help to develop physical pictures of the numerically observed results.

In this thesis we employ the time-convolutionless master equation up to second order (TCL2). Within this approach the equation of motion for the reduced density matrix of the

subsystem S is determined by the equation [39]

$$\partial_t \hat{\rho}_S(t) = -i[\hat{H}_S, \hat{\rho}_S(t)] - \int_0^t \mathrm{tr}_E\{[\hat{H}_{SE}, [\hat{H}_{SE}(\tau - t), \hat{\rho}_S(t) \otimes \hat{\rho}_E]]\}\mathrm{d}\tau, \tag{3.29}$$

where the time-dependent interaction Hamiltonian $\hat{H}_{SE}(t)$ is defined as

$$\hat{H}_{SE}(t) = \mathrm{e}^{i(\hat{H}_S + \hat{H}_E)t} \hat{H}_{SE} \mathrm{e}^{-i(\hat{H}_S + \hat{H}_E)t}. \tag{3.30}$$

Here, $\hat{H}_S$ ($\hat{H}_E$) describes the Hamiltonian of the subsystem (environment), respectively. $\hat{H}_{SE}$ describes the interaction between the subsystem and the environment. The equations of motion for the reduced density matrix depend on the model system and in particular on the form of the interaction. The model specific equations are presented and discussed in the subsequent chapters, in which we analyze the dynamics of the different model systems.

We close this section with a brief discussion of the parameter regime in which the TCL2 approach is expected to give good results. We note that for the spin-boson model a comparison of various perturbative approaches, including different master equations, with the numerically exact ML-MCTDH method was done in Ref. [32]. Since the TCL2 approach involves a perturbative treatment of the coupling between the subsystem S and its environment, its validity is restricted to the weak coupling regime. Furthermore, it is assumed that the correlations in the environment decay much faster than the system's relaxation rate and the internal dynamics of the subsystem S [39]. For the spin-boson model, for instance, the perturbative master equations capture the reduced spin dynamics less accurate for an adiabatic environment [32]. This also implies that for low temperatures the master equations are less accurate, as a higher temperature typically reduces the correlations.

4. Dynamics of the spin-boson model: A case study of environment-induced effects

A key property of thermalizing quantum systems is that the reduced state of a subsystem is driven towards a thermal equilibrium state by the interaction with its remainder: The remainder acts as an effective environment. The aim of this chapter is to investigate different environment induced effects in a clean set up. To do this, we consider the spin-boson model, which consists of a single spin, the subsystem of interest, and an environment of harmonic oscillators.

In the first part, section 4.1, we introduce the spin-boson model and discuss some details which are relevant for the present work. This includes the specific models of the environment which we consider, the perturbative equations of motion which we use to analyze the dynamics, and the numerical treatment within the ML-MCTDH framework. In section 4.2 we analyze under which situations an environment can drive a system towards an equilibrium state and discuss indications for thermalization. Furthermore, we identify situations in which the environment fails to thermalize the spin. To this end, we investigate the dynamics of the spin using the concepts derived and discussed in 2.5.3. We demonstrate three qualitatively different asymptotic behaviors of the spin and explain how these can be classified based on the measure for the influence of the initial state of an open system on its dynamics. In section 4.3 we investigate a less-well understood effect of an environment: memory effects. Employing a recently proposed measure for non-Markovian behavior based on the information exchange between the open system and its environment, we examine memory effects in a broad range of parameter and employ our numerically exact results to validate perturbative approaches and demonstrate certain limitations.

4.1 The spin-boson model

The spin-boson model, which involves a spin, or more generally a two-level system, interacting linearly with a bath of harmonic oscillators, is a paradigmatic model to describe

dissipative quantum dynamics [125, 126]. Despite its simplicity, the spin-boson model can be used to describe a variety of different processes and phenomena, including electron transfer [127] and macroscopic quantum coherence [128]. On the other hand, the spin-boson model is also interesting from a more fundamental point of view as it shows a transition from coherent dynamics to incoherent decay as well as a quantum phase transition [36, 57, 58] and exhibits qualitatively different asymptotic behaviors. In the context of thermalization, one central question is under which circumstances the harmonic oscillators can equilibrate or even thermalize the spin as $t \to \infty$. Just recently, the equilibration of the spin was observed in an experimental realization of the model using trapped ions: for a sufficiently large environment, i.e. sufficiently many harmonic oscillators, the spin approaches an equilibrium state and stays close to this state for most of the time [129–131].

As mentioned above, the spin-boson model consists of a single spin which is linearly coupled to a bath of harmonic oscillators. In mass-weighted coordinates, the Hamiltonian describing this model reads

$$H = \Delta\hat{\sigma}_x + \frac{1}{2}\sum_{n=1}^{N}(\hat{p}_n^2 + \omega_n^2\hat{q}_n^2) + \hat{\sigma}_z\sum_{n=1}^{N} c_n\hat{q}_n, \tag{4.1}$$

where $\hat{\sigma}_x$ and $\hat{\sigma}_z$ are the Pauli matrices, Δ denotes the coupling between the two spin states, and ω_n, $\hat{q}_n$, and $\hat{p}_n$ represent the frequency, position, and momentum of the bath oscillators, respectively; c_n denotes the coupling strength of the spin to the n-th harmonic oscillator of the bath.

To discuss environment-induced effects in the spin-boson model, we consider the influence of the harmonic oscillators, which constitute the environment, on the dynamics of the spin. For the spin-boson model, it was shown that the influence of the harmonic oscillators on the spin is completely determined by the spectral density of the harmonic oscillators defined as [125, 126]

$$J(\omega) = \frac{\pi}{2}\sum_{n=1}^{N}\frac{c_n^2}{\omega_n}\delta(\omega - \omega_n). \tag{4.2}$$

In order to investigate different environment induced effects, like dissipation and decoherence, unique and non-unique asymptotic states, and non-Markovian effects in the dynamics of the spin, we consider two different models for the environment, i.e. two different spectral densities: the well-known Ohmic spectral density $J_O(\omega)$ and a gapped spectral density $J_G(\omega)$ which is inspired by the experimental realization of the spin-boson model in Ref. [131]. The Ohmic spectral density is defined as [125, 126]

$$J_O = \frac{\pi}{2}\alpha\omega\mathrm{e}^{-\omega/\omega_c}, \tag{4.3}$$

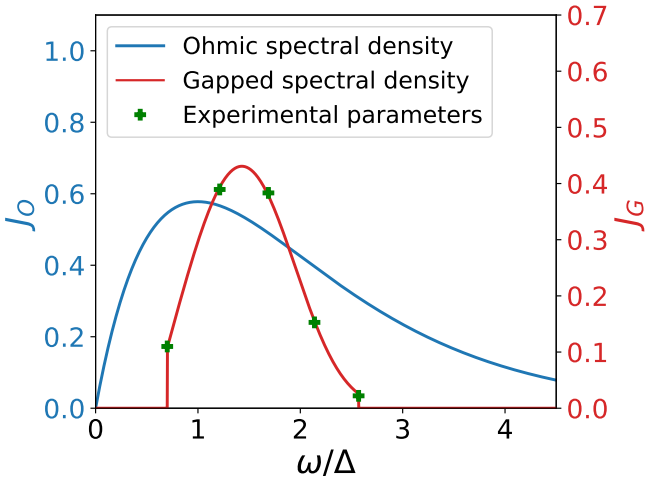

Figure 4.1: The two considered spectral densities for $\alpha = 1$. In blue (left axis) the Ohmic spectral density is shown for $\omega_c = \Delta$. In red (right axis) the gapped spectral density is shown. The green markers denote the experimental parameters. Note that the gapped spectral density is zero below $\omega_{\min}$ and above $\omega_{\max}$

where α denotes the system-bath coupling strength and ω_c the characteristic frequency of the bath. The Ohmic spectral density is arguably one of the most studied models for the environment in the spin-boson model. In particular, it is known that qualitative different dynamics of the spin can be observed, depending on the coupling strength α. For $\alpha \lesssim 0.5$ the spin exhibits a coherent decay, whereas for $0.5 \lesssim \alpha \lesssim 1$ one finds an incoherent decay to a unique asymptotic state [34]. For $1 \lesssim \alpha$ and $T = 0$ the spin localizes in its initial state, i.e. the asymptotic state of the spin depends on the initial state [57, 58, 125, 126, 132]. This model is thus well suited to discuss the measure for the local memory introduced in Sec. 3.2.

The second model for the environment we consider is a gapped spectral density described by the function

$$J_G(\omega) = \frac{\pi}{2}\alpha a(\omega - b)\mathrm{e}^{-(\frac{\omega-b}{c})^3}\chi_{[\omega_{\min},\omega_{\max}]}, \tag{4.4}$$

where a, b, and c are fitting parameters which we determine by a least square fit of the function (4.4) to the parameters of the experimental realization with 5 environmental harmonic oscillators. For the parameters we find $(a, b, c) = (0.677, 0.541, 1.28)$. The distinct feature of the experimental set up is that the lowest frequency of the environmental degrees of freedom is given by the frequency of the ion trap, which is always non-zero [131]. This implies that the corresponding spectral density is zero below some $\omega_{\min} > 0$, leading to a gap in the spectrum of the environment. The support of the spectral density, i.e. $\omega_{\min}$ and $\omega_{\max}$ are determined by experimental parameters, and α denotes the coupling strength. As we will discuss later, the existence of the gap in the spectral density can lead to a failure of *subsystem equilibration* for sufficiently strong coupling α. The qualitative differences of the

two spectral densities are presented in Fig. 4.1 for $\alpha = 1$.

Up to date, no analytic solution for the dynamics of the spin-boson model is known. Our analysis of environment-induced effects is based on two approaches. On the one hand we employ perturbative equations of motion and their analytic solution. This approach allows us to analyze the dynamics in the weak coupling regime, i.e. $\alpha \ll 1$. To simulate the dynamics of the spin-boson model in the full parameter regime, we employ the ML-MCTDH approach introduced in section (3.2), for which it was demonstrated that it can be used to simulate the dynamics in a broad range of coupling strengths [34].

In the weak coupling regime, i.e. $\alpha \ll 1$, the TCL2 method discussed in Sec. 3.3.2 can be used to derive a generalized master equation for the reduced density matrix of the spin [39,125,133]. The state of the spin is completely characterized by the three components of the Bloch vector, i.e. by the three expectation values of $\hat{\sigma}_x$, $\hat{\sigma}_y$, and $\hat{\sigma}_z$. Within the TCL2 approach, the equations of motion for these three expectation values are [32, 39]

$$\partial_t \langle \hat{\sigma}_x \rangle (t) = -\Gamma_{xx}(t) \langle \hat{\sigma}_x \rangle (t) - \Gamma_x(t) \tag{4.5a}$$

$$\partial_t \langle \hat{\sigma}_y \rangle (t) = -2\Delta \langle \hat{\sigma}_z \rangle (t) - \Gamma_{yz}(t) \langle \hat{\sigma}_z \rangle (t) - \Gamma_{yy}(t) \langle \hat{\sigma}_y \rangle (t) \tag{4.5b}$$

$$\partial_t \langle \hat{\sigma}_z \rangle (t) = 2\Delta \langle \hat{\sigma}_y \rangle (t), \tag{4.5c}$$

where the time-dependent rates $\Gamma_{ij}(t)$ are determined by the spectral density $J(\omega)$ and Δ, and are defined in [32]. These equations can be solved numerically to obtain the dynamics of the spin in the weak coupling regime.

To analyze the dynamics of the spin analytically, we consider the stationary rate approximation, i.e. we replace the time dependent rates $\Gamma_{ij}(t)$ with their long time limit, in the following denoted with $\Gamma_{ij} \coloneqq \lim_{t\to\infty} \Gamma_{ij}(t)$. Within this approximation, the three equations (4.5a), (4.5b), and (4.5c) constitute a system of first order autonomous differential equations which can be solved analytically. Their solution read

$$\langle \hat{\sigma}_x \rangle (t) = \mathrm{e}^{-\Gamma_{xx} t} \langle \hat{\sigma}_x \rangle (0) - \frac{\Gamma_x}{\Gamma_{xx}} (1 - \mathrm{e}^{-\Gamma_{xx} t}) \tag{4.6a}$$

$$\begin{aligned} \langle \hat{\sigma}_y \rangle (t) = \mathrm{e}^{-\Gamma_{yy}/2t} \Bigg(& \cos(\tilde{\Delta} t) \langle \hat{\sigma}_y \rangle (0) - \frac{\Gamma_{yy}}{2\tilde{\Delta}} \sin(\tilde{\Delta} t) \langle \hat{\sigma}_y \rangle (0) \\ & - \frac{2\Delta - \Gamma_{yz}}{\tilde{\Delta}} \sin(\tilde{\Delta} t) \langle \hat{\sigma}_z \rangle (0) \Bigg) \end{aligned} \tag{4.6b}$$

$$\begin{aligned} \langle \hat{\sigma}_z \rangle (t) = \mathrm{e}^{-\Gamma_{yy}/2t} \Bigg(& \frac{2\Delta}{\tilde{\Delta}} \sin(\tilde{\Delta} t) \langle \hat{\sigma}_y \rangle (0) + \cos(\tilde{\Delta} t) \langle \hat{\sigma}_z \rangle (0) \\ & + \frac{\Gamma_{yy}}{2\tilde{\Delta}} \sin(\tilde{\Delta} t) \langle \hat{\sigma}_z \rangle (0) \Bigg), \end{aligned} \tag{4.6c}$$

where $\tilde{\Delta}$ denotes the renormalized tunneling frequency of the spin which is given by $\tilde{\Delta} =$

$\frac{1}{2}\Big(8\Delta(2\Delta-\Gamma_{yz})-\Gamma_{yy}^2\Big)^{1/2}$. These equations describe the time-evolution of the three components of the Bloch vector for weak coupling and large ω_c for an arbitrary initial state of the spin. We note that the stationary rate approximation, leads to errors in the transient dynamics, i.e. on the dynamics on short time scales.

The analytic equation for $\langle\hat{\sigma}_z\rangle$ given by Eq. (4.6c) is derived using perturbation theory in the coupling strength α. For an initial state of the spin of the form $(\langle\hat{\sigma}_x\rangle\ \langle\hat{\sigma}_y\rangle\ \langle\hat{\sigma}_z\rangle) = (0\ 0\ 1)$ a renormalized perturbation theory, employing a resummation of all terms linear in the coupling strength of a path integral solution [126], can be used to derive another analytic solution for $\langle\hat{\sigma}_z\rangle(t)$ reading

$$\langle\hat{\sigma}_z\rangle(t) = \mathrm{e}^{-\gamma t}\Big[\cos(\tilde{\Delta}t) + \frac{\gamma}{\tilde{\Delta}}\sin(\tilde{\Delta}t)\Big], \tag{4.7}$$

where the renormalized frequency $\tilde{\Delta}$ and the damping depend on the characteristic bath frequency ω_c and the coupling strength α and are given by

$$\tilde{\Delta} = [\Gamma(1-2\alpha)\cos(\pi\alpha)]^{\frac{1}{2(1-\alpha)}}\Big(\frac{2\Delta}{\omega_c}\Big)^{\frac{\alpha}{1-\alpha}}2\Delta \tag{4.8}$$

$$\gamma = \frac{\pi}{2}\alpha\tilde{\Delta}\mathrm{e}^{-\frac{\tilde{\Delta}}{\omega_c}}. \tag{4.9}$$

We note that the solution for $\langle\hat{\sigma}_z\rangle$ given by Eq. (4.7) has the same functional form as the solution of the TCL2 equation for this particular initial state of the spin. However, the renormalized frequency $\tilde{\Delta}$ and the damping γ differ. To be more precise, the renormalized frequency $\tilde{\Delta}$ in the TCL2 solution and Eq. (4.9) have the same Taylor expansion at $\alpha = 0$, and hence, they coincide for $\alpha \to 0$.

The approaches discussed so far are based on a perturbative treatmenf of the coupling α, and thus, are only valid in the weak coupling regime [32, 34]. In order to investigate the dynamics of the spin-boson model in the full parameter regime, we employ the ML-MCTDH approach introduced in section 3.2, to simulate the dynamics numerically. It was previously demonstrated that the ML-MCTDH approach can be used to simulate the dynamics in a broad range of coupling strengths [34]. In the following we briefly explain how the ML-MCTDH approach can be used to simulate the dynamics of the spin-boson model. The general concept of the method is described in Sec. 3.2. The two spectral densities introduced above describe a condensed phase environment with a formally continuous distribution of bath modes. The ML-MCTDH approach can only be used to propagate the wave function for a system with a finite number of degrees of freedom. For finite timescales, a finite number of bath modes can be used to represent the condensed phase environment, thus making the treatment with the ML-MCTDH approach feasible. To simulate the dynamics of the spin-boson model for the condensed phase we thus simulate the dynamics for an environment

consisting of N harmonic oscillators, and consider N as a convergence parameter. To ensure convergence to the continuum limit over the timescale considered, we employ several hundreds of modes. In the past, different discretization have been used [34, 134]. While the expectation value of $\hat{\sigma}_z$ converges well for different discretization schemes, we find numerically that the expectation values of $\hat{\sigma}_x$ and $\hat{\sigma}_y$ converges faster for an equidistant discretization. In the following we thus use an equidistant discretization. The implementation of the ML-MCTDH theory we use, has up to four dynamical layers plus one static layer.

4.2 Initial state dependence in the dynamics of the spin-boson model

An environment can drive a small system towards thermal equilibrium by inducing decoherence and dissipation. In this section we investigate different aspects of this phenomenon for the spin-boson model. In particular, we discuss under which situations an environment can drive an open system to thermal equilibrium, under which circumstances the environment fails to thermalize the system, and how one can classify this based on the dynamics of the open system. Our analysis is based on the influence of the initial state of the open system on its dynamics. In particular, the influence of the initial state on the asymptotic behavior of the open system as $t \to \infty$ can be used to classify the dynamics into thermal and non-thermal. To investigate this influence, we employ the measure developed in 2.5.3 to investigate the dependency of the initial state of the spin on its dynamics.

An open quantum system can exhibit three qualitatively different asymptotic behaviors as $t \to \infty$. First, the open system can relax to a unique asymptotic state. This is the expected behavior if the open system is thermalized by its environment. Second, the open system can relax to an asymptotic state which depends on the initial state. This represents a violation of *subsystem state independence*. Last, the open system may not relax to an asymptotic state and the reduced state of the subsystem $\hat{\rho}_S(t)$ remains time-dependent at all times. This is a violation of *subsystem equilibration*. A non-unique asymptotic state or a reduced state which remains time-dependent at all times are thus indications for non-thermal behavior. In these situations the environment is not able to thermalize the open system.

Our goal is to discuss the influence of the initial state of the spin on its dynamics for a fixed initial state of the environment. We consider the zero temperature limit of the environment, i.e. the harmonic oscillators are initially all in their ground state. In this limit it is known that for an Ohmic spectral density the spin localizes in its initial state above a critical coupling strengths [36, 57, 58], i.e. the asymptotic state of the spin exhibits a dependence on its initial state. We further assume that the initial state of the spin is pure. Hence, it can be parametrized by the two Bloch angles θ and φ. The corresponding wave function of the spin, as well as graphical representation in terms of the Bloch vector is shown in Fig. 4.2.

a)

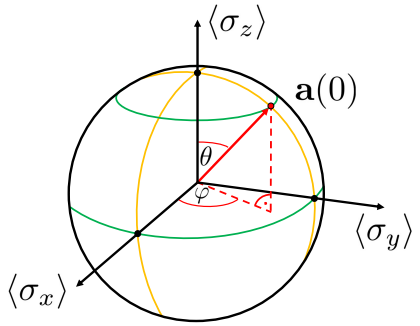

b)

$$|\psi(0)\rangle_{\text{spin}} = \cos\frac{\theta}{2}\,|\uparrow\rangle + \mathrm{e}^{i\varphi}\sin\frac{\theta}{2}\,|\downarrow\rangle \qquad (4.10)$$

Figure 4.2: The initial state of the spin parametrized by the two Bloch angles θ and φ. In the left panel the graphical representation in terms of the three dimensional Bloch vector is shown. The red dot represents the Bloch vector corresponding to the wave function $|\psi(0)\rangle_{\text{spin}}$. In the right panel the corresponding wave function is shown.

To analyze the asymptotic behavior of the spin we consider properties of the dynamical map. More precisely, we consider the action of the dynamical map on the Bloch vector representation of the reduced state of the spin, i.e. we consider the two quantities $\mathbf{M}(t)$ and $\mathbf{b}(t)$. As discussed in Sec. 2.5.3, the matrix $\mathbf{M}(t)$ can be used to investigate the influence of the initial of the open system on its dynamics and on the asymptotic behavior. To obtain the dynamical map we simulate the dynamics of the spin-boson model for four different initial states of the spin using the ML-MCTDH approach. Using the time-dependent Bloch vectors for the different initial states of the spin, Eq. (2.11) can be inverted to obtain $\Phi_{t;ij,kl}(t)$. Using $\Phi_{t;ij,kl}(t)$, and Eq. (2.14), $\mathbf{M}(t)$ and $\mathbf{b}(t)$ can be calculated numerically.

The remainder of this section is organized according to the three possible asymptotic behaviors of an open system. In the first part, 4.2.1, we discuss the relaxation to a unique asymptotic state. We find this behavior in the weak coupling regime for the Ohmic and gapped spectral density. In part two, 4.2.2, and three, 4.2.3, we extend our investigations to the strong coupling regime for the Ohmic spectral density and the gapped spectral density, respectively. In this regime the dynamics of the spin differs significantly between the two spectral densities. For the Ohmic spectral density we find a violation of *subsystem state independence*, whereas for the gapped spectral density we find a failure of *subsystem equilibration*.

4.2.1 Thermalization: Relaxation to a unique stationary state

The first situation we discuss is the relaxation of the spin to a unique stationary state. We find this behavior in the weak coupling regime for both spectral densities. As discussed in section 2.5.3, the singular values of the matrix $\mathbf{M}(t)$ can be used to discuss the influence of the initial state of the spin on its dynamics. In the following, we denote the singular values of $\mathbf{M}(t)$ with $s_i(t)$ and sort them in descending order, i.e. $s_1(t) \geq s_2(t) \geq s_3(t)$. In Fig. 4.3

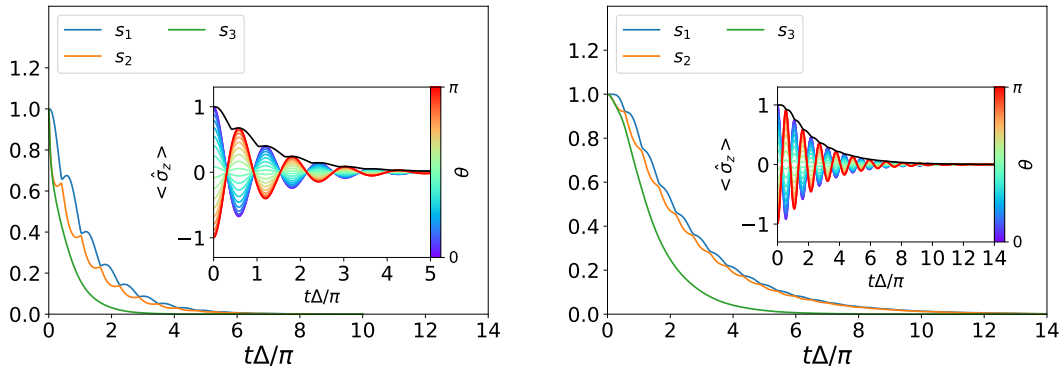

Figure 4.3: The three singular values of $\mathbf{M}(t)$ as a function of time for $\alpha = 0.1$. In the left plot the results for the Ohmic spectral density for $\omega_c = 20\Delta$ is shown, in the right plot for the gapped spectral density. In both plots the inset shows $\langle \hat{\sigma}_z \rangle$ for different initial states of the spin for $\varphi = 0$ and varying θ. The black line in the inset shows $s_{max}(t)$.

the singular values of $\mathbf{M}(t)$ are shown for the Ohmic and the gapped spectral density for $\alpha = 0.1$, together with the expectation value of $\hat{\sigma}_z$ for different initial states of the spin.

We first note that for vanishing coupling α the expectation value of $\hat{\sigma}_z$ oscillates with a frequency given by Δ. The qualitative effect of the environment is very similar for the two spectral densities. The coupling to the environment induces a damping of the oscillations and leads to a renormalization of the frequency, i.e. the frequency of the spin is decreased. As shown in Fig. 4.3, the expectation value of $\hat{\sigma}_z$ decays to zero for different initial states of the spin. This is an indication that the asymptotic state of the spin is in fact independent of its initial state. It is, however, no general proof of *subsystem state independence* as this only shows that the expectation value of $\hat{\sigma}_z$ approaches the same asymptotic value for a subset of all possible initial states of the spin.

Employing the measure for the influence of the initial state developed in section 2.5.3 we can analyze the asymptotic behavior without referring to the dynamics for a particular initial state. It directly follows from Eq. (2.14) that $\mathbf{M}(0) = \mathbb{1}$. Consequently, all three singular values are initially one. As can be seen in Fig. 4.3, the three singular values decay to zero for both spectral densities, reflecting the vanishing influence of the initial state on the state of the open system at a later time. The first two singular values exhibit periodic modulations. We find that $s_1(t) > s_2(t)$ for all times, i.e. the two singular values never cross. The third singular value decays monotonically. Furthermore, the largest singular value, denoted by the black lines in the insets, provides an upper bound for the influence of the initial state on expectation values at time t. Note that according to Eq. (2.29) the quantity $\delta_{1,2}(t; \hat{\sigma}_z)$ is bounded by $4s_{\max}(t)$, while we find $\delta_{1,2}(t; \hat{\sigma}_z) \leq 2s_{\max}(t)$. This is related to the fact that in the derivation of Eq. (2.29) no property of the observable $\hat{O}$ was used. For $\hat{O} = \hat{\sigma}_z$ one can employ that the expectation value of $\hat{\sigma}_x$ and $\hat{\sigma}_y$ vanishes in both eigenstate of $\hat{\sigma}_z$. Using

this, one can show that $\delta_{1,2}(t;\hat{\sigma}_z)$ is bounded by $2s_{\max}(t)$.

For the Ohmic spectral density, one can use the weak coupling solution of the expectation values of $\hat{\sigma}_x$, $\hat{\sigma}_y$, and $\hat{\sigma}_z$, given by Eqs. (4.6a), (4.6b), and (4.6c), to relate the time-dependent expectation values of the spin with the singular values of $\mathbf{M}(t)$. We emphasize again that the analytic solution is only valid for small α and large ω_c [32, 125, 126]. The derivation of the weak coupling solution of $\mathbf{M}(t)$ and $\mathbf{b}(t)$ are provided in Appendix A.2. The analytic solution reveals that the periodically modulated singular values $s_1(t)$ and $s_2(t)$ are related to the coherent decay of $\langle\hat{\sigma}_y\rangle$ and $\langle\hat{\sigma}_z\rangle$. The two singular values are exponentially damped, with the same damping as $\langle\hat{\sigma}_y\rangle$ and $\langle\hat{\sigma}_z\rangle$. The frequency of the periodic modulations of $s_1(t)$ and $s_2(t)$ is given by $2\tilde{\Delta}$, where $\tilde{\Delta}$ denotes the renormalized frequency of the spin. The monotonically decaying singular value $s_3(t)$ describes the monotonic decay of $\langle\hat{\sigma}_x\rangle(t)$. Both, the singular value $s_3(t)$ and $\langle\hat{\sigma}_x\rangle$, decay exponentially with the same decay rate.

We conclude that in the weak coupling regime the harmonic environment drives the spin towards a unique asymptotic state for both spectral densities considered here.

4.2.2 Local memory of the initial condition: Relaxation to a non-unique asymptotic state

Next, we consider the dynamics of the spin for the Ohmic spectral density in the strong coupling regime and discuss how a non-unique asymptotic state can be detected by employing properties of the dynamical map characterized by $\mathbf{M}(t)$ and $\mathbf{b}(t)$.

For the Ohmic spectral density the spin localizes in its initial state above a critical coupling strength α_c [34, 36, 57, 58, 125]. For sufficiently strong coupling α the asymptotic state of the spin depends on its initial state, i.e. some information about the initial state of the spin is stored in local observables. Thus, we expect that for $\alpha < 1$ the spin relaxes to a unique asymptotic state, whereas for $1 < \alpha$ the asymptotic state depends on the initial state, i.e. we expect a violation of *subsystem state independence* for $1 < \alpha$. We note that for finite ω_c/Δ both critical couplings shift to larger values [32, 34, 36, 135]. In Fig. 4.4, the first and second singular value of $\mathbf{M}(t)$ are shown for $\omega_c = 20$ for different values of the coupling strength α. The third singular value shows a very similar behavior as the second one and is thus not shown. In addition, the expectation value of $\hat{\sigma}_z$ for different initial states of the spin is shown for $\alpha = 1.2$.

At $t = 0$ the dynamical map is the identity and, thus, all three singular values are initially one. In contrast to the weak coupling regime, all three singular values decay monotonically to zero for $0.5 < \alpha < 1$. They show, however, an opposite trend upon increasing the coupling strength. The time scale associated with the decay of $s_2(t)$ and $s_3(t)$ becomes shorter upon increasing the coupling strength. The decay of $s_1(t)$ slows down and eventually approaches

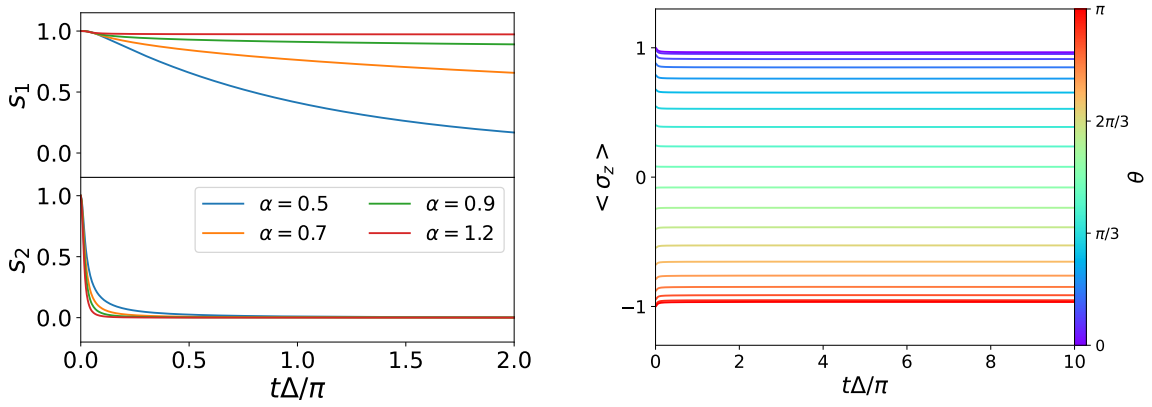

Figure 4.4: In the left panel the first and second singular value of $\mathbf{M}(t)$ as a function of time for different values of α are shown. In the right panel the expectation value of $\hat{\sigma}_z$ as a function of time for different initial states parametrized by θ is shown. In this plot $\omega_c = 20\Delta$, $\alpha = 1.2$, and $\varphi = 0$. The results show that the asymptotic state of the spin depends on the initial state of the spin.

a non-zero value as $t \to \infty$ for $1 \lesssim \alpha$, indicating a non-vanishing influence of the initial state on the asymptotic state of the spin. This behavior of $\mathbf{M}(t)$ implies that for $1 \lesssim \alpha$ the spin relaxes to an asymptotic state which depends on the initial state. This violation of *subsystem state independence* manifests itself in a dependence of expectation values on the initial state of the spin at all times. We demonstrate this for $\langle \hat{\sigma}_z \rangle$ in the right panel of Fig. 4.4 for $\alpha = 1.2$. For all initial states of the spin, the expectation value becomes stationary as $t \to \infty$. However, the asymptotic value of $\langle \hat{\sigma}_z \rangle$ depends on the initial state of the spin. The fact that only one singular value of $\mathbf{M}(t)$ approaches a non-zero value means that the image of $\mathbf{M}_\infty = \lim_{t\to\infty} \mathbf{M}(t)$ is one dimensional. This implies that some initial states are mapped to the same asymptotic state.

To classify those initial states which are mapped to the same asymptotic state, we use the singular value decomposition of $\mathbf{M}_\infty$, given by $\mathbf{M}_\infty = \mathbf{V}_\infty \mathbf{S}_\infty \mathbf{W}_\infty^T$. In the following we assume that only one singular value of $\mathbf{M}(t)$ is non vanishing as $t \to \infty$, as it is the case for the localization of the spin discussed above. In this case, the limit of the dynamical map as $t \to \infty$ (see Eq. (2.14)) can be written as

$$\mathbf{a}_\infty = s_{\infty,1} \langle \mathbf{w}_{\infty,1}, \mathbf{a}(0) \rangle \mathbf{v}_{\infty,1} + \mathbf{b}_\infty, \tag{4.11}$$

where $\mathbf{v}_{\infty,1}$ ($\mathbf{w}_{\infty,1}$) are the vectors formed by the first column of the matrix $\mathbf{V}_\infty$ ($\mathbf{W}_\infty$), respectively, and $\langle \mathbf{x}, \mathbf{y} \rangle = \sum x_i, y_i$ is the standard scalar product between the real vectors $\mathbf{x}$ and $\mathbf{y}$. From this equation it follows that all initial states, for which the scalar product $\langle \mathbf{w}_{\infty,1}, \mathbf{a}(0) \rangle$ is equal, are mapped to the same asymptotic state. That means that all initial

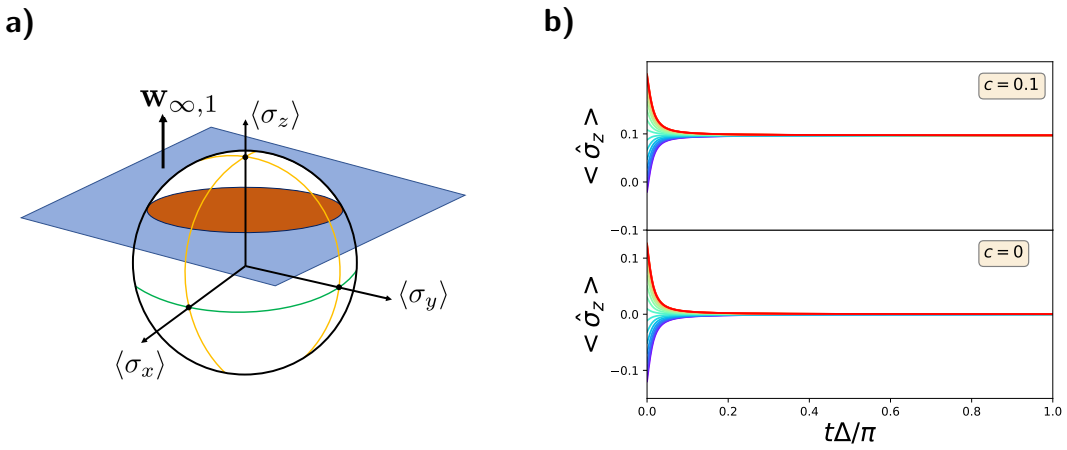

Figure 4.5: In the left panel the set of initial states, which lead to the same asymptotic state is indicated. The plane which is defined by the vector $\mathbf{w}_{\infty,1}$ is represented by the light blue area. The intersection of this plane with the Bloch sphere is represented by the orange area. In the right panel the expectation value of $\hat{\sigma}_z$ for different initial states in this set is shown.

states contained in the set

$$\mathcal{P}_c = \{\mathbf{a}(0) \in B(\mathbb{R}^3) | \langle \mathbf{w}_{\infty,1}, \mathbf{a} \rangle = c\} \tag{4.12}$$

are mapped to the same asymptotic state. This set is the intersection between a plane and the Bloch sphere. The constant c parametrizes a family of planes which are all parallel to each other. One example for a set $\mathcal{P}_c$ is shown in Fig. 4.5a). Note that the asymptotic state of the spin depends on the constant c, i.e. for different sets $\mathcal{P}_c$ the asymptotic state is different. For the parameters considered in Fig. 4.4 we find $\mathbf{w}_{\infty,1} \approx (0 \quad 0.13 \quad 0.99)$. The planes, defined by $\mathbf{w}_{\infty,1}$ are thus tilted compared to the XY-plane. For the angle between the planes defined by $\mathbf{w}_{\infty,1}$ and the XY-plane we find $\approx 7.25°$. In Fig. 4.5b) we show the expectation value of $\hat{\sigma}_z$ for different initial states to demonstrate our findings. In the upper plot the different initial states of the spin are all in $\mathcal{P}_{0.1}$, whereas in the lower plot they are in $\mathcal{P}_0$. As one can see, the asymptotic value of $\langle\hat{\sigma}_z\rangle$ is equal for all initial states in one $\mathcal{P}_c$ but differs for different c.

The localization of the spin can be explained in terms of a renormalized system frequency $\tilde{\Delta}$. This approach, first used by Silbey and Harris [136, 137], employs a variational Polaron transformation to map the Hamiltonian of the spin-boson model to $\tilde{H} = \tilde{\Delta}\sigma_x + H_{\text{env}} + \tilde{H}_I$, where $\tilde{\Delta}$ describes a renormalized frequency and $\tilde{H}_I$ describes a modified interaction between the spin and the environment. Note that H_{env} describes the harmonic oscillators and is not changed by the transformation. Minimizing the Bogoliubov-Peierls upper bound with respect to the variational parameters of the transformation yields an implicit equation for

the renormalized system frequency $\tilde{\Delta}$ [138, 139]. In their two papers Silbey and Harris demonstrated that the renormalized system frequency captures the qualitative dynamics of the spin and yields good results even in low order perturbation theory. For an Ohmic spectral density the resulting renormalized spin frequency $\tilde{\Delta}$ as a function of the coupling strength α is shown in Fig. 4.6. The renormalized system frequency decreases monotonically for increasing coupling strength α. Above a critical coupling α_c it vanishes thus explaining the localization of the spin in its initial state.

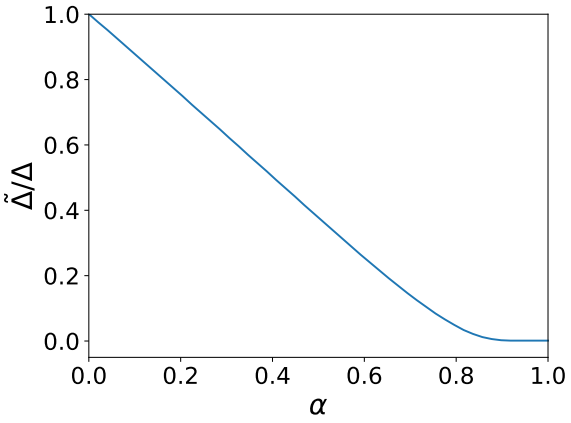

Figure 4.6: Renormalized system frequency $\tilde{\Delta}$ for $\omega_c = 20\Delta$ obtained from the variational calculation described in Refs. [136, 137].

We conclude that for the spin-boson model with an Ohmic spectral density the spin always approaches a time-independent asymptotic state. For coupling strengths $\alpha \lesssim 1$ the asymptotic state is unique, i.e. we find indications of thermalization of the spin. For couplings $1 \lesssim \alpha$ and $T = 0$, the spin localizes and the initial state of the spin influences the asymptotic state. Thus, the spin equilibrates but we find a failure of *subsystem state independence*.

4.2.3 Failure of subsystem equilibration

The third and last possible asymptotic behavior of an open system is that the reduced state remains time-dependent at all times, i.e. the the open system does not relax to an asymptotic state. This represents a violation of *subsystem equilibration*. As we demonstrate in the following, this type of behavior can be found for the gapped spectral density for sufficiently strong coupling α.

In Fig. 4.7a) the three singular values of $\mathbf{M}(t)$ are shown for the gapped spectral density for strong coupling $\alpha = 1.2$. All three singular values exhibit a fast initial decay. After the initial decay, the smallest singular value decays further and remains close to zero, while the other two singular values of $\mathbf{M}(t)$ exhibit undamped oscillations. Since the limit $\lim_{t\to\infty} \mathbf{M}(t)$ does not exist, there exists at least one initial state for which the asymptotic state does not

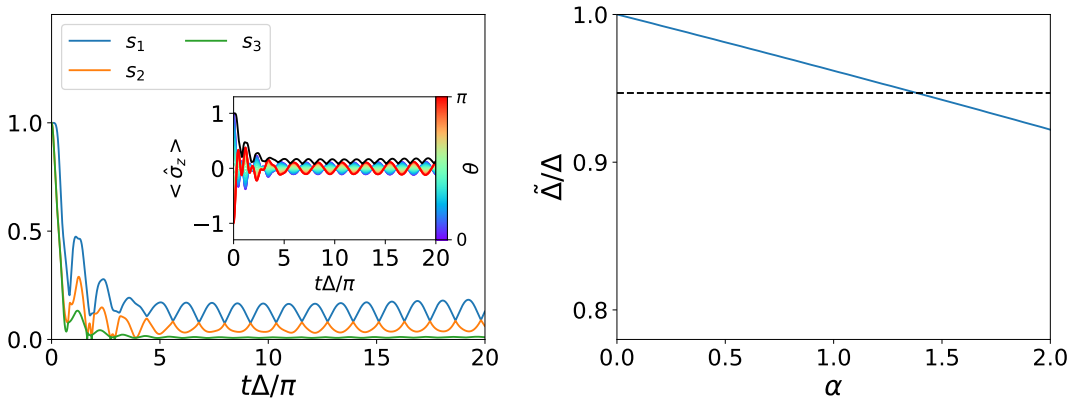

Figure 4.7: in the left panel the three singular values of $M(t)$ as a function of time for $\alpha = 1.2$ are shown. The inset shows the expectation value of σ_z for different initial states of the open system, where $\varphi = 0$. The black line in the inset shows the largest singular value of $M(t)$. In the right panel the renormalized spin coupling $\tilde{\Delta}$ as a function of the coupling strength for the gapped spectral density is shown. The dashed line represent the smallest bath frequency.

exist, and the state of the spin remains time-dependent at all times. For longer times, i.e. $t\Delta/2\pi > 5$ the period of the oscillations of the singular values have twice the frequency of the spin, similar to our findings for the weak coupling regime discussed in Sec. 4.2.1. We note that for small times, i.e. $t\Delta/2\pi < 5$, the singular values cross, whereas for larger times the singular values do not cross.

The failure of subsystem relaxation and the influence of the initial state on the dynamics can be seen in the expectation value of $\hat{\sigma}_z$ shown in the inset of Fig. 4.7. At short times the expectation value exhibits a complex behavior. Here, we will not discuss the transient dynamics. Instead we focus on the long-time dynamics of the spin. For $t\Delta/2\pi > 5$ the expectation value of $\hat{\sigma}_z$ exhibits undamped oscillations demonstrating the failure of *subsystem equilibration*. The initial state has an influence on the dynamics at all times. Nevertheless, the largest singular value, denoted by the black line in the inset of Fig. 4.7, provides an upper bound for the influence of the initial state at all times t.

Qualitatively, this behavior can be explained in a similar way as the localization in the strong coupling regime of the Ohmic spectral density, i.e. in terms of a variational polaron transformation and a renormalized spin frequency introduced by Silbey and Harris. In Fig. 4.7b) the renormalized spin frequency $\tilde{\Delta}$ is shown as a function of the coupling strength. The renormalized system frequency is a monotonically decreasing function. For sufficiently strong coupling α, the renormalized spin frequency $\tilde{\Delta}$ is smaller than the smallest bath frequency. For the transformed Hamiltonian, the influence of the environment can be understood in perturbation theory [136, 137]. Thus, we conclude that for sufficiently strong coupling the environment fails to equilibrate the spin since there is no spectral weight at the renormalized spin tunneling. For $\alpha = 1.2$ the renormalized system frequency is close

to the smallest bath frequency. For this situation we find that the environment cause a partial decoherence of the spin, as $\langle\hat{\sigma}\rangle_z$ is damped at short times. However, the environment cannot equilibrate the spin completely and the state of the spin remains time-dependent.

4.3 Non-Markovian effects in the spin-boson model at zero temperature

Dissipation and decoherence are arguably the best-known effects of an environment. As discussed in the previous section, they can induce relaxation of the open system's state to an equilibrium state. Besides these well-understood effects, the environment can also act as a memory for the open system leading to non-Markovian dynamics in the time evolution of the open system. In this section we investigate memory effects and non-Markovian behavior in the dynamics of the spin-boson model with an Ohmic spectral density. We will follow the lines of our publication [140],

Non-Markovian effects in the spin-boson model at zero temperature
Sebastian Wenderoth, Heinz-Peter Breuer, and Michael Thoss
Physical Review A, **104**, 012213 (2021)
DOI: 10.1103/PhysRevA.104.012213

In the first part, 4.3.1, we give a short overview of non-Markovianity in the dynamics of open quantum systems and discuss how memory effects can be quantified using the distinguishability between quantum states. Using the numerically exact ML-MCTDH approach we investigate memory effects in the spin-boson model at zero temperature, where non-Markovian effects are expected to be particularly pronounced [141]. The numerical results are supported by analytic results obtained from the weak coupling solution given by (4.7). We first focus on the scaling regime ($\omega_c \gg \Delta$) in Sec. 4.3.2. In Sec. 4.3.3 we discuss memory effects for $\omega_c \approx \Delta$.

4.3.1 Measuring non-Markovianity in quantum systems

Memory effects in the time-evolution of an open system are usually associated with the presence of a memory kernel in the Nakajima-Zwanzig equation which describes the time-evolution of the reduced density matrix of an open quantum system [113–115, 142]. A time-local master equation, like the time-convolutionless master equation [116, 117] is consequently associated to a Markovian time-evolution. This definition of non-Markovianity, however, is insufficient since memory effects induced by the environment can be, and in fact are, included in the time-dependent rates of the time-local master equation [141]. Moreover,

a definition of non-Markovianity should provide a general mathematical characterization which does not rely on a specific representation of the dynamics.

In order to define quantum non-Markovianity in a representation independent way, different mathematical and physical concepts have been developed in recent years. Definitions of non-Markovianity can be based on the divisibility properties of the underlying dynamical map, or on the correlations of the open system with an ancilla system [143–146]. For recent reviews of this topic see e.g. [147–149]. Our analysis of non-Markovianity is based on a physically motivated definition of non-Markovianity using the distinguishabiliy between quantum states [150, 151]. In a recent review the different approaches have been related to each other resulting in a hierarchy of concepts of quantum non-Markovianity [152]. According to this, the definition based on the distinguishability is the most restrictive concept of quantum non-Markovianity: An increasing distinguishability implies non-Markovianity according to all other concepts. A monotonically decreasing distingusihability, however, does not imply a Markovian time-evolution according to other concepts.

In the following we explain in more detail how the distinguishability can be used to quantify memory effects in the time-evolution of an open quantum system. The central quantity in this approach is the trace distance between two quantum states $\mathcal{D}(\hat{\rho}_1, \hat{\rho}_2)$ defined by Eq. (2.19). The trace distance can be interpreted as the distinguishability between the two states ρ_1 and ρ_2 [153]. Assuming that the initial state factorizes between the open system and the environment, the time evolution of the open system is determined by a family of completely positive and trace preserving (CPT) maps $\Phi(t)$ (see section 2.2 for more details). Any pair of initial states $\rho_{1,2}(0)$ then evolves into $\rho_{1,2}(t) = \Phi(t)\rho_{1,2}(0)$.

To quantify the time-dependent distinguishability, and hence the information flow between the open system and its environment, we consider the time-dependent trace distance defined as

$$\mathcal{D}(t) = \mathcal{D}(\rho_1(t), \rho_2(t)). \tag{4.13}$$

Note that CPT maps are contractions for the trace distance, i.e., $\mathcal{D}(t) \leq \mathcal{D}(0)$ [154]. The CPT property alone, however, does not imply monotonicity of the trace distance as a function of time. If $\mathcal{D}(t)$ is a monotonically decreasing function of time the two states $\rho_1(t)$ and $\rho_2(t)$ become less and less distinguishable. This can be interpreted as a continuous loss of information from the open system to the environment, and consequently, the dynamics is defined to be Markovian. A temporal increase of the trace distance, on the other hand, can be interpreted as a flow of information from the environment back to the open system, which is a unique signature of memory effects, and thus, of the non-Markovian character of the dynamics. On the basis of this interpretation one can define a measure for the degree of

non-Markovianity of the dynamics as [150]

$$\mathcal{N} = \int_{\sigma>0} \sigma(t)\mathrm{d}t, \tag{4.14}$$

where $\sigma(t) = \frac{d}{dt}\mathcal{D}(t)$ and the integral extends over all time intervals in which $\sigma(t) > 0$. By definition, this measure is strictly zero if the trace distance decreases monotonically, i.e., if there is no information backflow from the environment to the system, which corresponds to Markovian dynamics. Such a behavior occurs, e.g., if the family of dynamical maps $\Phi(t)$ is CP-divisible [148]. The simplest and best known example is given by a dynamical semigroup with a time-independent generator in Lindblad form. By maximizing over the initial state pair the measure defined by Eq. (4.14) becomes a property of the dynamical map alone.

4.3.2 Memory effects and non-Markovianity in the scaling regime

In the following we investigate memory effects in the spin-boson model at zero temperature using the time-dependent trace distance (4.13) and the measure for the non-Markovianity defined by Eq. (4.14). We begin our discussion of non-Markovian effects in the scaling regime, i.e. $\omega_c \gg \Delta$.

To evaluate the time-dependent trace distance defined in Eq. (4.13), we simulate the dynamics for two different initial states of the spin using the ML-MCTDH approach. The state of the environment is fixed, and, since we are interested in the zero temperature limit, all harmonic oscillators are initially in the ground state. We further assume that there are initially no correlations between the spin and its environment.

To calculate the time-dependent trace distance we employ the representation of the reduced state of the spin in terms of the Bloch vector $\mathbf{a}(t) = (\langle\hat{\sigma}_x\rangle(t), \langle\hat{\sigma}_y\rangle(t), \langle\hat{\sigma}_z\rangle(t))^T$, where $\langle\hat{\sigma}_i\rangle(t) = \langle\psi(t)|\hat{\sigma}_i|\psi(t)\rangle$. Employing this representation, Eq. (4.13) can be expressed as

$$\mathcal{D}(t) = \frac{1}{2}||\mathbf{a}_1(t) - \mathbf{a}_2(t)||_2, \tag{4.15}$$

where $\mathbf{a}_{1(2)}(t)$ is the time-dependent Bloch vector corresponding to the first (second) initial state, respectively, and $||\vec{x} - \vec{y}||_2$ denotes the Euclidean distance between the two vectors $\mathbf{x}$ and $\mathbf{y}$. It was shown that initial system states leading to a maximal non-Markovianity $\mathcal{N}$ must have the maximal initial trace distance $\mathcal{D}(0) = 1$ and, hence, must have orthogonal supports [155]. For the present case of a spin this implies that the initial states must be a pair of pure orthogonal states (antipodal points on the Bloch sphere).

In the following, we focus on a particular process defined by the dynamical map and the initial state pair. We consider the two eigenstates of $\hat{\sigma}_z$, $\rho_1(0) = |\uparrow\rangle\langle\uparrow|$ and $\rho_2(0) = |\downarrow\rangle\langle\downarrow|$

as the two initial states. For this specific choice of the initial states, the time evolution of $\mathbf{a}_2$ can be related to that of $\mathbf{a}_1$ by employing a symmetry of the spin-boson model. The technical proof is provided in Appendix A.3. Using this and the relation $\langle\hat{\sigma}_y\rangle(t) = \frac{1}{2\Delta}\partial_t\langle\hat{\sigma}_z\rangle(t)$, the trace distance can be written in terms of $\langle\hat{\sigma}_z\rangle_1$ and its derivative as

$$\mathcal{D}(t) = \sqrt{\Big[\langle\hat{\sigma}_z\rangle_1(t)\Big]^2 + \Big[\frac{1}{2\Delta}\partial_t\langle\hat{\sigma}_z\rangle_1(t)\Big]^2}, \tag{4.16}$$

where $\langle\hat{\sigma}_z\rangle_1(t)$ denotes the expectation value of $\hat{\sigma_z}$ with respect to the first initial state, i.e. $\mathbf{a}_1$. Taking the derivative of (4.16) with respect to time, it directly follows that $\partial_t\langle\hat{\sigma}_z\rangle_1(t_\mathrm{s}) = 0$ implies $\partial_t\mathcal{D}(t_\mathrm{s}) = 0$, i.e. if $\langle\hat{\sigma}_z\rangle_1$ has a stationary point at t_s, the trace distance also has a stationary point at t_s. Physically, this means that non-Markovian intervals either start or end at stationary points of $\langle\hat{\sigma}_z\rangle$. We note that this result does not rely on perturbation theory, and thus, Eq. 4.16 holds for all parameters.

Before discussing the numerical results we mention that the analytic solution of $\langle\hat{\sigma}_z\rangle$, defined by Eq. (4.7), can be used to derive an analytic expression for the trace distance $\mathcal{D}(t)$ which is valid for weak couplings α. The corresponding equation reads

$$\mathcal{D}(t) = \mathrm{e}^{-\gamma t}\sqrt{\frac{1}{2}\Big[1+\eta\Big] + \beta\sin(2\tilde{\Delta}t) + \frac{1}{2}\Big[1-\eta\Big]\cos(2\tilde{\Delta}t)}, \tag{4.17}$$

where, β, and η are constants which depend on the coupling strength α and on the characteristic bath frequency ω_c and are defined as

$$\begin{aligned}\beta &= \frac{\gamma}{\tilde{\Delta}}\\ \eta &= \beta^2 + \frac{\tilde{\Delta}}{2\Delta}(1+\beta)^2.\end{aligned} \tag{4.18}$$

We highlight one particular property of the analytic solution which is particularly important for our analysis. Using Eq. (4.17) it is easy to show that

$$\mathcal{D}(t + \frac{\pi}{\tilde{\Delta}}) = \mathrm{e}^{-\frac{\pi\gamma}{\tilde{\Delta}}}\mathcal{D}(t) \tag{4.19}$$

holds for all times t. In the weak coupling regime we thus expect that the trace distance exhibits an exponential decay with periodic modulations.

As a starting point of our discussion of memory effects, we recapitulate the dynamics of the spin and discuss the corresponding dynamics of the trace distance [34, 125, 126]. In the left panel of Fig. 4.8 the dynamics of the spin for different values of the coupling strength α for $\omega_c = 40\Delta$ is shown. Since $\langle\hat{\sigma}_y\rangle(t) = \frac{1}{2\Delta}\partial_t\langle\hat{\sigma}_z\rangle(t)$ holds, we only show the dynamics of $\langle\hat{\sigma}_x\rangle$ and $\langle\hat{\sigma}_z\rangle$.

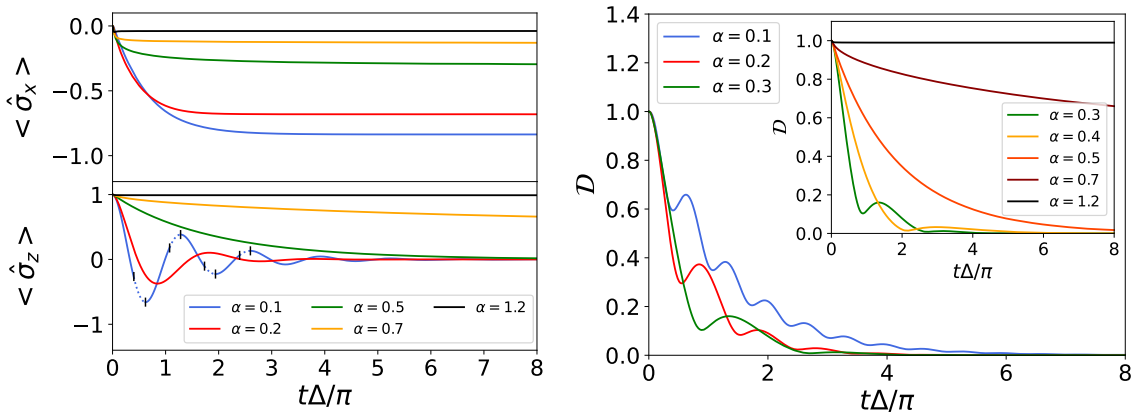

Figure 4.8: In the left panel the expectation value of $\hat{\sigma}_x$ and $\hat{\sigma}_z$ in the three different dynamical regimes of the spin-boson model for $\omega_c = 40\Delta$ are shown. In the right panel the corresponding trace distance is shown. For $\alpha = 0.1$ the first four non-Markovian intervals are marked by dashed lines. The figures are taken from [140]. ©2021 American Physical Society

To discuss relations between the time evolution of the spin and the time-dependent trace distance we give a short recap of the dynamics of the spin. The dynamics of the spin can be grouped into three qualitatively different dynamical regimes: In the weak coupling regime ($\alpha < 0.5$) the spin decays coherently to its stationary value. For increasing coupling strength, the oscillation frequency of $\langle \hat{\sigma}_z \rangle$ decreases. The intermediate regime ($0.5 < \alpha < 1$) is characterized by a monotonic or incoherent decay of the spin. Upon increasing the coupling strength further, the decay slows down and eventually the spin localizes for coupling strengths larger than $\alpha \approx 1$. In all three regimes $\langle \hat{\sigma}_x \rangle$ relaxes monotonically to its equilibrium value.

In the right panel of Fig. 4.8 the corresponding trace distance is shown. Similar to the dynamics of the spin itself, the behavior of the trace distance can be grouped into three different regimes. For weak coupling ($\alpha \lesssim 0.5$), the trace distance exhibits an overall decay to zero with periodic modulations including temporal increases, which indicate the presence of memory effects. This is consistent with the above mentioned property of the analytic solution given by Eq. (4.19). In the regime of incoherent decay, i.e. ($0.5 \lesssim \alpha \lesssim 1$), the trace distance decays monotonically. The decay slows down upon increasing the coupling strength. In both regimes, the overall decay reflects a relaxation of the spin to an equilibrium state, where the equilibrium state is independent on the initial state (see discussion in Sec. 4.2.1). For couplings $1 \lesssim \alpha$ the trace distance relaxes monotonically to a non-zero value indicating a dependence of the asymptotic state on the initial state as discussed in Sec. 4.2.2.

Summarizing this, we find that the coherent decay of the spin is non-Markovian, whereas incoherent decay and localization is Markovian. In the following we analyze the non-Markovian regime in more detail. As mentioned above, a stationary point of $\langle \hat{\sigma}_z \rangle$ implies a stationary point of the trace distance. Numerically we find that the corresponding stationary points

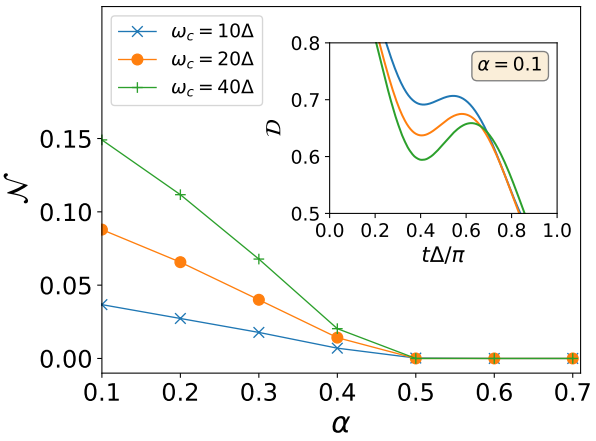

Figure 4.9: Non-Markovianity $\mathcal{N}$ as a function of the coupling strength α for different characteristic frequencies ω_c. The symbols represent the data, the lines are a guide to the eye. The inset shows the first increase of the trace distance for different values of ω_c for $\alpha = 0.1$. The figure is taken from [140]. ©2021 American Physical Society

of the trace distance are all local maxima and, therefore, the non-Markovian intervals end at the extremal points of $\langle \hat{\sigma}_z \rangle$. This is demonstrated in Fig. 4.8 for $\alpha = 0.1$. We find this behavior for all couplings $\alpha < 0.5$, as long as $\omega_c \gg \Delta$. As the coupling strength approaches the coherent-to-incoherent transition ($\alpha \approx 0.5$), the renormalized frequency $\tilde{\Delta}$ vanishes, leading to a monotonically decaying spin. Additionally, the increases in the trace distance become weaker as $\alpha \to 0.5$. Thus, the non-Markovian intervals shift to infinite time and memory effects disappear as the dynamics changes from coherent to incoherent decay. As a result, the regime of incoherent decay ($0.5 \leq \alpha \leq 1$) is Markovian.

Next, we want to quantify the non-Markovianity as a function of the coupling strength α. To this end, we use the cumulative measure $\mathcal{N}$ defined in Eq. (4.14). We first consider the behavior of $\mathcal{N}$ as $\alpha \to 0$. In this limit we are not able to converge $\mathcal{N}$ as the decay slows down and we are unable to simulate the dynamics of the spin for long enough times. In the weak coupling regime, however, the analytic solution given by Eq. (4.17) can be used to analyze the non-Markovianity. We discuss the validity of the weak coupling solution in detail at the end of this section. First note that for $\alpha = 0$ the evolution of the spin is unitary, and thus, $\mathcal{D}(t) = 1$ holds for all times. Consequently, $\mathcal{N} = 0$, as expected for a unitary time-evolution. To calculate the asymptotic behavior of $\mathcal{N}$ as $\alpha \to 0$, we employ the above mentioned property of the analytic solution, i.e. $\mathcal{D}(t + \frac{\pi}{\tilde{\Delta}}) = \mathrm{e}^{-\frac{\pi\gamma}{\tilde{\Delta}}}\mathcal{D}(t)$. Employing this property the summed non-Markovianity can be written as

$$\mathcal{N} = \frac{\mathcal{N}_1}{1 - \mathrm{e}^{-\pi\frac{\gamma}{\tilde{\Delta}}}}, \tag{4.20}$$

where the $\mathcal{N}_1$ denotes the information back flow during time interval $[0, \frac{\pi}{\tilde{\Delta}}]$ and the denominator accounts for the infinitely many, periodically reoccurring information back flows. The

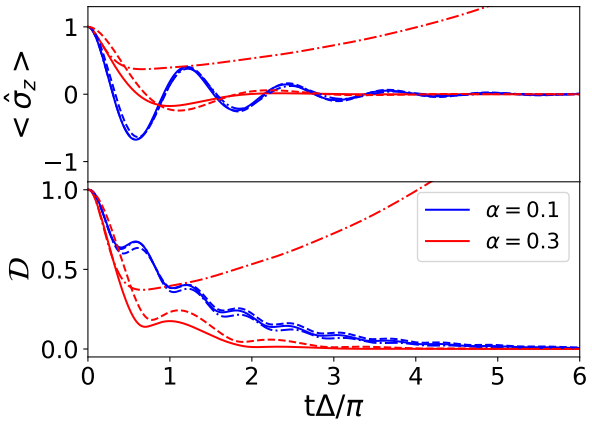

Figure 4.10: Comparison between the numerically exact results (solid lines), the TCL2 master equation approach (dashed-dotted lines), and the analytical equations (4.7) (dashed lines), for $\alpha = 0.1$ [blue curves] and $\alpha = 0.3$ [red curves]. Here, we set $\omega_c = 20\Delta$. The figure is taken from [140]. ©2021 American Physical Society

derivation of Eq. (4.20) is provided in Appendix A.4. As $\alpha \to 0$ the information back flow during one interval decreases. However, there are infinitely many of them. Using the Taylor expansion for the analytic expression of $\mathcal{D}(t)$, γ, and $\tilde{\Delta}$ for small α one finds

$$\mathcal{N} \sim -\frac{2}{\pi^2} \mathrm{e}^{\frac{2\Delta}{\omega_c}} \left[\ln\left(\frac{2\Delta}{\omega_c}\right) + \gamma_{\mathrm{EMC}} + \frac{\pi^2}{4} \mathrm{e}^{-\frac{2\Delta}{\omega_c}} \right] \quad \text{as } \alpha \to 0, \tag{4.21}$$

where γ_{EMC} denotes the Euler-Mascheroni constant. Since this limit is finite, we find that $\lim_{\alpha\to 0} \mathcal{N} > 0$, and thus, $\mathcal{N}$ is not analytic at $\alpha = 0$. The physical intuition of this result is that the relaxation time diverges as $\alpha \to 0$, and thus, memory effects are present at all times although the individual information back flows become infinitesimal.

For $\alpha > 0.1$ we can use the ML-MCTDH approach to obtain $\mathcal{N}$ numerically. Fig. 4.9 shows $\mathcal{N}$ as a function of the coupling strength α for different values of ω_c. Because the trace distance exhibits memory effects in the regime of coherent decay, i.e. for $\alpha < 0.5$, the measure of non-Markovianity $\mathcal{N}$ is non-zero. In this regime, the cumulative information back flow decreases monotonically as a function of the coupling strength. For a monotonically decaying spin, i.e. for $\alpha = 0.5$, the trace distance decays monotonically, and consequently, the non-Markovianity $\mathcal{N}$ vanishes. For an increasing characteristic bath frequency ω_c the non-Markovianity increases. The origin of this behavior can be seen in the inset of Fig. 4.9: the information back flow during one period is larger for larger ω_c.

We close this section with a discussion of the performance of the different perturbative approaches. Using the numerically exact results obtained from the ML-MCTDH approach, we can test the validity and demonstrate limitations of the analytic solution defined by Eq. (4.17) and the TCL2 master equation defined by Eqs. (4.5a), (4.5b), and (4.5c). We note that the TCL2 approach was previously used to investigate memory effects in the spin-

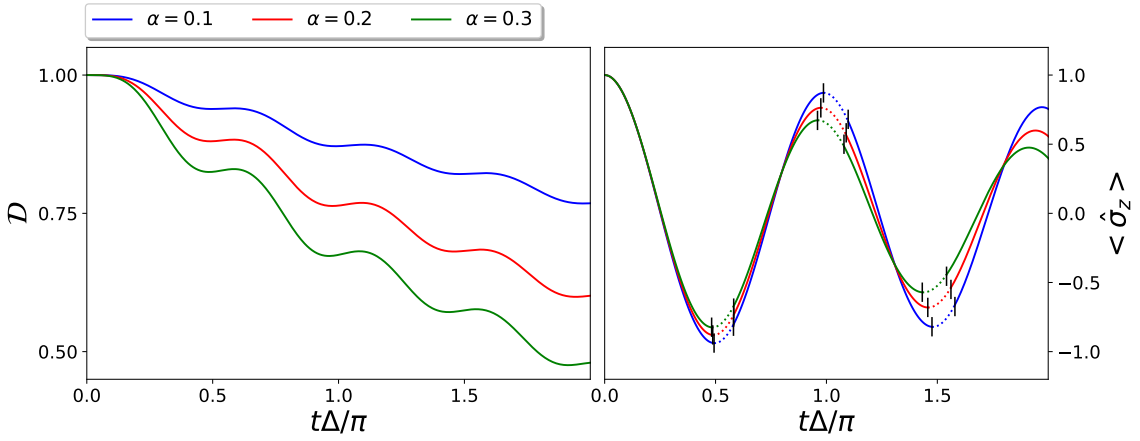

Figure 4.11: Dynamics of the trace distance (left) and $\hat{\sigma}_z$ (right) for $\omega_c = \Delta$ in the weak coupling regime. For better visualization, only results for short times are shown. The non-Markovian intervals of $\hat{\sigma}_z$ are marked by dashed lines. The figure is taken from [140]. ©2021 American Physical Society

boson model [141]. In Fig. 4.10 the numerical exact results obtained with the ML-MCTDH approach, together with the other two methods is shown.

For $\alpha = 0.1$ the TCL2 master equation approach, as well as the analytical equations (4.7) and (4.17), give qualitatively good results for $\langle\hat{\sigma}_z\rangle$ and $\mathcal{D}$. As the coupling strength increases, the approximations become less accurate and eventually break down. Although the analytic solution still gives qualitatively good results for $\alpha = 0.3$, the deviations from the numerically exact solution are larger compared to the results for $\alpha = 0.1$. The TCL2 approach, on the other hand, predicts unphysical results for longer times, in particular $\langle\hat{\sigma}_z\rangle$ and $\mathcal{D}$ exceed one. This indicates that perturbation theory, as it is employed in the TCL2 method, is no longer valid for this value of the coupling strength. The analytic approach, on the other hand, uses renormalized perturbation theory, employing a resummation of all terms linear in the coupling strength of a path integral solution [126], and thus has a broader range of validity.

4.3.3 Memory effects and non-Markovianity for a slow environment

In the following, we discuss non-Markovian effects outside the scaling limit, focusing on the particularly interesting crossover regime $\omega_c \approx \Delta$, where the timescales of spin and bath are similar. In this regime the perturbative solutions introduced above are not valid and we are restricted to numerical results.

For weak coupling α, shown in Fig. 4.11 for $\omega_c = \Delta$, the overall dynamics are very similar to the scaling regime, i.e. the spin shows damped, coherent oscillations and the trace distance decays to zero with periodic modulations. The memory effects, however, exhibit a qualitatively different behavior. Unlike in the scaling regime, the non-Markovian intervals

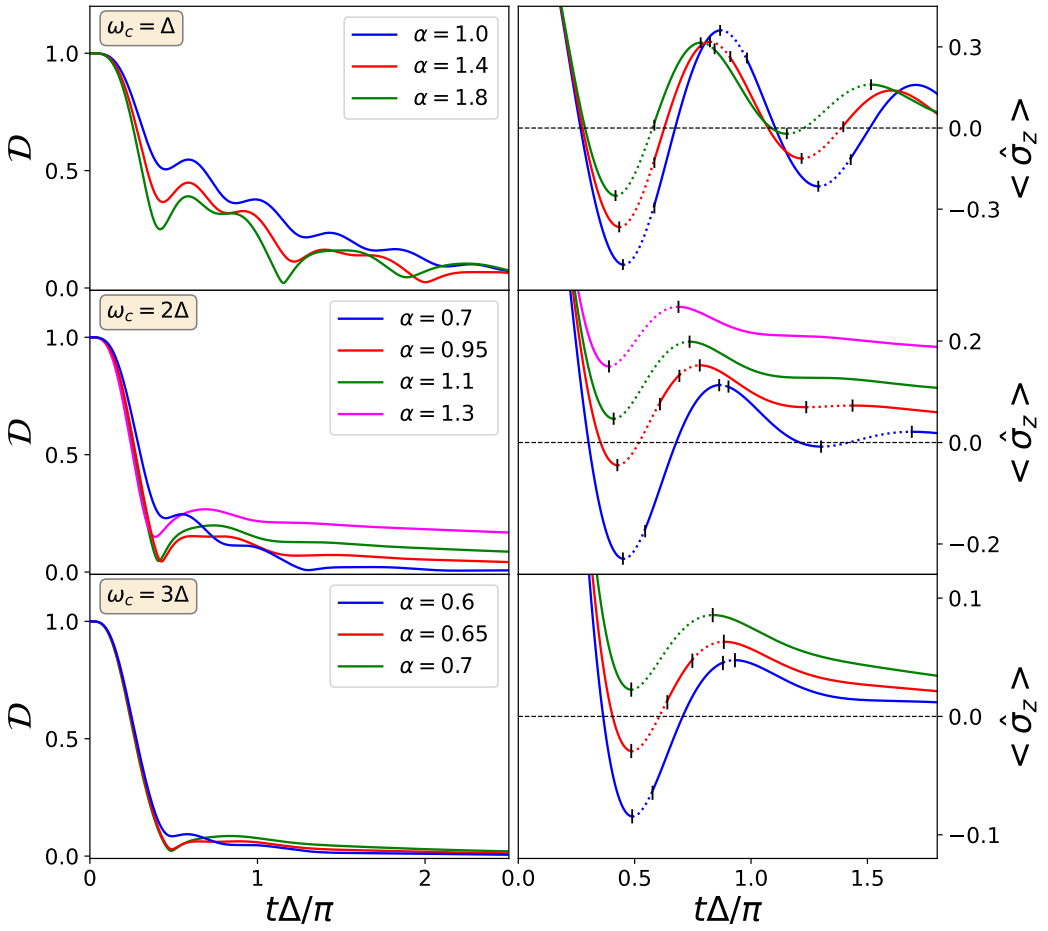

Figure 4.12: Dynamics of the trace distance (left) and $\langle \sigma_z \rangle$ (right) for different characteristic frequencies ω_c in the moderate and strong coupling regime. The non-Markovian intervals are marked with dashed lines. For better visualization not all non-Markovian intervals are marked. The figure is taken from [140]. ©2021 American Physical Society

begin at the extremal points of $\langle \hat{\sigma}_z \rangle$, indicating that $\mathcal{D}$ has local minima at the extremal points of $\langle \hat{\sigma}_z \rangle$.

We find further differences of the non-Markovian behavior for stronger coupling α. The numerical results are depicted in Fig. 4.12. The dynamics in this regime depends sensitively on ω_c and, thus, we show results for different values of ω_c. In contrast to the scaling regime, the dynamics of the spin is partially coherent for $\alpha \geq 0.5$ (see also Refs. [32, 34]), with an initial decay which does not slow down as the coupling strength is increased. We find a qualitatively different non-Markovian behavior in the crossover regime, $\omega_c \approx \Delta$. To demonstrate this, consider the first local minimum and maximum of $\langle \hat{\sigma}_z \rangle$ for the case $\omega_c = 2\Delta$ in Fig. 4.12. In the weak to moderate coupling regime (up to $\alpha \approx 0.7$), the stationary points of $\mathcal{D}$ associated to the two local extrema of $\langle \hat{\sigma}_z \rangle$ are both local minima and, thus, both non-Markovian intervals begin at the local extrema. As the coupling strength is

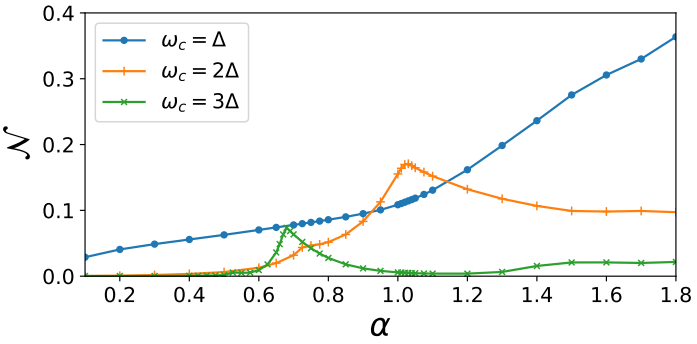

Figure 4.13: Non-Markovianity $\mathcal{N}$ as a function of the coupling strength α for different characteristic frequencies ω_c. The figure is taken from [140]. ©2021 American Physical Society

increased, the non-Markovian interval associated to the local maximum of $\langle\hat{\sigma}_z\rangle$ first shrinks to zero and then extends to the left (i.e. to shorter times) with fixed end point at the local maximum of $\langle\hat{\sigma}_z\rangle$. Eventually the two distinct intervals merge to a single non-Markovian interval extending from the local minimum to the local maximum. Upon further increasing the coupling strength, the initial decay becomes weaker and the following increase in the trace distance becomes smaller. This transition in the non-Markovian behavior results in a non-monotonic dependence of the memory effects on the coupling strength α caused by this pair of extrema of $\langle\hat{\sigma}_z\rangle$, i.e. memory effects first increase with α up to the point at which the two intervals merge and then decrease again. Similar transitions in the non-Markovian behavior are observed for later local extrema of $\langle\hat{\sigma}_z\rangle$, albeit for weaker coupling α.

This dependence of memory effects on the coupling strength α is reflected in the cumulative measure for non-Markovianity $\mathcal{N}$ which is shown in Fig. 4.13.For weak coupling α, $\mathcal{N}$ is very small for $\omega_c \in [2\Delta, 3\Delta]$, whereas it assumes significant values for $\omega_c = \Delta$. This is consistent with previous investigations of memory effects in the spin-boson model employing perturbative master equations, which predict Markovian dynamics if the effective spectral density of the environment is flat around the transition frequency of the spin [141], i.e. for $\omega_c = 2\Delta$. In the moderate and strong coupling regime, the transitions in the non-Markovian behavior discussed above give rise to different features in the non-Markovianity measure. For $\omega_c = 2\Delta$ and $\omega_c = 3\Delta$, the transition of the first local minimum and maximum of $\langle\sigma_z\rangle$ lead to a pronounced maximum of $\mathcal{N}$. Additionally, we find structures at $\alpha \approx 0.71$ and $\alpha \approx 0.52$ for $\omega_c = 2\Delta$ and $\omega_c = 3\Delta$, respectively, which coincide with the transition of non-Markovian behavior of the second local minimum and maximum of $\langle\sigma_z\rangle$. For $\omega_c = \Delta$, only the third oscillation of $\langle\sigma_z\rangle$ exhibits a transition at $\alpha \approx 1.4$, leading to weak shoulder in the non-Markovianity $\mathcal{N}$. Otherwise $\mathcal{N}$ increases monotonically over the shown range of coupling strengths.

4.4 Summary

In this chapter, we have investigated various aspects of the dynamics of the spin-boson model, with the goal to analyze different aspects of environment-induced effects. To this end we have employed the numerically exact ML-MCTDH framework, to simulate the dynamics in a broad range of parameters. In order to understand and analyze the numerical results we have used approximative analytic solutions for the dynamics of the spin.

In the first part, Sec. 4.2, we have examined the ability of an environment to equilibrate an open system, and discussed different situations in which this fails. To this end we have analyzed the measure to quantify the influence of the initial state on the dynamics of an open system developed in section 2.5.3. We have demonstrated that this measure can be used to not only classify the asymptotic behavior of the open system, but can also be used to quantify the influence of the initial state on expectation values of observables. We have discussed the failure of *subsystem state independence* in the strong coupling regime of an Ohmic spectral density and have identified an example of the failure of *subsystem equilibration*. In both situations the non-thermal behavior can be explained in terms of a renormalized spin coupling.

In the second part, 4.3, we have explored memory effects in the spin-boson model at zero temperature. Our results cover a broad range of parameters and reveal a rich dynamical behavior. While in the scaling limit of a fast bath, the dynamics transition from non-Markov to Markov as the decay of the spin changes from coherent to incoherent decay, the crossover regime, without separation of timescales between spin and bath, exhibits a complex, non-monotonic dependence of the non-Markovianity on the coupling strength. Furthermore, we have used our numerically exact results to test the validity of the perturbative approaches and demonstrate certain limitations.

5. Local memory and delocalization mechanisms in disordered systems

A key feature of thermalizing quantum systems is the *subsystem state independence*, i.e. the asymptotic state of subsystems is independent of their initial state, provided that their initial state does not change macroscopic observables of the total system. This implies that in thermalizing systems no information about the initial state is stored in local observables. One example of non-thermal behavior, a failure of *subsystem state independence*, can thus be detected by investigating the local memory of subsystems. Many-body localized systems (introduced in Sec. 2.4.3) constitute one class of systems which are expected to retain some memory about their initial state in local observables. These systems are characterized by a suppression of transport [22–24] and an extensive set of local conserved quantities [25,26]. As the asymptotic state of subsystem is described by a generalized Gibbs state (see Sec. 2.4.2), i.e. depends on all conserved quantities, we expect to find signatures of the initial state in local observables at all times. In this chapter, we discuss and analyze the local memory in thermalizing and non-thermalizing systems. As discussed above, the local memory is expected to exhibit qualitatively different behavior for thermalizing and localized systems, and thus, can serve as a further indicator for the thermal or non-thermal behavior. The spin-glass order parameter, defined by Eq. (2.26), is one possibility to quantify this local memory and was previously used to detect thermal and non-thermal behavior [55, 88, 156]. Other approaches considered the information backflow from an environment to a system by monitoring the bipartite entanglement shared between a probe-qubit and a system-qubit [157] or the Holevo quantity, an information theoretic measure that gives an upper bound for the accessible information of a quantum state [158].

In this thesis, we quantify the local memory by considering the reduced dynamics of a single spin and employ the concepts derived in Sec. 2.5.3. We investigate the dynamics of the XXZ Heisenberg spin chain, a paradigmatic model in the context of many-body localization. Depending on the parameters, this model can exhibit three different dynamical phases: Anderson localization, many-body localization, and thermalizing behavior, thus making it a perfect model for discussing local memory in different phases. By investigating

the local memory, and particularly the loss of this to the environment, we can identify some of the underlying mechanisms which are responsible for the spreading of information in the system. Additionally, this approach of investigating thermal and non-thermal behavior is based on local properties of the system. In comparison to the other approaches presented in Sec. 2.5, like spectral properties of the Hamiltonian or the entanglement entropy, this approach is experimentally more accessible.

This chapter is organized as follows. In section 5.1 we introduce the disordered XXZ Heisenberg spin chain and explain in detail how we quantify the local memory in this model. The goal of the second part, 5.2, is to understand and analyze different delocalization mechanisms by investigating the loss of local memory in different set ups. In Sec. 5.3, we discuss the local memory across the thermal-to-localized transition in terms of the mechanisms identified before. We finish with a summary in 5.4.

5.1 Disordered XXZ Heisenberg spin chain

In this chapter, we investigate the local memory in the disordered XXZ Heisenberg spin chain. The disordered XXZ Heisenberg spin chain consists of a linear chain of spins with nearest neighbor interactions and random local fields and is described by the Hamiltonian

$$\hat{H}_{XXZ} = \sum_{l=1}^{L} h_l \hat{S}_l^z + J \sum_{l=1}^{L-1} \left(\hat{S}_l^x \hat{S}_{l+1}^x + \hat{S}_l^y \hat{S}_{l+1}^y \right) + J_z \sum_{l=1}^{L-1} \hat{S}_l^z \hat{S}_{l+1}^z, \tag{5.1}$$

where $\hat{S}_l^x$, $\hat{S}_l^y$, and $\hat{S}_l^z$ denote the x, y, and z component of the l-th spin. As usual they are given by $\hat{S}^x = \frac{1}{2}\hat{\sigma}^x$ and similarly for the other two components. Here $\hat{\sigma}^x$, $\hat{\sigma}^y$, and $\hat{\sigma}^z$ are the three Pauli matrices. The h_l are random variables which are uniformly distributed in the interval $[-W, W]$, where W is the disorder strength. J describes the interaction of neighboring spins in x and y direction, whereas J_z describe the interaction of neighboring spins in z direction. The model is schematically shown in Fig. 5.1. To discuss the underlying mechanisms of the system we note that the Hamiltonian (5.1) can be written as

$$\hat{H}_{XXZ} = \sum_{l=1}^{L} h_l \hat{S}_l^z + \frac{J}{2} \sum_{l=1}^{L-1} \left(\hat{S}_l^+ \hat{S}_{l+1}^- + \hat{S}_l^- \hat{S}_{l+1}^+ \right) + J_z \sum_{l=1}^{L-1} \hat{S}_l^z \hat{S}_{l+1}^z, \tag{5.2}$$

where $\hat{S}_l^{\pm} = \hat{S}_l^x \pm i\hat{S}_l^y$ are the raising and lowering operators for the spin at site l. The coupling in x and y direction of the spin induces spin flips between neighboring spins, whereas the coupling in z direction describes an antiferromagnetic interaction. From Eq. (5.2) it is also apparent that the total spin in z direction is conserved under the time-evolution.

The disordered XXZ Heisenberg chain can exhibit three different dynamical phases depending on the parameters of the model. For $J_z = 0$, the Hamiltonian defined by Eq. (5.2)

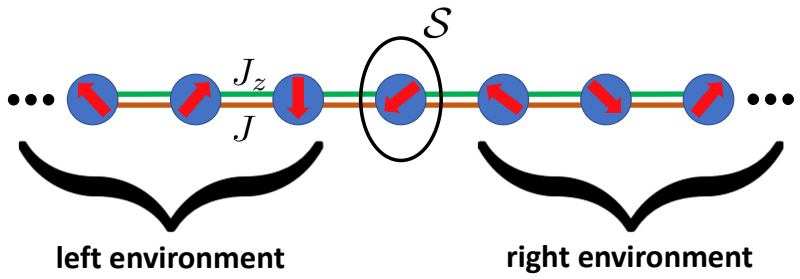

Figure 5.1: Schematic illustration of the disordered XXZ Heisenberg spin chain. The spins are represented by the red arrows in blue circles. The orange and green lines represent the coupling J and J_z, respectively. The black circle indicates the subsystem $\mathcal{S}$, of which we want to quantify the local memory, i.e. a single spin in the middle of the spin chain. The remaining spins constitute the environment, which can be separated into a left and right environment.

can be mapped to non-interacting fermions on a lattice with random local disorder using the Jordan-Wigner transformation [159]. In his seminal paper, Anderson showed that in such systems transport is absent for any non-zero disorder strength W [22], a phenomenon nowadays known as Anderson localization. Due to the absence of transport for $J_z = 0$, the XXZ Heisenberg spin chain is localized for any disorder strength W and subsystems never thermalize. For $J_z \neq 0$, on the other hand, the XXZ Heisenberg spin chain exhibits a transition from thermalizing to many-body localized behavior as the disorder strength is increased. For weak disorder, the model exhibits thermal behavior: the spectrum of the Hamiltonian (5.1) displays a Wigner-Dyson distribution [83, 88] and local expectation values relax to their thermal value and remains close to it for almost all times [156]. For sufficiently strong disorder the system displays many-body localized behavior: the spectrum has Poissonian statistics [83, 88] and some information about the initial state is retained in local observables [31, 160].

For $J_z \neq 0$ the disordered XXZ Heisenberg model thus exhibits a transition from thermal to localized behavior. The value of the critical disorder strength W_c, at which this transitions occurs, is currently under debate. For $J_z = J$ the critical disorder W_c was estimated to be between $3J - 4J$, based on spectral properties of the Hamiltonian [88, 161]. However, more recent investigations of the stability of many-body localization with respect to rare thermal regions estimated the critical coupling to be larger than $7J$ [94]. The reason for this discrepancy between the values for the critical disorder lies in the different mechanisms responsible for thermalization. For weak disorder, the eigenstates are delocalized over the whole system, and thus, the spectrum of the Hamiltonian follows a Wigner-Dyson distribution. For higher disorder strengths, the eigenstates are not delocalized over the full system and the spectrum of the Hamiltonian follows a Poissonian distribution. However, for sufficiently large system sizes, regions in which the local disorder is small exists almost surely.

These small regions can locally thermalize and form a finite thermal region. It was argued that such finite thermal regions can seed an 'avalanche'-like mechanism which ultimately leads to a thermalization of the full system [92–94]. Many-body localization can survive in the thermodynamic limit if this avalanche-like process eventually stops (see Sec. 2.5.1). This second mechanism, however, is only present in large enough systems. Since spectral properties can only be investigated for small systems, this effect is not apparent in the existing spectral investigations. In this thesis, we focus on the first mechanisms and do not discuss the effect of rare thermal regions on the local memory.

To investigate the local memory in the spin chain, we employ the concepts developed in Sec. 2.5.3. That means, we consider a single spin of the chain as an open system. The remainder of this spin acts as an environment. Throughout this chapter, we consider the spin in the middle of the chain as the open system, of which we want to quantify the local memory. In the following we denote this spin as the *central spin*. The environment thus consists of all spins except the central one. The environment can be separated further into the left environment, consisting of all spins to the left of the central spin, and the right environment, consisting of all spins to the right of the central spin. This separation of the spin chain is indicated in Fig. 5.1. The time-evolution of the spin of interest is described by a dynamical map of the form (2.14), i.e. by the two quantities $\mathbf{M}(t)$ and $\mathbf{b}(t)$. As argued in Sec. 2.5.3 the largest singular value of $\mathbf{M}(t)$ can be interpreted as a measure for the local memory. In general, the dynamical map, and thus the local memory, depends on the initial state of the environment $\hat{\rho}_E(0)$, as can be seen from the definition (2.7). In this chapter, we assume that the initial state of the environment is always a pure state and that the initial state factorizes between the central spin and the environment. In the following, we denote the initial state of the environment with $|\Psi_E(0)\rangle$. The state of the environment thus assumes the form

$$|\Psi_E\rangle = |\psi_{E,\mathrm{left}}\rangle \otimes |\psi_{E,\mathrm{right}}\rangle\,, \tag{5.3}$$

where $|\psi_{E,\mathrm{left}}\rangle$ ($|\psi_{E,\mathrm{right}}\rangle$) denotes the state of the left (right) environment.

To quantify the local memory of the central spin, we calculate the dynamical map for the central spin, i.e. we calculate $\mathbf{M}(t)$ and $\mathbf{b}(t)$ defined by Eq. (2.14). To this end, we simulate the dynamics for four different initial states of the central spin, while keeping the state of the environment fixed. From these four trajectories the dynamical map of the central spin can be reconstructed as discussed in Sec. 2.2. Here, we use exact diagonalization (ED) to simulate the dynamics of the system. This is motivated by the following considerations. We are interested in the asymptotic behavior of the local memory. For many-body localized systems, the time scale of the relaxation to the asymptotic state can be of the order of $\mathcal{O}\left(10^5\right)$. Simulating the dynamics of the system on these time scales with propagation

methods, like the ML-MCTDH approach, is very challenging. In the ergodic regime, on the other hand, the entanglement entropy is extensive. This implies that a large number of SPFs is required to converge the expectation values obtained with the ML-MCTDH approach, thus limiting the system sizes treatable within the ML-MCTDH approach also to relatively small systems. We emphasize that for the small system considered here the local memory never becomes zero, even if the system thermalizes. If not stated otherwise, all results are disorder averaged over 1000 disorder realizations.

5.2 Loss of local memory and delocalization mechanisms

In this section, we investigate different processes which lead to a loss of local memory. We first note that the Hamiltonian (5.1) conserves the total spin in z direction. Hence, the quantity

$$S^z_{\mathrm{tot}} = \sum_{l=1}^{L} \langle \Psi(t) | \hat{S}^z_n | \Psi(t) \rangle \tag{5.4}$$

is conserved under the time evolution. This means that the subspaces corresponding to different values of S^z_{tot} can be considered separately, which reduces the numerical effort. In order to discuss different delocalization mechanisms, we focus on the dynamics within the two subspaces corresponding to a total magnetization of $S^z_{\mathrm{tot}} = -(L-1)/2$ and $S^z_{\mathrm{tot}} = -(L-2)/2$. That is, we consider initial states in which only one or two spins are initially in the state $|\uparrow\rangle$, while the remaining spins are initially in the state $|\downarrow\rangle$. The dimension of these two subspaces scale linearly and quadratically with the chain length, respectively. Hence, we can simulate the dynamics for relatively large system sizes, thus reducing the influence of finite size effects. In Fig. 5.2 the disorder averaged expectation value of $\hat{S}^z$ of the central spin is shown for different chain length to demonstrate the finite size effects. The results for $L = 11$ differ from the results for larger chain lengths, thus showing that for $L = 11$ finite size effects are still pronounced. The results for $L = 21$, $L = 31$, and $L = 41$, are similar and the finite size effects have only a minor influence on the dynamics. We note that for higher disorder strengths W, the influence of finite size effects is smaller, as the system is deeper in the localized phase. In the following, we always consider a chain length of $L = 31$. For this chain length, finite size effects have a small influence, but the simulations are still numerically feasible for all different initial conditions we consider.

The remainder of this section is separated into two parts, according to different parameter regimes of the model we consider. In the first part, 5.2.1 we discuss dynamics in Anderson localized systems and the loss of local memory due to spin flip processes. In the second part, 5.2.2, we investigate the influence of the antiferromagnetic interaction on the local memory. The influence of this interaction is of particular importance since this interaction can either

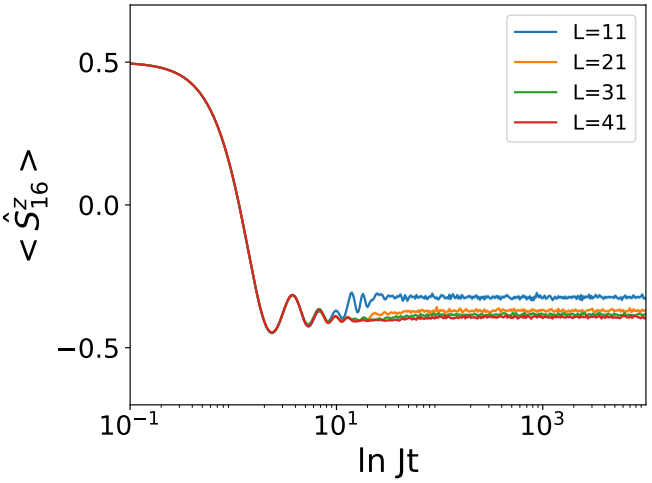

Figure 5.2: Disorder averaged expectation value of $\hat{S}^z$ of the central spin for different chain length L. The shaded area represents the error of the mean. Here we set $W = 0.5J$ and $J_z = 0$. The finite size effects are smaller for higher disorder strengths W as the system becomes stronger localized for higher disorder strength.

induce thermalization of the system (weak disorder W) or many-body localization (strong disorder W).

5.2.1 Local memory in Anderson localized systems

We first discuss the local memory in Anderson localized systems, i.e. we consider $J_z = 0$ for which it is known that the system is localized for any non-vanishing disorder strength W. For this special situation the interaction between the spins only induces spin-flips, thus creating entanglement between different spins. To simplify the discussion, we define the many-body states $|\Phi_k\rangle$, in which the k-th spin is in the up state $|\uparrow\rangle$ and the rest is in the down state $|\downarrow\rangle$, i.e.

$$
\begin{aligned}
|\Phi_1\rangle &= |\uparrow\downarrow\downarrow \ldots\rangle \\
|\Phi_2\rangle &= |\downarrow\uparrow\downarrow\downarrow \ldots\rangle \\
|\Phi_3\rangle &= |\downarrow\downarrow\uparrow\downarrow\downarrow \ldots\rangle \\
&\ldots
\end{aligned}
$$

To understand the dynamics of the system in this regime, we first discuss the expectation values of $\hat{S}^z_l$. This will later help us to analyze the loss of information. We first consider the dynamics of the spin chain for the initial state $|\Phi_{16}\rangle$, i.e. the state of the central spin is initially in the state $|\uparrow\rangle$ and all other spins are in the down state. In Fig. 5.3a) the disordered magnetization pattern, i.e. the expectation value of $\hat{S}^z_l$ as a function of l is shown at different times for $W = 1J$.

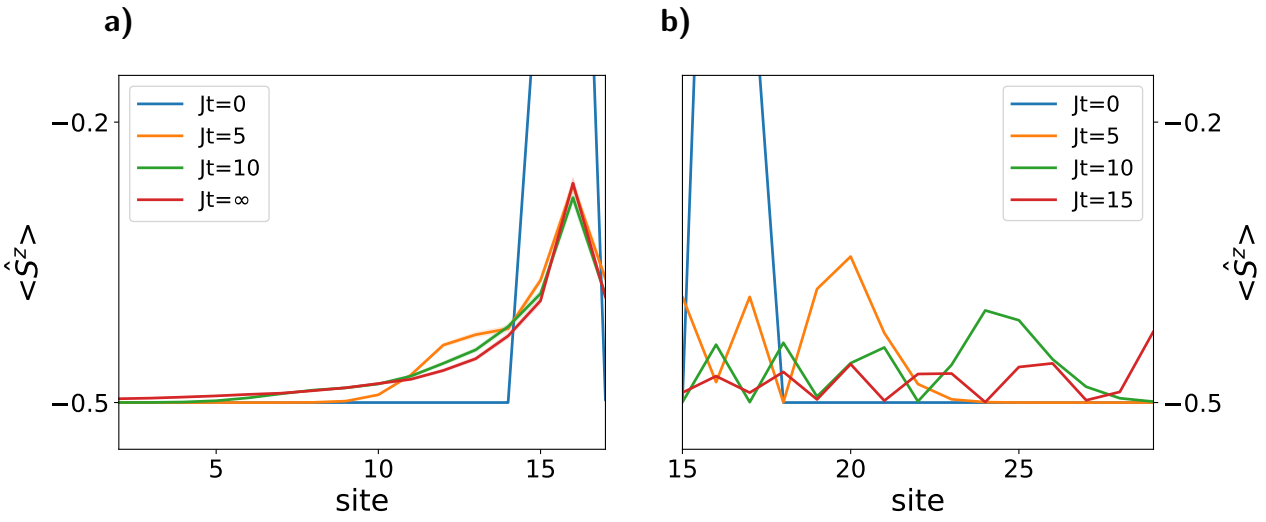

Figure 5.3: Expectation value of S_l^z as a function of the site l for different times Jt for $L = 31$. The spin chain is initially in the state $|\Phi_{16}\rangle$. In the left panel the disorder averaged results for $W = 1J$ are shown. In the right panel the results for $W = 0$ are shown, for which the system is not localized. In both cases the expectation values are symmetric around $l = 16$.

The spin chain is initially in the state $|\Phi_{16}\rangle$. Consequently, $\langle \hat{S}_l^z(0)\rangle = 1/2$ for $l = 16$ and $-1/2$ else, resulting in a magnetization pattern which is peaked at $l = 16$. As can be seen from the expectation values at $Jt = 5$ (orange curve) there is a wave front at $l \approx 11$ and $l \approx 21$. For $|l - 16| \lesssim 5$ the expectation value of $\hat{S}_l^z$ has changed, whereas the expectation value of $\hat{S}_l^z$ for spins which are further away is still $\approx -1/2$. This wave front propagates over time with a finite velocity, which can be seen by comparing the curves at different times. For $Jt = 10$ (green curve), we find that $\langle \hat{S}_l^z\rangle = -1/2$ for $l \lesssim 5$. Over time the wave front smears out. For $Jt = 10$, for example, the wave front is broader and weaker pronounced compared to $Jt = 5$. As $t \to \infty$ the magnetization pattern approaches an exponentially localized form. Formally, expectation values of finite dimensional systems do not have a well-defined limit as $t \to \infty$. However, for non-vanishing disorder the fluctuations of the disorder-averaged expectation values of $\hat{S}_l^z$ around their time-averaged value are negligible, i.e. the disorder-averaged expectation values approach an asymptotic value for $W \neq 0$. In contrast to that, transport is not suppressed for vanishing disorder and transport is possible for $W = 0$. The magnetization pattern does not approach a localized form, as can be seen in Fig. 5.3b). We emphasize that for non-vanishing disorder W, the expectation value of the central spin, i.e. $\langle \hat{S}_{16}^z\rangle$, is similar for all times $Jt \gtrsim 2$ and does not change significantly at later times.

To explain this behavior, we first note that spin flips can only occur between neighboring spins which are anti aligned, i.e. spins which have opposite spin. In this case, the interaction entangles these two spins, resulting in a change of the expectation value of $\langle \hat{S}_l^z\rangle$ of these two spins. For the subspace considered in Fig. 5.3, this means that the Hamiltonian couples

the state $|\Phi_k\rangle$ with the two states $|\Phi_{k-1}\rangle$ and $|\Phi_{k+1}\rangle$. Initially, the spin chain is in the state $|\Phi_{16}\rangle$. At short times, the interaction thus induces transitions from $|\Phi_{16}\rangle$ to $|\Phi_{15}\rangle$ and $|\Phi_{17}\rangle$, and with this a change of $\hat{S}^z_{15}$, $\hat{S}^z_{16}$, and $\hat{S}^z_{17}$. After these first spin-flips, the wave function has some contribution from the states $|\Phi_{15}\rangle$ and $|\Phi_{17}\rangle$, allowing for spin-flips with the spins at $l = 14$ and $l = 18$. For vanishing disorder, i.e. $W = 0$, these consecutive spin-flips continue, thus giving rise to transport. This is demonstrated in Fig. 5.3b): the magnetization pattern does not remain localized as $t \to \infty$. For $W > 0$, the system is Anderson localized. The spin-flip processes are suppressed and the above described cascade eventually stops, thus giving rise to the above described dynamics of the magnetization pattern. This cascade-like process of entanglement spreading implies that the information of the initial state of the central spin propagates with a finite velocity, a result also known as the Lieb-Robinson bound in quantum systems: There is an upper limit of the speed at which information can propagate in non-relativistic quantum systems [162].

Next, we discuss the local memory resulting from the above described dynamics of the spin chain. To this end, we calculate the dynamical map for the central spin for different initial states of the environment $|\Psi_E(0)\rangle$ (see Sec. 5.1) and consider the largest singular value of $\mathbf{M}(t)$ as a measure for the local memory. To start with, we consider a particular simple initial state of the environment: we investigate the local memory for an environment, in which all spins are in the state $|\downarrow\rangle$. We refer to this state as the polarized environment. In this situation, the initial state of the environment, denoted by $|\Psi_{E,0}\rangle$, is given by

$$\begin{aligned} |\Psi_{E,0}\rangle &= |\psi_{\text{left},0}\rangle \otimes |\psi_{\text{right},0}\rangle\,, \\ |\psi_{\text{left},0}\rangle &= |\downarrow\rangle^{\otimes 15}\,, \\ |\psi_{\text{right},0}\rangle &= |\downarrow\rangle^{\otimes 15}\,. \end{aligned} \tag{5.5}$$

In Fig. 5.4a) the expectation value of S^z_{16} is shown for different disorder strengths W if the spin chain is initially in the state $|\Phi_{16}\rangle$, i.e. the central spin is initially in the state $|\uparrow\rangle$. Additionally, we show the largest singular value of $\mathbf{M}(t)$, in the following denoted with $s_{\max}(t)$. The expectation value of $\hat{S}^z_{16}$ and $s_{\max}$ exhibit a very similar dynamical behavior. At $Jt = 0$ we find that $\langle \hat{S}^z_{16}\rangle = 1/2$ and $s_{\max} = 1$, as expected from the initial configuration. At short times ($Jt \lesssim 1$) both exhibit a decay, whose strength decreases with increasing disorder strength. At intermediate times ($Jt \lesssim 10$) the two observables show damped oscillations. For higher disorder strength W the oscillations are more pronounced and persists for longer times. In the long time limit, both quantities, $\hat{S}^z_{16}$ and $s_{\max}$, approach an asymptotic value and stays close to this value. The asymptotic value of both observables increases for increasing disorder strength.

The dynamical behavior of the two quantities can be explained in the following way. The

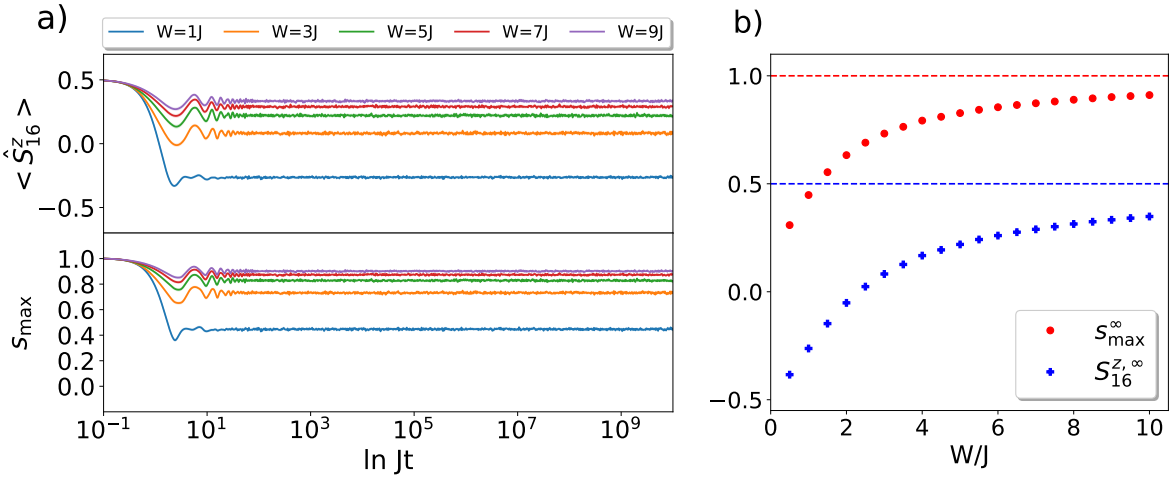

Figure 5.4: In the upper plot of a) the disorder averaged expectation value of $\hat{S}^z_{16}$ as a function of time is shown for different disorder strengths if the spin chain is initially in the state $|\Phi_{16}\rangle$. In the lower part the corresponding disorder averaged largest singular value of the dynamical map $\mathbf{M}$, $s_{\max}$, is shown. The shaded area represents the error of the mean. In b) the corresponding time-averaged quantities are shown. In both cases, the time-averaged values can be interpreted as the asymptotic values. The dashed lines represent the corresponding limit for a perfectly localized system ($W \to \infty$).

initial decay of the two observables is caused by the hybridization of the central spin with its neighbors. This hybridization is induced by spin-flip processes. These spin flips entangle neighboring spins, which lead to a change of the expectation value of $\hat{S}^z_{16}$. If the spins get entangled, the information about the initial state of the middle spin is partially contained in the entanglement between the spins, and is thus not accessible by measurements of a single spin. Consequently, the local memory, quantified by $s_{\max}$, decreases. For increasing disorder strength these spin-flips are suppressed, and thus, the initial decay becomes weaker for increasing disorder strength. The oscillations at intermediate times are caused by coherent oscillation between the central spin and its direct neighbors. For stronger disorder strength the interaction with the other spins is suppressed, and thus, these coherent oscillations persists for longer times.

The reason for the similar dynamical behavior of the two quantities is the polarized initial state of the environment, defined by Eq. (5.5). For this special choice, there is a close relation between the local memory of the central spin and the corresponding expectation value of $\hat{S}^z_{16}$: If the middle spin is initially in the state $|\downarrow\rangle$, the state of the total system assumes the form $|\downarrow\downarrow ...\rangle$. This is an eigenstate of the Hamiltonian, and is thus time-independent. This implies that the local memory of the central spin vanishes if and only if the reduced state of the spin relaxes to the state $|\downarrow\rangle\langle\downarrow|$ for all possible initial states of the middle spin, thus explaining the direct relation between the two quantities.

In Fig. 5.4b) the time-averaged quantities $S^{z,\infty}_{16} := \langle\langle \hat{S}^z_{16}(t)\rangle\rangle_t$ and $s^{\infty}_{\max} := \langle s_{\max}(t)\rangle_t$ are shown, where $\langle f(t)\rangle_t$ denotes the time average of a function $f(t)$ defined in Eq. (2.18). As

can be seen from the results in Fig. 5.4a) this time average is dominated by the long-time dynamics, and can thus be interpreted as the asymptotic value of the two quantities. In particular the asymptotic value of $s^{\infty}_{\max} = \lim_{t\to\infty} s_{\max}(t)$ represents the local memory about the initial state on long times, and can thus be used as an indicator for thermal and non-thermal behavior. The dashed lines represent the values for a perfectly localized system, i.e. for the limit $W \to \infty$. For weak disorder, we find $S^{z,\infty}_{16} \approx -1/2$ and $s^{\infty}_{\max} \ll 1$, indicating a weak localization. As the disorder strength increases both asymptotic values increase monotonically and approach the limit of a perfectly localized system, i.e. for $S^{z,\infty}_{16} \to 1/2$ and $s^{\infty}_{\max} \to 1$ as $W \to \infty$. This dependence can be explained in terms of the Anderson localization of the system. For any non-zero disorder strength, the system exhibits Anderson localization, and the magnetization pattern approaches an exponentially localized form (see Fig. 5.3). The decay length of this exponential form, however, depends on the disorder strength: for higher disorder strength the decay length decreases [22]. For increasing disorder strength, the dynamics are stronger localized, thus explaining the dependence of $S^{z,\infty}_{16}$ and $s^{\infty}_{\max}$. Although the system is localized for any disorder strength W the information about the initial state of the central spin can distribute over more sites for weaker disorder strength.

From this discussion we conclude that for this simple situation, i.e. $J_z = 0$ and an environment in which all spins are initially in the state $|\downarrow\rangle$, the loss of local memory is related to the initial hybridization of a spin with its direct neighbors, mediated by spin-flip processes. The time scale of this loss of information is approximately given by $Jt \sim 1$. As the hybridization is suppressed and the system becomes more localized for higher disorder strength W, the loss of information decreases as W increases.

In general, the dynamical map, and thus the local memory, depends on the initial state of the environment. In the following we discuss this influence for an Anderson localized system, i.e. for $J_z = 0$. To keep the analysis simple, we assume that in the initial state of the environment one spin is in the state $|\uparrow\rangle$ and all other spins are in the state $|\downarrow\rangle$. We parametrize the position of the environmental spin which is in the state $|\uparrow\rangle$ by its distance d to the central spin. The corresponding initial state of the environment, denoted with $|\Psi_{E,d}\rangle$, is given by

$$\begin{aligned} |\Psi_{E,d}\rangle &= |\psi_{\mathrm{left},d}\rangle \otimes |\psi_{\mathrm{right},0}\rangle\,, \\ |\psi_{\mathrm{left},0}\rangle &= |\downarrow\rangle^{\otimes(15-d)} \otimes |\uparrow\rangle \otimes |\downarrow\rangle^{\otimes(d-1)}\,, \\ |\psi_{\mathrm{right},0}\rangle &= |\downarrow\rangle^{\otimes 15}\,. \end{aligned} \tag{5.6}$$

Thus, in the state $|\Psi_{E,d}\rangle$, the spin with index $n = 16-d$ is in the state $|\uparrow\rangle$ and the remaining environmental spins are initially in the state $|\downarrow\rangle$.

In Fig. 5.5 the largest singular value is shown for different initial states of the environment,

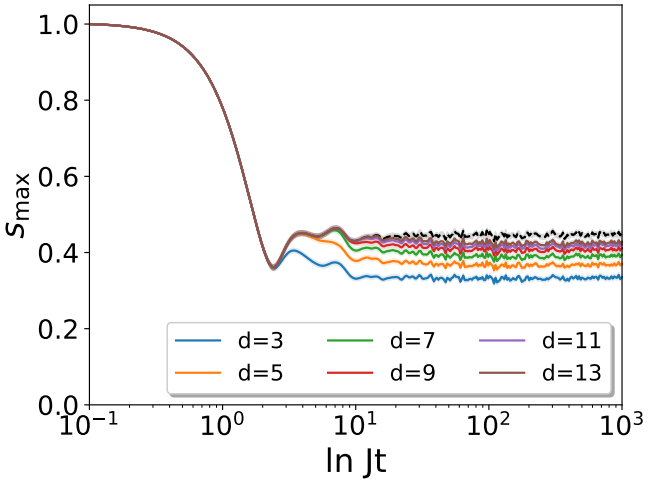

Figure 5.5: Disorder averaged largest singular value of the dynamical map $\mathbf{M}(t)$ as a function of time for different distances d. The parameters are $W = J$ and $J_z = 0$. The black line represent the results for for a polarized initial state of the environment (5.5). The inset shows the entanglement entropy of the central spin with the environment.

i.e. for different distances d between the central spin and the flipped spin in the environment. The qualitative influence of the environmental state on the local memory is similar for all considered disorder strengths, and thus, we only present data for the case $W = J$. On short times scales, $Jt \lesssim 1$, $s_{\max}$ exhibits a decay which is independent of the initial state of the environment, i.e. it is independent of the distance d and the decay is equal to the decay observed for the polarized environmental state. On intermediate time scales ($1 \lesssim Jt$), the initial state of the environment has an influence on $s_{\max}$. If the environment is initially in a state of the form $|\Psi_{E,d}\rangle$, the local memory is smaller compared to the polarized initial state of the environment. For increasing distance d this effect becomes weaker and shifts to later times. As the distance increases, the results obtained for an initial state of the environment of the form $|\Psi_{E,d}\rangle$ approaches the one for the polarized initial state $|\Psi_{E,0}\rangle$.

As discussed previously, the loss of information on short time scales ($Jt < 1$), i.e. the initial decay of $s_{\max}$, is related to the hybridization of the central spin with its direct neighbors. Consequently, this loss is independent of the state of the environment. The influence of the environmental state on longer time scales, as well as its dependence on d can be explained in the following way. The speed at which information can travel through the system has a finite velocity (see previous discussion). If the distance between the flipped spin in the environment and the central spin is larger, i.e. for larger distances d, it takes a longer time until this flipped spin can influence the central spin, thus explaining the shift of the influence of the environmental state on $s_{\max}$ with increasing d. Similar to the localization of the central spin shown in Fig. 5.3, the influence of the flipped spin in the environment is also localized. For increasing d the flipped spin gets further away from the central spin, and thus its asymptotic influence becomes weaker. As $d \to \infty$ this influence should vanish and the results should

be equal to the local memory for $|\Psi_{E,d\to\infty}\rangle$ should be equal to the results for $|\Psi_{E,0}\rangle$. As the localization length decreases upon increasing the disorder strength, the influence of the flipped environmental spin becomes weaker as the disorder strength is increased.

The local memory, quantified by $s_{\max}$, decreases over time to a non-zero value, indicating a partial loss of the local memory. This means that part of the information about the initial state of the central spin is not accessible by measuring the central spin. The information about the initial state can either be stored in the entanglement between the central spin and its remainder or in the corresponding state of the environment [148, 163]. In the following we investigate the influence of the environmental state, i.e. the influence of $|\Psi_{E,d}\rangle$, on these two aspects. To quantify the entanglement between the central spin and its environment we consider the von Neumann entropy of the reduced state of the central spin defined as

$$S_{16} = -\mathrm{tr}\{\hat{\rho}_{16} \ln \hat{\rho}_{16}\}, \tag{5.7}$$

where $\hat{\rho}_{16}$ denotes the reduced state of the central spin. To analyze the information which is contained in the environmental state, we investigate the influence of the initial state of the central spin on the corresponding reduced state of the environment. To do this, we consider two different initial states of the total system $|\Psi^{(1)}(0)\rangle$ and $|\Psi^{(2)}(0)\rangle$, which differ only in the state of the central spin. For these two different initial states we calculate the reduced state of the environment at a later time t, i.e. we calculate $\hat{\rho}_E^{(i)}(t) = \mathrm{tr}_{16}\{|\Psi^{(i)}(t)\rangle \langle\Psi^{(i)}(t)|\}$, where $\mathrm{tr}_{16}\{\cdot\}$ denotes the partial trace over the central spin. To discuss the influence of the initial state of the central spin on the reduced state of the environment, we consider the time-dependent distance between the two reduced states of the environment defined by

$$\mathcal{D}_E(t) = \mathcal{D}(\hat{\rho}_E^{(1)}(t), \hat{\rho}_E^{(2)}(t)), \tag{5.8}$$

where $\hat{\rho}_E^{(1)}(t)$ ($\hat{\rho}_E^{(2)}(t)$) denotes the reduced state of the environment corresponding to the first (second) initial state of the system, and $\mathcal{D}(\hat{\rho}_E^{(1)}, \hat{\rho}_E^{(2)})$ denotes the trace distance between density matrices defined by Eq. (2.19). If this distance is zero, the initial state of the central spin has no influence on the reduced state of the environment. If, on the other hand, the distance is non-zero, different initial states of the central spin lead to different reduced states of the environment.

In Fig. 5.6, the two quantities, S_{16} and $\mathcal{D}_E(t)$, are shown for different initial states of the environment. For the entanglement entropy we consider $|\uparrow\rangle$ as the initial state of the central spin. For the distance between the two environmental states $\mathcal{D}_E(t)$ we consider $|\uparrow\rangle$ and $|\downarrow\rangle$ as the initial state of the central spin. At time $t = 0$ the state of the system factorizes between the central spin and the environment, and thus, the entanglement entropy is zero at $t = 0$. Additionally, the two considered initial states $|\Psi^{(1)}(0)\rangle$ and $|\Psi^{(2)}(0)\rangle$ differ only

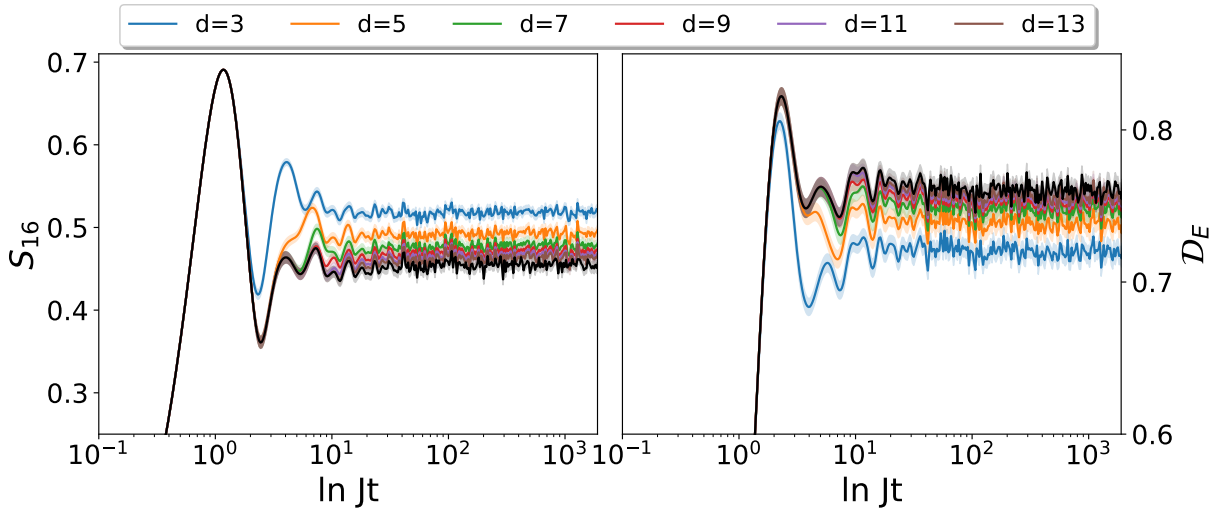

Figure 5.6: In the left panel the disorder averaged entanglement entropy S_{16} is shown for different initial states of the environment. In the right panel the disorder averaged distance between the reduced state of the environment for two different initial states of the central spin $\mathcal{D}_E$ is shown. The black line represents the result for the polarized environment.

in the state of the central spin. Hence, the reduced state of the environment is equal for $|\Psi^{(1)}(0)\rangle$ and $|\Psi^{(2)}(0)\rangle$ and $\mathcal{D}_E$ vanishes for $t = 0$. Both quantities exhibit an initial increase on the same time scale as the initial decay of $s_{\max}$ discussed before (see Fig. 5.5). Hence, the information about the initial state of the central spin is stored in the entanglement between the central spin and its remainder, as well as, in the reduced state of the environment. The initial increase is independent of the initial state of the environment, and thus, we conclude that this increase is caused by the hybridization of the central spin with its neighbors.

After this initial increase, both quantities approach an asymptotic value and stays close to this for all times. This takes place on a time scale of $1 \lesssim Jt \lesssim 10$. On these time scales we find an influence of the initial state of the environment: compared to the polarized environment, a flipped spin in the environment increases the asymptotic value of the entanglement entropy, whereas the asymptotic value of $\mathcal{D}_E$ is decreased. For increasing distance d both effect become weaker. This means that upon decreasing the distance d, the information about the initial state contained in the entanglement entropy increases, whereas the information stored in the state of the environment decreases. Given that the local memory, quantified by $s_{\max}$, decreases as d becomes smaller we conclude that the flipped spin in the environment increases the entanglement between the central spin and its environment, thus reducing the local memory of the central spin.

From our discussion we conclude that the local memory in Anderson localized systems is partially lost on two time scales. On short time scales $1 \lesssim Jt$ the central spin hybridize with its direct neighbors, leading to a decrease of the local memory. The state of the environment can further reduce the local memory by creating entanglement between the environment and

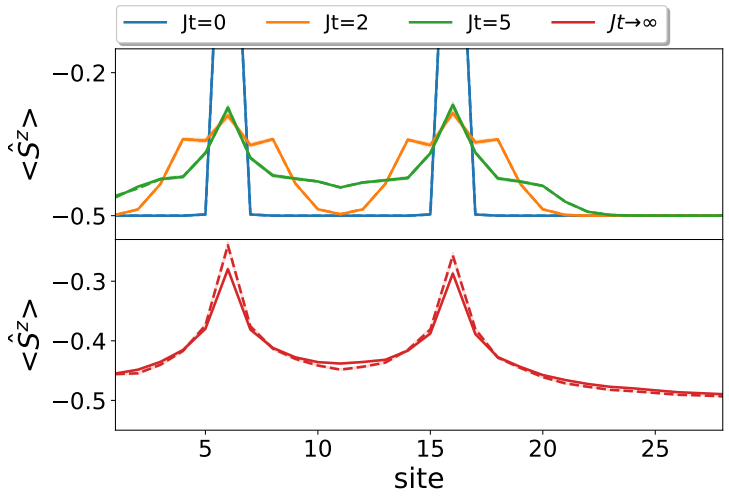

Figure 5.7: Disorder averaged expectation value of S_l^z as a function of l at different times. At time $t = 0$, the spins at $l = 6$ and $l = 16$ are in the up state, whereas the remaining spins are in the down state. The dashed lines, not visible in the upper plot, represent the results for $J_z = 0$.

the central spin. As argued above, this effect is observable on a time scale $1 \lesssim Jt \lesssim \mathcal{O}(L)$. For increasing disorder strength W the system becomes more localized and the loss of local memory is reduced, as expected for Anderson localized systems. We emphasize that for any non-zero disorder strength W some information about the initial state is retained locally for all times.

5.2.2 Influence of interaction in two particle systems

As a next step, we examine the influence of the antiferromagnetic interaction J_z on the local memory. Note that for $J_z \neq 0$ the Hamiltonian cannot be expressed in terms of non-interacting fermions, and thus, the dynamics cannot be understood in terms of single-particle states. In order to discuss the influence of the antiferromagnetic interaction in the simplest set up, we consider the dynamics of the central spin when the environment is initialized in a state of the form $|\Psi_{E,d}\rangle$ defined by Eq. (5.6). That means that the spin at site $n = 16 - d$ is initially in the state $|\uparrow\rangle$ and the remaining spins of the environment are in the state $|\downarrow\rangle$. To analyze the influence of the antiferromagnetic interaction we compare the results for $J_z = 0$ and $J_z = J$. In the following plots, the dashed lines always represent the results for $J_z = 0$, whereas the solid lines represent the results for $J_z = J$.

Similar to the previous section, we begin with a discussion of the expectation values of $\hat{S}_l^z$ as a function of l at different times. To demonstrate the effect of the antiferromagnetic interaction we consider the initial state, in which the spins at $l = 6$ and $l = 16$ are in the state $|\uparrow\rangle$ and the remaining spins are in the state $|\downarrow\rangle$. Fig. 5.7 shows the resulting expectation values of $\hat{S}_l^z$ as a function of l for $W = J$ at different times. For $Jt \lesssim 5$, the dynamics of

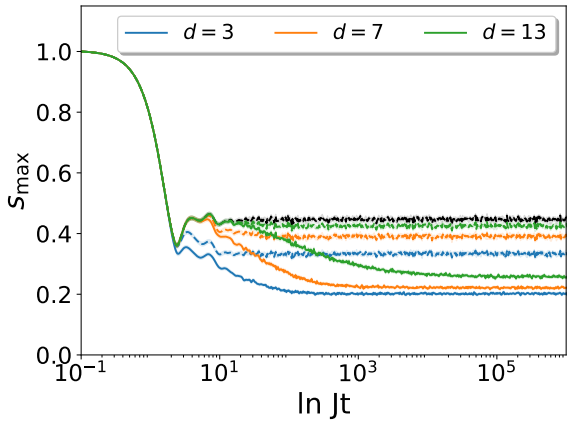

Figure 5.8: Disorder averaged largest singular value of the dynamical map $\mathbf{M}$ as a function of time for different distances d. The disorder strength is $W = J$. The colored dashed lines (three horizontal lines) represent the results for $J_z = 0$, the black line is the result for $J_z = 0$ for an environment which is initially in a polarized state.

the expectation values $\hat{S}_n^z$ is similar to the dynamics of the magnetization pattern discussed above: The spin-flips induce a spreading of the magnetization around the two spins which are initially in the state $|\uparrow\rangle$. At short times, $Jt < 5$, the dynamics of the spin chain is independent of the antiferromagnetic interaction, i.e. the results for $J_z = 0$ and $J_Z = J$ are equal. At later times we find an influence of the antiferromagnetic interaction, as can be seen in the lower plot of Fig. 5.7. In particular, the antiferromagnetic interaction leads to a broadening of the magnetization pattern, and hence to a further delocalization of the spins. The fact that the antiferromagnetic interaction only influences the dynamics on later times can be explained as follows. In the subspace of a total magnetization of $-(L-2)/2$, the antiferromagnetic interaction influences those states in which the two up spins are next to each other. These states are initially not occupied, thus the antiferromagnetic interaction has not influence on short time scales. Since the magnetization spreads with a finite velocity (see Sec. 5.2.1), the antiferromagnetic interaction influences the dynamics only at later times, once the corresponding states are occupied.

Next, we analyze how this antiferrmagnetic induced delocalization affects the local memory in the spin chain. To this end, we consider the central spin as an open system and consider the largest singular value of $\mathbf{M}(t)$ as a measure for the local memory. In the following, we choose $|\Psi_{E,d}\rangle$, defined by Eq. (5.6), as the initial state of the environment. In Fig. 5.8 the largest singular value of $\mathbf{M}(t)$ for different distances d is shown. In this plot we set $W = J$, the dashed lines represent the non-interacting results ($J_z = 0$), and the black line represents the result for a polarized environment, i.e. for an initial state of the form $|\Psi_{E,0}\rangle$. On short time scales, $Jt \lesssim 1$, $s_{\max}$ exhibits a decay which is independent of the antiferromagnetic interaction J_z and of the distance d. Since this decay is caused by the hybridization of the central spin with its direct neighbors this is not surprising. In the Anderson localized system,

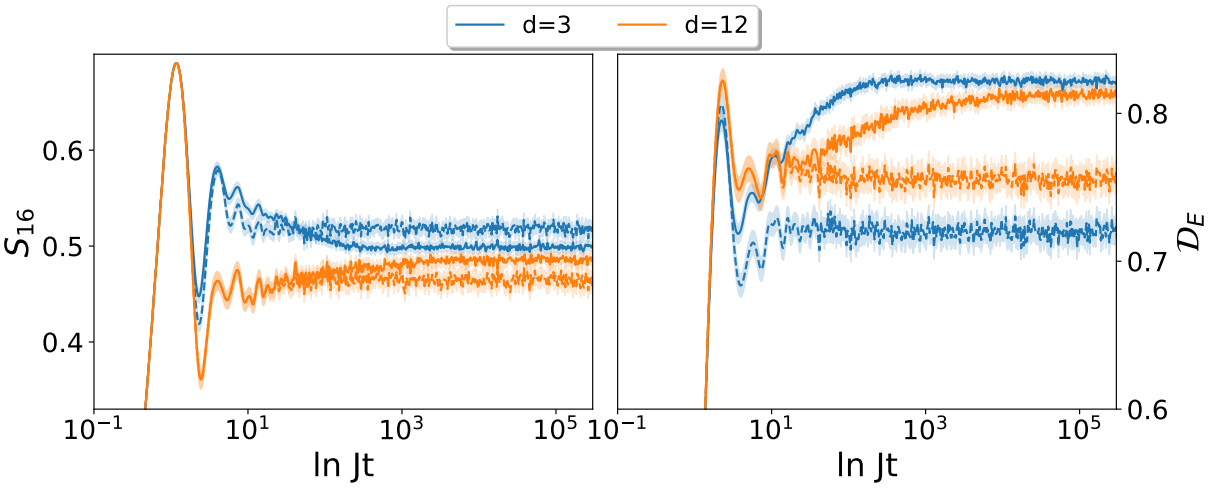

Figure 5.9: In the left panel the disorder averaged entanglement entropy S_{16} is shown for two different initial states of the environment. In the right panel the corresponding disorder averaged distance between the reduced state of the environment $\mathcal{D}_E$ is shown. The dashed lines represent the result for $J_z = 0$.

a flipped spin in the environment leads to a decrease of the local memory caused by an increased entanglement between the central spin and its environment. This process decreases the local memory on a time scale of $1 \lesssim Jt \lesssim \mathcal{O}(L)$ and can be seen by a comparison between the black line (polarized environment) and the dashed colored lines ($J_z = 0$). The antiferromagnetic interaction leads to a further decrease of the local memory on a slow, logarithmic like time scale, i.e. for times $10^1 \lesssim Jt \lesssim 10^3$. For an increasing distance d the onset of this second time scale shifts to larger times, as can be seen by the deviations between the dashed ($J_z = 0$) and solid ($J_z = J$) lines in Fig. 5.8. This shift originates from the finite spreading of entanglement, which we already discussed above.

As discussed previously, the information about the initial state of the central spin is either stored in the entanglement between the central spin and its environment or in the state of the environment. For $J_z = 0$ we have found that a flipped spin in the environment increases the entanglement between the central spin and its environment, thus leading to a decrease of the local memory. To discuss the influence of a flipped spin in the environment for the case $J_z = J$, we show the entanglement entropy and the distance between the reduced states of the environment, defined by Eq. (5.8), in Fig. 5.9. At time $t = 0$ the entanglement entropy, as well as, the distance $\mathcal{D}_E$ are zero. As discussed previously for the case $J_z = 0$, this follows from the initial state and the definition of the quantity $\mathcal{D}_E$. For $J_z = J$ both quantities exhibit an initial increase. This initial increase is caused by the hybridization of the central spin with its direct neighbors, and is thus independent of the distance d and of the antiferromagnetic interaction J_z. On longer time scales ($10^1 \lesssim Jt \lesssim 10^3$), the antiferromagnetic interaction induces a slow change, similar to the observed decay of $s_{\max}$. The qualitative influence of the antiferromagnetic interaction depends on the distance d.

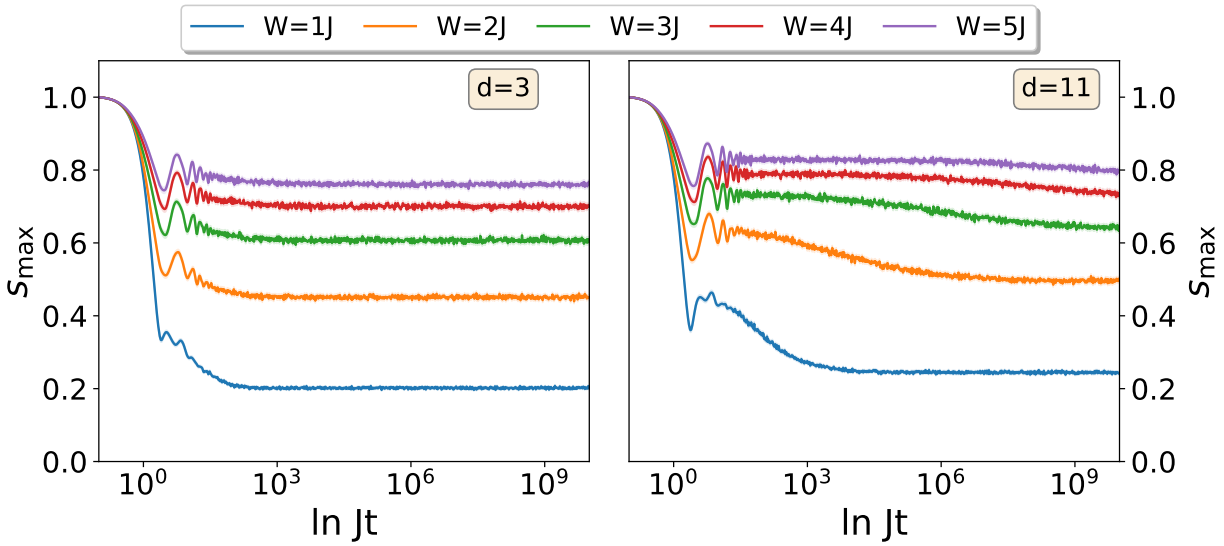

Figure 5.10: The disorder averaged largest singular value of $\mathbf{M}(t)$ as a function of time for different disorder strengths W. In the left plot the distance is $d = 3$, while in the right plot $d = 11$. After the initial decay, we find a logarithmic decay of $s_{\max}$ for all investigated disorder strength. The strength, as well as the onset of this time scale depends on the disorder strength and the distance d.

For small distances (blue curve) the antiferromagnetic interaction reduces the entanglement entropy and increases the corresponding distance between the environmental states. For larger distances, exemplified for $d = 12$, on the other hand, the antiferromagnetic interaction induces an increases of the entanglement entropy and $\mathcal{D}_E$. Given that $s_{\max}$ is decreased by the antiferromagnetic interaction for small and large distances d, we conclude that for small distances d the antiferromagnetic interaction transfers the information about the initial state of the central spin to the state of the environment. For larger distances d, the antiferromagnetic interaction increases $\mathcal{D}_E$ and leads to a higher entanglement between the central spin and its environment, which is both indicating a loss of local memory.

We finish this section with a qualitative discussion of the influence of the disorder strength on the decay of $s_{\max}$ induced by the antiferromagnetic interaction. In Fig. 5.10 the largest singular value of $\mathbf{M}$ is shown for two different distances and different disorder strengths W. The decay of $s_{\max}$ on short time scales ($1 \lesssim Jt$) is caused by the hybridization between the central spin with its direct neighbors. Consequently, it is independent of the antiferromagnetic interaction and exhibits the same dependency of the disorder strength, which we already discussed in 5.2.1, i.e. it becomes weaker as the disorder strength is increased. For larger disorder strengths W the spin-flips are suppressed, thus leading to a weaker hybridization of the central spin with its neighbors. For later times, the antiferromagnetic interaction gives rise to a slow logarithmic decay of $s_{\max}$. This decay exhibits some qualitative difference for small and large distances d. For $d = 3$ the slow decay starts almost directly after the initial decay at $Jt \sim 1$. In this case, the onset of this time scale is independent of the disorder

strength. For $d = 11$, on the other hand, the onset of the second time scale exhibits a strong dependence on the disorder strength: for increasing disorder it shifts to larger times. In both cases, the overall loss of information induced by the antiferromagnetic interaction, i.e. the loss associated to the slow time scale, decreases as the disorder strength is increased.

The decreasing influence of the antiferromagnetic interaction for increasing disorder strength can be explained as follows. Although the system is interacting, i.e. the system is not Anderson localized, the dynamics of of the magnetization pattern shown in Fig. 5.7 and the non-vanishing local memory suggest that the system is still localized. For increasing disorder strength, the dynamics are stronger localized. For the environmental states considered in Fig. 5.10, this implies that the occupation of those states which are influenced by the antiferromagnetic interaction, i.e. states with two up spins next to each other, are stronger suppressed.

Qualitatively, the dependence of the onset of the slow decay can be explained in the following way. During the time-evolution of the wave function the states which are influenced by the antiferromagnetic interaction (two up spins next to each other) get occupied by spin-flip processes. The first states which get occupied and are influenced by the antiferromagnetic interaction are the ones where the two up spins are approximately in the middle of the flipped spin in the environment and the central spin, i.e. at a distance $\approx d/2$ from the central spin. This leads to a first delay of the influence of the antiferromangetic interaction on $s_{\max}$. Once these states are occupied, the antiferromagnetic interaction can influence the dynamics of the spin chain. The first influence of this interaction is thus observable in the dynamics of the spins with a distance of $\approx d/2$ from the central spin. However, this influence also propagates with a finite velocity through the system, leading to a further delay of the influence of J_z on $s_{\max}$. We find that for short distances, i.e. $d = 3$ the delay is almost independent of the disorder, whereas for large distances ($d = 11$), the delay shifts to significantly larger times as the disorder strength increases. Giving a more precise microscopic explanation for this process remains an open question.

Summarizing this section, we find that for the initial states considered in this section the dynamics still exhibit clear signatures of localization even for $J_z \neq 0$, i.e. if the system is not Anderson localized. This can be seen by the asymptotic magnetization pattern Fig. 5.7 and a non-vanishing asymptotic value of $s_{\max}$. The antiferromagnetic interaction J_z induces a further delocalization mechanism in the system which manifests itself in a broader magnetization pattern and a slow decay of the local memory. This time scale displays similarities with the logarithmic time scale of the half chain entanglement entropy, which is typically associated to many-body localization [68].

5.3 Local memory across the ETH-MBL phase transition

In the following, we investigate the local memory across the ETH-MBL phase transition. That means we analyze the local memory as the dynamics changes from thermalizing to localized and explore the possibility to extract information about the phase from the local memory. Here, we focus on initial states of the total system which have a total magnetization close to 0. For these initial states the critical disorder strength W_c, i.e. the disorder strength at which the dynamics changes from thermalizing to localized, was estimated to be around $W = 3J - 4J$. For a more detailed discussion about the phase transition in the XXZ Heisenberg spin chain see Sec. 5.1.

To quantify the local memory we proceed in a similar way as in the previous section. We consider the spin in the middle of the chain as an open system, the remaining spins constitute the environment, and calculate the dynamical map for the central spin from the time-dependent wave function of the total system. To obtain the later we use exact diagonalization. Since the dimension of the considered subspaces grow exponentially with the system size, we are restricted to relatively small system sizes. Thus we discuss the dynamics for $L \in [9, 11, 13, 15]$. In particular, we consider the following initial states for the different system sizes

$$|\Psi(0)\rangle_9 = |\uparrow\downarrow\uparrow\downarrow\rangle \otimes |\sigma\rangle \otimes |\downarrow\uparrow\downarrow\uparrow\rangle \tag{5.9}$$

$$|\Psi(0)\rangle_{11} = |\downarrow\uparrow\downarrow\uparrow\downarrow\rangle \otimes |\sigma\rangle \otimes |\downarrow\uparrow\downarrow\uparrow\downarrow\rangle \tag{5.10}$$

$$|\Psi(0)\rangle_{13} = |\uparrow\downarrow\uparrow\downarrow\uparrow\downarrow\rangle \otimes |\sigma\rangle \otimes |\downarrow\uparrow\downarrow\uparrow\downarrow\uparrow\rangle \tag{5.11}$$

$$|\Psi(0)\rangle_{15} = |\downarrow\uparrow\downarrow\uparrow\downarrow\uparrow\downarrow\rangle \otimes |\sigma\rangle \otimes |\downarrow\uparrow\downarrow\uparrow\downarrow\uparrow\downarrow\rangle\,. \tag{5.12}$$

The reason for choosing these states is that the vicinity of the central spin is equal for all system sizes. This allows for a better comparison between the results for different system sizes. To calculate the dynamical map for the central spin we proceed as described above: we calculate the time-dependent wave function of the system for four different initial states of the central spin, while keeping the initial state of the environment fixed. Using Eqs. (2.11) and (2.14), the quantities $\mathbf{M}(t)$ and $\vec{b}(t)$ can be calculated.

We begin our discussion with an overview of the dynamics. In Fig. 5.11 the largest singular value of $\mathbf{M}(t)$ as a measure for the local memory is shown for different system sizes. In the main plot the disorder strength is $W = 1.5J$, in the inset the results for $W = 5J$ are shown. To distinguish the different mechanisms we show the results for $J_z = 0$ (dashed lines) and for $J_z = J$ (solid lines). We first discuss the dynamics of the local memory for $J_z = 0$, i.e. for which the system is Anderson localized (dashed lines). At short times we find a decrease of $s_{\max}$. This initial decay is caused by the hybridization of the spin with its neighboring spins, and is thus independent of the system size. For $J_z = 0$ the spin flips

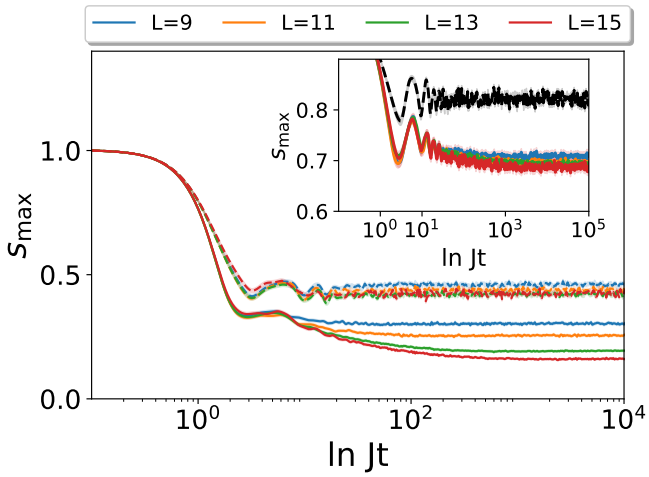

Figure 5.11: The disorder averaged largest singular value $s_{\max}$ as a function of time for different systems sizes. In the main plot the disorder is $W = 1.5J$. The dashed lines represent the results for $J_z = 0$. In the inset the disorder is $W = 5$. The black dashed line represents the results for $L = 15$ and $J_z = 0$.

create entanglement between the central spin and the environment, thus leading to a loss of local memory. This takes place on a time scale $Jt \approx 10$. Consequently, $s_{\max}$ approaches its asymptotic value on these time scales. For $L = 9$ to $L = 13$ we find a decrease of the asymptotic value indicating a dependency of the local memory on the system size. The asymptotic value of $s_{\max}$ for $L = 13$ and $L = 15$, however, is similar. From this we conclude that for $J_z = 0$ some information about the initial state is stored in local observables, which is the expected behavior for Anderson localized systems. From a comparison with the results for $W = 5J$, we find that for higher disorder the local memory increases, i.e. the dynamics are more localized.

As discussed in the Sec. 5.1, the antiferromagnetic interaction can either drive the system towards thermal equilibrium or induce many-body localization, depending on the disorder strength W. In the following, we discuss the influence of this antiferromagnetic interaction on the local memory. From the results presented in Fig. 5.11 we find two effects which we explain in the following. The first effect can be seen on short time scales. The initial decay of $s_{\max}$ is similar for $J_z = 0$ and $J_z \neq 0$. However, at $Jt \approx 1$ we find a further decrease of $s_{\max}$ induced by the antiferromagnetic interaction. This decrease of the local memory does not depend on the chain length. Thus, we conclude that this effect is caused by the interaction of the central spin with its vicinity which is equal for the different system sizes. The second effect can be seen on longer time scales, i.e. for times $10^1 \lesssim Jt \lesssim 10^3$. In this regime, we find a slow decay of $s_{\max}$, which, in contrast to the influence of J_z on short time scales, exhibits a dependence on L. For increasing system size L the decay extends over a longer time scale and the asymptotic value decreases with system size. For increasing L more information about the initial state of the central spin is lost during the time-evolution.

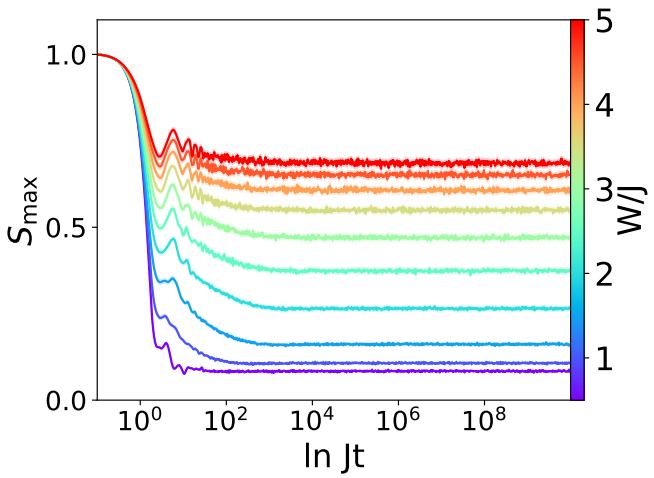

Figure 5.12: The disorder averaged largest singular value of $\mathbf{M}$ as a function of time for different disorder strengths. The system size is $L = 15$.

This is an indication for thermal behavior. This slow decay is similar to the loss of local information which we found for the environmental states with a single flipped spin (see Sec 6.2.2). By increasing the system size, we add spins at the two ends of the spin chain. For $W = 1.5J$ these added spins eventually get entangled with the central spin thus causing a loss of the local memory of the central spin. For $W = 5J$ we find a qualitatively similar influence of the antiferromagnetic interaction. The dependency on the system size, however, is much weaker. In particular the results for $L = 13$ and $L = 15$ are very similar, showing that the added spins have only a weak influence on the local memory of the central spin.

Next, we discuss the influence of the disorder strength on the local memory and on the different time scales. In Fig. 5.12 the largest singular value of $\mathbf{M}(t)$ is shown for different disorder strengths. Here, the system size is always $L = 15$. For all shown disorder strengths, $s_{\max}$ exhibits the initial decay discussed above. This initial decay is caused by the hybridization of the central spin with its neighbors. This hybridization becomes weaker for increasing disorder strength, hence the initial decay of $s_{\max}$ becomes weaker as the disorder strength increases. For all disorder strength except for $W = 0.5J$ (purple line) the largest singular value exhibits the above discussed slow, logarithmic decay. For $1.5J \geq W$ the decay of $s_{\max}$ induced by the antiferromagnetic interaction slows down and becomes weaker. For weak disorder $0.5J \lesssim W$ the suppression of the transport due to the disorder is very weak. In this case the loss of local memory induced by the spin flips is already large and the additional decay induced by the antiferromagnetic interaction is not visible. The asymptotic value of $s_{\max}$ shows a clear trend as a function of the disorder strength: as W is increased the asymptotic value of the local memory increases, indicating a stronger localization.

As a last aspect, we discuss the dependence of the asymptotic value of $s^{\infty}_{\max}$ on the disorder strength. We obtain the asymptotic value as the mean of $s_{\max}$ in the interval

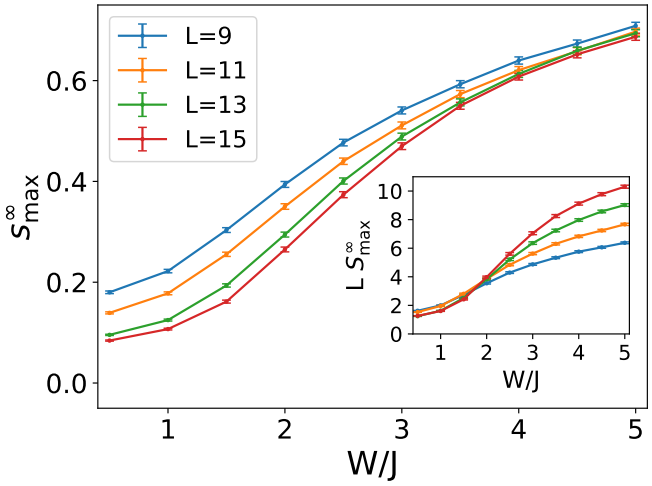

Figure 5.13: The plateau value of $s_{\max}$ as a function of the disorder for different chain lengths L. The plateau value is calculated as the mean of $s_{\max}$ in the interval $Jt \in [10^8, 10^{10}]$. In the inset the asymptotic value times the chain length is shown to demonstrate the scaling behavior.

$Jt \in [10^8, 10^{10}]$. In Fig. 5.13 this is shown as a function of the disorder strength for different system sizes L. In the inset we plot $Ls_{\max}$ to indicate the scaling of the local memory with the system size. For all system sizes L the asymptotic value of $s_{\max}$ increases monotonically with the disorder strength. For higher disorder the transport is stronger suppressed, thus explaining this general trend. For weak disorder strength $W \lesssim 3J$ the asymptotic value of $s_{\max}$ decreases with increasing system size, whereas for higher disorder strength the influence of the system size becomes smaller. This indicates that the local memory is not influenced by the spins at the end of the chain for sufficiently strong disorder. This is a clear indication for localization. In the limit $W \to \infty$ the dynamics become trivially localized independently of the system size. Thus all curves should approach 1 in this limit, independently of the system size.

As can be seen from the inset of Fig. 5.13, the asymptotic value of $s_{\max}$ scales approximately with L^{-1}, for $W \lesssim 2J$ and slower for $2J \lesssim W$. From this we conclude that in the weak disorder case, the information about the initial state of the central spin is distributed over the full system. This is a clear indicator for thermal behavior. For disorder strengths $W \gtrsim 2$ the asymptotic value of the local memory scales slower, indicating that the information is not distributed uniformly over the full system. At this point we emphasize that recent investigations of the stability of many-body localization suggest that for $W \gtrsim 3$ the localization is destroyed by rare thermal regions [94]. Using only ED we cannot investigate the effect of such rare thermal regions on the local memory as this approach is limited to small system sizes.

5.4 Summary

In this chapter we have applied the measure to quantify the influence of the initial state of an open system on its dynamics to study the local memory in the disordered XXZ Heisenberg spin chain. We explored the possibility to extract information about the phase of the model from the local memory.

In section 5.2 we have analyzed the local memory in the XXZ Heisenberg spin model for a particular simple class of initial states. By analyzing the loss of local memory of a single spin we have identified different delocalization mechanisms: In Anderson localized systems the hybridization between a spin and its environment creates entanglement leading to a partial loss of local memory. For $J_z \neq 0$ we have found a slow decay of the local memory induced by the antiferromagnetic interaction. This decay exhibits similarities to the time scale usually associated to MBL physics.

In the second part, 5.3, we have investigated local memory across the thermalizing to many-body localized transition and identified different time scales of the loss of local memory. On short time scales the interaction of the spin with its vicinity gives rise to a loss of the local memory which is independent of the system size. For longer times we have found a slow, logarithmic decay of the local memory which extends over a longer time for increasing system sizes. As the disorder strength increases, both effects become weaker and the system retains more information about the initial state in local observables. Last, we have discussed the asymptotic value of the local memory as an indicator for thermal behavior. In the weak disorder regime, i.e. for $W \lesssim 2J$, the asymptotic value of the local memory scales approximately with L^{-1}. The information about the initial state spreads over the total system, which is an indication of thermal behavior.

It has been argued that in the thermodynamic limit rare thermal regions can drive disordered systems towards thermal equilibrium [92–94]. In the present discussion we used exact diagonalization to investigate local memory, and thus, are restricted to small system sizes. For future work it might be interesting to investigate this by coupling a many-body localized system to a macroscopic environment and study the loss of local memory in the presence of a thermal environment.

6. Effect of non-local interactions in a centrally coupled many-body localized system

Recently, the first experimental observations of many-body localization (MBL) have been reported [156, 164, 165]. In these experiments trapped ions are used to realize certain physical models which are expected to show MBL. The interaction between the ions in the experimental set up is typically long-ranged, i.e. the interaction between different ions is not restricted to a nearest neighbor interaction but decays with the distance between the ions as $r^{-\alpha}$. However, in many of the existing theoretical literature of MBL systems with short range interaction, like the disordered XXZ Heisenberg spin chain discussed in the previous chapter, are considered [31, 66–69, 88, 97, 166–168]. This also includes the formal proof of MBL in one particular system [27]. The stability of MBL in long-range interacting systems, in particular in the thermodynamic limit, is still an open question. This stability was already discussed by Anderson for non-interacting systems [22]. In his paper he argued that localization can exist in systems with long range hopping if the hopping strength decays sufficiently fast. In recent years these considerations have been extended to interacting systems by different theoretical approaches. It was argued that MBL can exist in long-range interacting systems if long-range interactions decay sufficiently fast [169, 170]. Furthermore, it was hypothesized that a one dimensional system can exhibit MBL for low temperatures and low energy densities if the interaction scales as $\sim r$ [171]. Recently, it was pointed out that long-range hopping has a stronger influence on the delocalization than long-range interactions [172].

The above mentioned publications about long-range interactions considered direct interactions between the constituents, which decay with the distance. A different kind of non-local interactions can be realized by coupling all degrees of freedom of the many-body localized system to one central degree of freedom. The thus introduced long-range interactions are qualitatively different compared to direct interactions. First, the long-range interactions mediated by the central degree of freedom do not decay with the distance, i.e. all con-

stituents of the many-body localized systems are coupled equally. Second, the delocalization mechanisms induced by the long-range interactions are mediated via the central degree of freedom and not by the direct interaction. Nandkishore et al. considered the influence of a bath of interacting bosons on a fully MBL system [173]. They showed that a bath with a continuous density of states thermalizes the localized system for any non-zero coupling. Ponte et al. investigated the influence of a central two-level system on a fully many-body localized system, i.e. they consider a system of non-interacting local integrals of motion and showed that the central two-level system can induce thermalization of the full system for sufficiently strong coupling [91]. In [174] the influence of a centrally coupled spin on the disordered XXZ Heisenberg spin chain was considered. It was demonstrated that the central spin influences the critical disorder strength W_c and can in fact delocalize the spin chain completely.

In this chapter we investigate the stability of MBL with respect to a centrally coupled d level system. To this end, we consider the dynamics of a disordered spin chain with antiferrmagnetic nearest neighbor interaction. We introduce long-range interactions to the model by adding a centrally coupled system with d levels to the model. In contrast to previous investigations of such systems, we consider the case of $d > 2$ and place a constant "magnetic field" on the central degree of freedom. As we discuss in the first section of this chapter, this has some crucial implications for the stability of MBL in these systems. Furthermore, we extend the investigations to much larger systems than previously investigated by employing the ML-MCTDH approach.

In this chapter we will loosely follow the lines of our publication [175],

> *Non-Markovian effects in the spin-boson model at zero temperature*
> Nathan Ng, **Sebastian Wenderoth**, Rajagopala Reddy Seelam, Eran Rabani, Hans-Dieter Meyer, Michael Thoss, and Michael Kolodrubetz
> Physical Review B, **103**, 134201 (2021)
> DOI: 10.1103/PhysRevB.103.134201
>

We augment the discussion with further details and extend the analysis of the strong coupling regime, in which the system is expected to obey the eigenstate thermalization hypothesis.

This chapter is organized as follows: In 6.1 we introduce the centrally coupled spin model which we investigate, explain how we simulate the dynamics using the ML-MCTDH approach, and discuss some analytic results, which we use to analyze the dynamics of the system. In the second part, 6.2, we focus on the localized regime of the system. We investigate the interplay between the local and non-local interaction and examine the stability of localization in finite and infinite systems. In the last part, Sec. 6.3, we expand the discussion to the

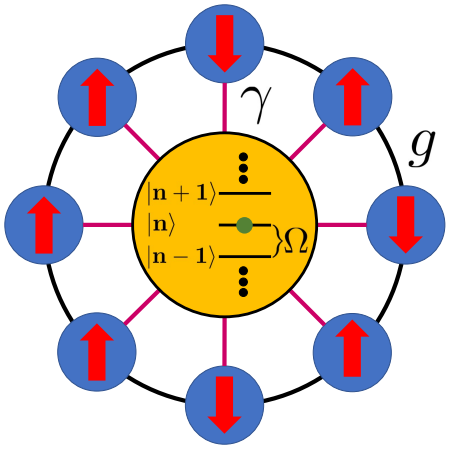

Figure 6.1: A schematic illustration of the centrally coupled spin chain. The spins are represented by red arrows in blue circles. The yellow dot represents the state of the qudit. Ω describes the energy difference between the different qudit levels, g describes the antiferromagnetic interaction between spins, and γ describes coupling between the qudit and each spin.

thermalizing regime and investigate subsystem equilibration for strong coupling between the spin chain and the central degree of freedom. Section 6.4 concludes this chapter with a summary.

6.1 Centrally coupled many-body localized system

In order to investigate the influence of long-range interactions in a many-body localized system, we consider a spin chain with antiferromagnetic interactions and random local disorder. The long-range interactions are introduced to the system by coupling a central degree of freedom to all spins in the chain. As the central degree of freedom, we consider a d level system, in the following denoted as *the qudit*. The model is described by the Hamiltonian

$$\begin{aligned} \hat{H} &= \hat{H}_0 + \Omega\hat{\mu}^z + \gamma\hat{H}_1(\hat{\mu}^+ + \text{h.c.}), \\ \hat{H}_0 &= \sum_{l=1}^{L} h\zeta_l\hat{\sigma}_l^z + g\hat{\sigma}_l^z\hat{\sigma}_{l+1}^z, \\ \hat{H}_1 &= \sum_{l=1}^{L} \hat{\sigma}_l^x, \end{aligned} \tag{6.1}$$

where $\hat{\mu}^z = \sum_{n=1}^{d} n\,|n\rangle\langle n|$ and $\hat{\mu}^+ = \sum_{n=1}^{d-1} |n+1\rangle\langle n|$. The states $\{|n\rangle\}$ label the states of the central degree of freedom. Here, $\hat{\sigma}_l^z$ and $\hat{\sigma}_l^x$ denote the Pauli matrices and the ζ_l are random variables drawn uniformly from the interval $[-1, 1]$. The chain length is denoted by L, and we consider periodic boundary conditions for the spin chain, i.e. we identify the index $L+1$ with 1. A schematic figure of the model is shown in Fig. 6.1. Throughout this

chapter, we consider a scaled spin-qudit coupling of the form

$$\gamma = \frac{\gamma_0}{\sqrt{L}}. \tag{6.2}$$

This particular scaling of the coupling γ guarantees that the qudit dynamics converge in the thermodynamic limit, i.e. for $L \to \infty$. Note that this is not trivial, since the environment consists of interacting modes. We elaborate on this later in this section. The dynamics of the qudit in the thermodynamic limit can be used to discuss some aspects of the dynamics of the spin chain as $L \to \infty$, a parameter regime which is inaccessible by numerical simulations.

The spin part of the Hamiltonian can be seen as a phenomenological model for many-body localization deep in the MBL phase. The spins represent localized bits (l-bits) and the exponentially localized interaction is restricted to only nearest neighbor interactions. For vanishing γ the spin chain is thus trivially localized, i.e. all $\hat{\sigma}_l^z$ are conserved quantities. The centrally coupled d level system induces flips of the l-bits, thus creating entanglement between different l-bits. This leads to a delocalization of the l-bits, which can potentially lead to thermalization of the system for a sufficiently strong coupling γ.

To discuss the effect of the centrally coupled qudit in more detail, we note that for large Ω an effective Hamiltonian, describing the dynamics of the spins, can be derived [176]: In the limit $d \to \infty$ the model defined by Eq. (6.1) can be mapped to a spin chain with an external drive, where the driving frequency is given by Ω and γ describes the coupling strength between the spin chain and the external drive [176, 177]. Using this representation of the model, an effective Hamiltonian for the spin chain, which is valid for finite d, can be derived. This effective Hamiltonian reads [176]

$$H_{eff} = H_0 + (H_1)^2 \frac{|d\rangle\langle d| - |1\rangle\langle 1|}{\Omega} + \mathcal{O}(\Omega^{-2}). \tag{6.3}$$

From this expression it follows that, in lowest order in Ω^{-1}, i.e. for $\gamma^2/\Omega \ll 1$, the centrally coupled qudit induces an all-to-all interaction, mediated by $(H_1)^2$, if the edge states of the qudit are occupied. Thus, we expect that for small edge occupation of the qudit, the long-range interactions mediated by the qudit only play a minor role in the dynamics. Based on these considerations and numerical investigations, a phase diagram was proposed in [176] and later modified in [175]. The resulting phase diagram is shown in the left panel of Fig. 6.2. In the limit $d \to \infty$, which corresponds to the right part of the phase diagram, the dynamics of the spin chain are equivalent to the dynamics of a spin chain with a periodic external drive. The external drive can thermalize the spins for sufficiently strong coupling γ, thus leading to a transition from localized to thermal behavior. As $d \to \infty$, the precise value of d should not matter, thus leading to a horizontal separation between the two phases in this limit. The value of the critical coupling γ_c, at which the dynamics of the spins change from

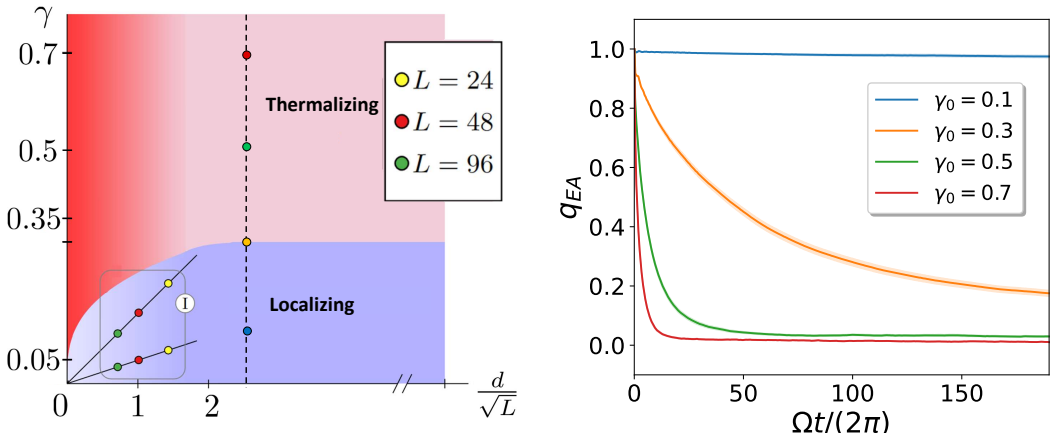

Figure 6.2: In the left plot a schematic phase diagram is shown. The phase diagram is taken from Ref. [175] and was modified. For sufficiently strong γ the central degree of freedom delocalizes the spins and eventually leads to a thermalization of the spins, indicated by the red region. For sufficiently low coupling γ, the spins remain localized, indicated by the blue region. The diagonal lines in the left part represent the parameters discussed in section 6.2. The dots on the vertical line represent the parameters for the data shown in the right plot, in which the generic behavior of the spin glass parameter q_{EA} is shown for thermalizing and non-thermalizing behavior of the spins.

localized to thermal, depends on the parameters of the Hamiltonian. For the parameter set we consider in this chapter, i.e. $h = 1.3$, $g = 1.07$, and $\Omega = \pi/0.8$, the critical coupling was estimated to be approximately $\gamma \approx 0.33$ [176]. The behavior for small $d/\sqrt{L}$, i.e. the left part of the phase diagram, is more complicated. As we discuss in Sec. 6.2, for fixed d, the spins always remain localized in the limit $L \to \infty$, if the coupling γ is scaled with $L^{-1/2}$. In this limit, the spins thus become localized above a certain chain length for any coupling strength γ. This limit corresponds to the diagonal lines in the phase diagram. To estimate the phase separation in the limit $L \to \infty$ for fixed d, the all-to-all interaction mediated by the qudit can be treated in a mean field approximation. Based on this consideration it was argued that couplings which tend to zero faster than $L^{-1/6}$ will result in a localized spin chain as $L \to \infty$. This scaling results in the curved blue region around the origin [175].

In order to investigate thermal and non-thermal behavior of the system we use different observables. To characterize the localization of the spin chain we consider the spin-glass order parameter q_{EA}, or Edwards-Anderson order parameter [95], defined as

$$q_{EA}(t) = \frac{1}{L}\sum_{l=1}^{L} \langle \Psi(0)|\hat{\sigma}_l^z(t)\hat{\sigma}_l^z|\Psi(0)\rangle \,, \tag{6.4}$$

which we already introduced and discussed in Sec. 2.5.2. Here $|\Psi(0)\rangle$ denotes the initial state of the system. The spin-glass order parameter measures the correlation of $\hat{\sigma}_l^z$ at time zero and at time t averaged over all spins. In thermalizing systems the asymptotic state of a single spin is independent of its initial state, and thus, we expect that for such systems the

correlations $\langle\Psi(0)|\hat{\sigma}_l^z(t)\hat{\sigma}_l(0)|\Psi(0)\rangle$ vanish. This implies that $q_{EA} \to 0$ as $t \to \infty$. If, on the other hand, the spins are not thermalized, some information about the initial state is stored in local observables, and consequently $|q_{EA}| > 0$ as $t \to \infty$. This is demonstrated in Fig. 6.2 for different points in the phase diagram for $L = 8$ and $d = 7$. The corresponding points in the phase diagram are indicated by the vertical line. Deep in the localized regime ($\gamma_0 = 0.1$) the spin-glass order parameter remains close to its initial value of 1, whereas in the thermalizing regime ($\gamma_0 \geq 0.5$) it decays to 0. In the intermediate regime ($\gamma_0 = 0.3$) we find a slow decay. For $\gamma_0 = 0.3$ it is not clear if q_{EA} decays to zero as $t \to \infty$.

To discuss the dynamics of the qudit we consider the qudit occupation variance $\Delta_{\mathcal{Q}}^2$ defined as

$$\Delta_{\mathcal{Q}}^2 = \langle(\mu^z)^2\rangle - \langle\mu^z\rangle^2 . \tag{6.5}$$

This quantity measures the width of the qudit occupation, i.e. $\Delta_{\mathcal{Q}}^2 = 0$ if only one level of the qudit is occupied, whereas it assumes larger values if multiple levels are occupied. For a uniform distribution, for example, we have $\Delta_{\mathcal{Q}}^2 = (d^2 - 1)/12$. Considering this quantity is motivated by the effective Hamiltonian defined by Eq. (6.3). For large Ω the central qudit mediates an all-to-all interaction if its edge states are occupied. In most of our discussion we initialize the qudit in the middle state. Hence, a small value of $\Delta_{\mathcal{Q}}^2$ signals a small occupation of the edge states, and negligible all-to-all interaction. In [175] it was shown that in the weak coupling regime the spin glass parameter and the qudit occupation variance are linearly related. The proof employs secular perturbation theory, which is expected to be valid up to times $t \sim \mathcal{O}(\gamma^{-1})$, and results in the relation

$$\Delta_{\mathcal{Q}}^2 \approx \frac{L}{2}(1 - q_{EA}). \tag{6.6}$$

If the coupling γ scales with $L^{-1/2}$, this relation is expected to be valid up to times $t \sim \mathcal{O}(\sqrt{L})$, and thus, we expect that Eq. (6.6) is valid for longer times as the chain length is increased.

As a third indicator for MBL we consider the entanglement entropy of the left half spin chain, denoted in the following by S_A, with the remainder, consisting of the other half of the chain and the qudit. As discussed in the previous chapters, a common indication for MBL is the logarithmic increases of the entanglement entropy. This characteristic spreading of entanglement is caused by the interaction between different local integrals of motion (LIOM), which decays exponentially with the distance between different LIOMs. We note that in the centrally coupled spin system the intuitive explanation for the logarithmic increase of the entanglement entropy breaks down as there is no clear notion of distance between different LIOMs. Still it was demonstrated that it is possible to see the logarithmic growth

in centrally coupled systems [174].

In this chapter, we set $h = 1.3$, $g = 1.07$, $\Omega = \pi/0.8$. If the model with these parameters is mapped on to the corresponding Floquet system (i.e., $d \to \infty$), it shows a localization-delocalization transition at a critical coupling $\gamma_c \lesssim 0.33$. Furthermore we restrict ourselves to central qudit size $d = 7$, which is large enough to display Floquet-like behavior but small enough that the finite qudit size plays an important role. As the initial state of the spin chain we consider the "super-Néel" state $|\uparrow\uparrow\downarrow\downarrow ...\rangle$. If not stated otherwise, the qudit is initially always in the state $|4\rangle$. The initial wave function of the system $|\Psi(0)\rangle$ is thus given by

$$|\Psi(0)\rangle = |\uparrow\uparrow\downarrow\downarrow ...\rangle \otimes |4\rangle \,. \tag{6.7}$$

6.1.1 Methodology

In the following we explain and discuss the methodology we use to simulate the dynamics of the system. On the one hand we employ the ML-MCTDH approach to simulate the dynamics of the system. On the other hand, we use the perturbative master equation approach introduced in Sec. 3.3.2, to simulate the dynamics of the qudit in the weak coupling and large L limit, i.e. for $\gamma_0 \ll 1$ and $L \to \infty$.

To simulate the dynamics of the system consisting of the qudit and the spin chain we employ the multilayer multiconfiguration time-dependent Hartree (ML-MCTDH) approach. A general overview of this method is given in section 3.2. In the present application we separate the wave function in the highest layer into one part describing the qudit and one part describing the spin chain. The part describing the spin chain is then further expanded in a binary way up to blocks of 12 spins. As an example this decomposition is shown in Fig. 6.3 for $L = 48$. All results are converged on the time scales presented. We note that in general, the results are easier to converge, i.e. require less SPFs, if the coupling γ is smaller. Additionally, we note that in the thermalizing regime we only obtain converged results if the full basis of the Hilbert space is used. That means that for this parameter regime we are restricted to small systems sizes.

To investigate the dynamics of the qudit in the thermodynamic limit, i.e. for $L \to \infty$, we consider the spin chain as an environment and employ the time-convolutionless master equation to derive an equation of motion for the reduced density matrix of the qudit. Although the Hamiltonian of the environment, i.e. $\hat{H}_0$ defined in Eq. 6.1, includes an interaction between different environmental modes, it is easy to check that $\hat{H}_0$ fulfills all assumption of the proof presented in Sec. 3.3.1. Thus, the model fulfills linear response in the thermodynamic limit, and it is possible to construct a harmonic environment with an

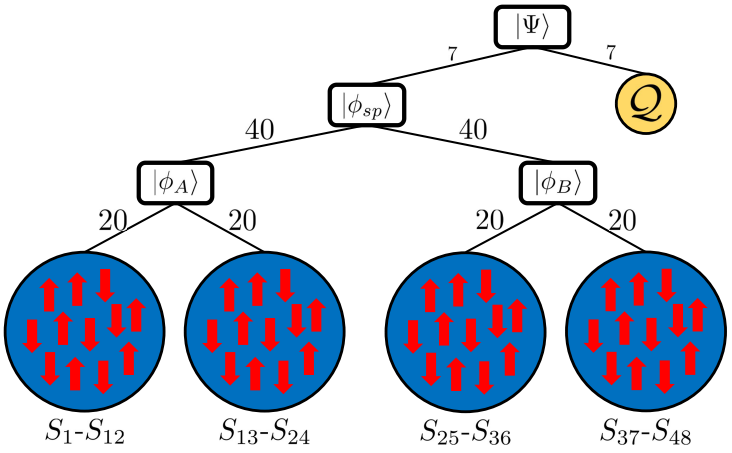

Figure 6.3: Tree representation of the ML-MCTDH wave function which we employ to propagate the wave function. In the first layer the wave function is separated into one part describing the qudit and one part describing the spin chain. The part describing the spin chain is then further expanded in a binary way up to blocks of 12 spins.

effective spectral density which leads to the same reduced qudit dynamics as the original environment as $L \to \infty$.

To do this we have to find a harmonic environment which results in the same force-force autocorrelation function defined as

$$C(t_1, t_2) = \frac{\gamma_0^2}{L} \sum_{l=1}^{L} \langle \Psi_{Env} | \hat{\sigma}_l^x(t_1) \hat{\sigma}_l^x(t_2) | \Psi_{Env} \rangle \,, \tag{6.8}$$

where $|\Psi_{Env}\rangle = |\uparrow\uparrow\downarrow\downarrow ...\rangle$ denotes the initial state of the spin chain. In general, the correlation function depends on the initial state of the spin chain, the interaction g, and the probability distribution of the local random fields. For the "super-Néel" state considered here a simple calculation shows that

$$C(t_1, t_2) = \gamma_0^2 \frac{\sin\Big(2h(t_1 - t_2)\Big)}{2h(t_1 - t_2)}, \tag{6.9}$$

where γ_0 is the unscaled coupling strength. For this particular initial state, the correlation function is thus independent of the antiferromagnetic interaction g. From this force-force autocorrelation function, the effective spectral density can be calculated as described in [101] yielding

$$J_{\text{eff}}(\omega) = \frac{\pi}{2} \frac{\gamma_0^2}{h} \chi_{[-2h,2h]}(\omega), \tag{6.10}$$

where χ_I is the characteristic function of the interval I, i.e. $\chi_I(\omega) = 1$ if $\omega \in I$ and 0 else. In the thermodynamic limit, i.e. $L \to \infty$, a harmonic environment with this spectral density

gives rise to the same reduced qudit dynamics as the environment consisting of the spins. We note that this statement is independent of the coupling strength γ_0.

Using the time-convolution less master equation up to second order introduced in Sec. 3.3.2, a master equation for the reduced state of the qudit can be derived reading

$$\partial_t \rho_{\mathcal{Q}}(t) = -i\Omega[\tau^z, \rho_{\mathcal{Q}}(t)] - \frac{\gamma_0^2}{\pi} k(t)[\tau^x, [\tau^-, \rho_{\mathcal{Q}}(t)]] - \frac{\gamma_0^2}{\pi} k^*(t)[\tau^x, [\tau^+, \rho_{\mathcal{Q}}(t)]], \quad (6.11)$$

where $k(t)$ is defined as

$$k(t) = \int_0^t C(\tau) \mathrm{e}^{i\Omega\tau} \mathrm{d}\tau, \quad (6.12)$$

with the bath correlation function $C(\tau)$ defined in terms of the effective spectral density $J_{\mathrm{eff}}(\omega)$ as

$$C(t) = \int J_{\mathrm{eff}}(\omega) \mathrm{e}^{-i\omega\tau} \mathrm{d}\omega. \quad (6.13)$$

This result allows us to investigate the qudit dynamics in the thermodynamic limit of the spin chain, i.e. $L \to \infty$.

6.2 Localized spin chain

We start the discussion with the regime in which the spin chain remains localized, even in the presence of long-range interactions. Following the discussion in the previous chapter, we expect this behavior for sufficiently weak coupling γ_0, which is indicated by a non-vanishing q_{EA}. In this section we investigate the weak and intermediate coupling regime, represented by the two diagonal lines in the schematic phase diagram in Fig. 6.2. Using the numerically exact results obtained from the ML-MCTDH approach and results obtained by the master equation approach, we discuss the dynamics and investigate the interplay between local and non-local interactions. The section is organized according to the two diagonal lines in the phase diagram in Fig. 6.2: in 6.2.1 we discuss the weak coupling regime, which corresponds to the lower diagonal line. The intermediate coupling regime, corresponding to the upper diagonal line, is subject to Sec. 6.2.2.

6.2.1 Weak coupling regime

We start our discussion in the weak coupling regime, i.e. $\gamma_0 \ll 1$. In Fig. 6.4 the spin glass parameter q_{EA} and the qudit variance are shown. Additionally, the scaled spin glass parameter is shown to demonstrate the validity of relation (6.6). All data are disorder averaged over $\mathcal{O}(10^1) - \mathcal{O}(10^2)$ realization. For larger system sizes fewer realization are

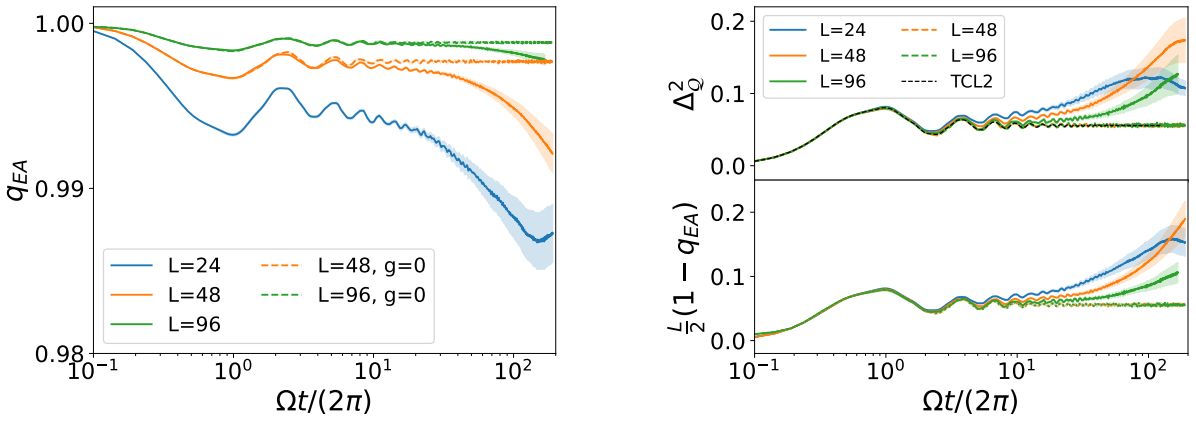

Figure 6.4: In the left panel, the spin glass order parameter q_{EA} is shown. The colored dashed lines represent the results for $g = 0$. In the right panel the qudit variance and the scaled spin glass order parameter are shown. The shaded area represents the error of the mean. The black dashed line represent the qudit variance obtained with the time-convolution less master equation with the effective spectral density. In all plots $\gamma_0 = 0.35$. The figures are taken from [175]. ©2021 American Physical Society.

needed. We first discuss the dynamics of the spin glass order parameter and the qudit variance. At $t = 0$, the spin glass parameter is one. On short time scales we find a decay of q_{EA} which is independent of the antiferromagnetic interaction g but depends on the system size. For increasing chain length the initial decay of q_{EA} becomes weaker. On longer time scales, $\Omega t/(2\pi) \gtrsim 2$, we find a slow decay of the spin glass parameter which is only present for $g \neq 0$. From this we conclude that the decay is induced by the antiferromagnetic interaction. This slow decay becomes weaker for increasing system size. We find a general trend of $q_{EA} \to 1$ as the system size is increased. Additionally the spin glass parameter is close to one ($q_{EA} > 0.98$) for all times and all system sizes considered. This suggests that for increasing system size the spin chain becomes more localized. This observation is supported by the formal expression of $\langle \hat{\sigma}_l^z(t) \rangle$, which reads

$$\langle \hat{\sigma}_l^z(t) \rangle = \langle \hat{\sigma}_l^z(0) \rangle + 2\gamma \int_0^t \langle \Psi(\tau) | (\hat{\mu}^+ + \hat{\mu}^-) \hat{\sigma}_l^x | \Psi(\tau) \rangle \, \mathrm{d}\tau, \tag{6.14}$$

where $|\Psi(t)\rangle$ is the wave function of the total system. Both operators appearing in the expectation value in the integral are bounded, and thus, the time-dependent expectation value $\langle \hat{\sigma}_l^z(t) \rangle$ is bounded by

$$\langle \hat{\sigma}_l^z(t) \rangle \leq \langle \hat{\sigma}_l^z(0) \rangle + 2\gamma C t. \tag{6.15}$$

Since $\gamma \sim L^{-1/2}$, we find that for a fixed time t the deviations of $\langle \hat{\sigma}_l^z(t) \rangle$ from its initial value decay with $L^{-1/2}$, or faster, as $L \to \infty$. We stress that this is only an upper bound on the scaling behavior. As we discuss later, our numerical data suggest that $q_{EA} \sim L^{-1}$ as $L \to \infty$.

The qudit occupation variance $\Delta_{\mathcal{Q}}^2$ exhibits an initial increase from zero to a small value ($\lesssim 0.1$), which is independent of the system size and the antiferromagnetic interaction. On longer time scales, $\Delta_{\mathcal{Q}}^2$ displays a slow increase which becomes weaker for increasing system size, similar to the slow decay of the spin glass parameter. For $g = 0$, the slow increase of the qudit occupation variance is absent. The results for $g = 0$ are independent of the system size and agree with the dynamics for $L \to \infty$ obtained with the time-convolution less master equation. In this regime (weak coupling γ_0), we expect that the master equation gives good results, i.e. the black line represents an accurate description of the qudit occupation variance for $L \to \infty$. In particular, the dynamics of the qudit become independent of the antiferromagnetic interaction in this limit. Hence, we expect that the dynamics of the qudit for $g \neq 0$ approach the results for $g = 0$ as $L \to \infty$. We emphasize at this point that, in contrast to the dynamics for $g \neq 0$, the results for $g = 0$ are converged with respect to the system size for $L = 96$. As suggested by Eq. (6.6) we find a good agreement between the qudit occupation variance and the scaled spin-glass parameter. In particular for $g = 0$ we find an almost perfect agreement on all time scales between the qudit variance and the scaled spin glass order parameter. The deviation of q_{EA} from 1 thus vanish with L^{-1} as $L \to \infty$, i.e. in the thermodynamic limit of $L \to \infty$ the spins of the chain remain localized.

We first explain the weak hybridization between the qudit and the spins for large L. This can be explained in terms of the effective spectral density. The support of the spectral density is $[-2h, 2h]$. The transition frequency of the qudit is Ω. For the chosen parameters we have $\Omega \approx 3h$, hence the spectral density has no weight at the transition frequency of the qudit, thus explaining the small hybridization. This exhibits similarities with the failure of *subsystem equilibration* described in the dynamics of the spin-boson model for the strong coupling regime of the gapped spectral density (see 4.2.3). In contrast to the situation in the spin-boson model, the Hamiltonian of the qudit does not induce dynamics, and thus, the state of the qudit is time-independent after the initial hybridization.

Next, we discuss the origin of the different time scales. The initial dynamics of both observables are independent of the antiferromagnetic interaction g. Thus, we conclude that these dynamics are induced by the hybridization of the qudit with each spin of the chain. The hybridization strength is determined by the coupling γ, i.e. the scaled coupling. Since this coupling is scaled with $L^{-1/2}$, the hybridization between a single spin and the qudit decreases as the system size increases, resulting in a weaker decay of q_{EA} for increasing chain length L is increased. Since the scaling of the coupling γ is chosen such that the overall influence of the environment is independent of the chain length, the qudit occupation variance on short times is independent of the system size. Since the second time scale is absent for $g = 0$, we conclude that it is induced by the antiferomagnetic interaction. The emergence of this slow time scale can be explained as follows. The state of the spin chain is

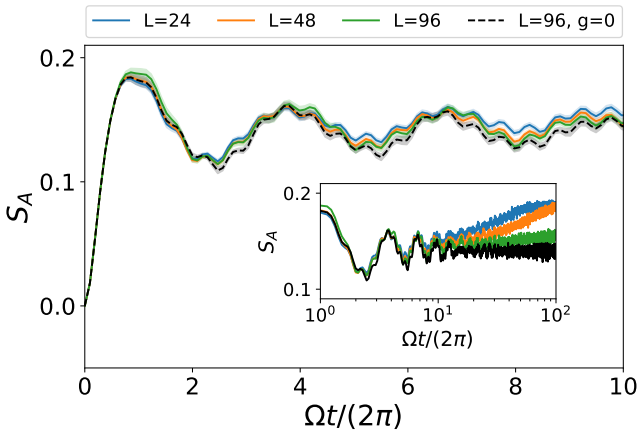

Figure 6.5: Half-chain entanglement entropy in the weak coupling regime, i.e. for $\gamma_0 = 0.35$. The shaded area represents the error of the mean. The main plot shows the short times, the inset shows the long time behavior. The black dashed line represents the results for $g = 0$.

initially in an eigenstate of H_0. Thus, the antiferromagnetic interaction within the spin chain do not entangle different spins in the chain. Due to the hybridization of the spins with the qudit the spins in the chains are tilted. In this situation the antiferromagnetic interaction can induce hybridization between different spins in the chain, resulting in a further delocalization of the spins, i.e. to a slow decay of q_{EA}. The tilting of the spins depends on the coupling γ. Since this scales with $L^{-1/2}$, this effect becomes weaker as the chain length is increased. More formally this can be phrased as follows: In the weak coupling regime the centrally coupled qudit induces partial flips of the spins in the chain, thus leading to a superposition of different spin patterns in the wave function. Since this is not an eigenstate of H_0 the antiferromagnetic interaction induces hybridization, thus leading to a further delocalization of the spins. From our results, however, we conclude that this is not sufficient to drive the spins towards a thermal equilibrium, since we find signature of localization, i.e. q_{EA} remains close to one, at all times considered.

A unique signature of many-body localization is the slow, logarithmic like growth of the entanglement entropy. To investigate the character of the localization we consider the entanglement entropy of one half of the spin chain with its remainder consisting of the other half and the qudit. In the following we denote this entanglement entropy with S_A. In Fig. 6.5 we show the short and long time dynamics of the entanglement entropy S_A. Let us first focus on the short time behavior of the entanglement entropy S_A, shown in the main plot of Fig. 6.5. On these time scales we find an increase of S_A, which is independent of the system size and the anti ferromagnetic interaction g. On longer time scales, shown in the inset, we find a slow increase of the entanglement entropy which is induced by the antiferromagnetic interaction g. The slope of this growth of the entanglement entropy decreases for increasing system size and approaches the results for $g = 0$. Following the discussion of the other two

observables we can assume that the results for $L = 96$ and $g = 0$ describe the results for $L \to \infty$.

As discussed above, the initial dynamics are induced by the hybridization between the qudit and the individual spins. The interaction between the individual spins and the qudit creates entanglement between them thus leading to an increase of S_A on short time scales. The scaling of the coupling γ is such that the influence of the spin chain on the qudit is independent of the system size, and thus, the initial increase of S_A is independent of the system size and of the antiferromagnetic interaction g. For the slow increase of the entanglement entropy we have two explanation. One possibility is that this increase is caused by the increased entanglement between the qudit and the spins, indicated by the increasing qudit variance $\Delta^2_{\mathcal{Q}}$ depicted in Fig. 6.4. A second possibility is that this increase is induced by the antiferromagnetic interaction along the spin chain. Based on our results we cannot exclude one or the other, leaving the origin of this slope as an open question.

6.2.2 Intermediate coupling regime

The discussion in the previous sections shows that for weak spin-qudit interaction the spin chain remains localized for all system sizes and time scales we considered. Furthermore, our analysis reveals that the delocalization of the spins is driven mostly by the local antiferromagnetic interaction and not by the long-range interaction mediated by the centrally coupled qudit. In the following we consider the intermediate coupling regime, $\gamma_0 = 1$, and investigate the stability of the localization with respect to increasing the spin-qudit coupling. In Fig. 6.6 the dynamics of the spin glass parameter q_{EA}, the qudit occupation variance $\Delta^2_{\mathcal{Q}}$, and the scaled spin glass parameter are shown. Qualitatively, the dynamics are similar to the above discussed weak coupling regime. On short time scales, the spin glass parameter exhibits an initial decay which depends on the system size, i.e. it becomes weaker for increasing system size. This decay is independent of the antiferromagnetic interaction, as the results for $g = 0$ and $g \neq 0$ coincide. On long time scales q_{EA} exhibits a slow decay for $g \neq 0$, which is absent for $g = 0$. Compared to the weak coupling regime, the spin glass parameter is significantly smaller, i.e. the spins are less localized for increasing coupling strength. As a function of the system size, however, we find a similar trend as in the weak coupling regime, i.e. $q_{EA} \to 1$ as $L \to \infty$. As the qualitative behavior is very similar to the weak coupling regime, the dynamics can be explained in a similar way: on short time scales the hybridization between the spins and the qudit induces a decay of q_{EA}. The strength of this hybridization is given by the scaled γ, and thus becomes weaker for increasing system size. On longer time scales the antiferromagnetic interaction leads to a hybridization of the spins along the chain. As the second mechanism is only present if the spins in the chain are entangled with the qudit, the second time scale becomes less pronounced as the system size increases and the effective coupling γ decreases.

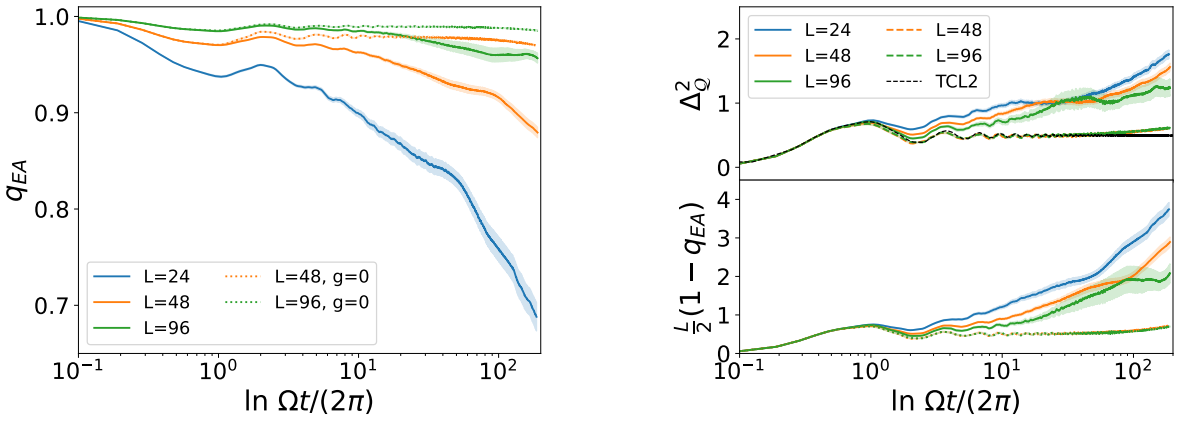

Figure 6.6: In the left plot the spin glass order parameter is shown for different chain length L. The colored dashed lines represent the results for $g = 0$. The shaded area represents the error of the mean. In the right plot the scaled spin glass order parameter and the qudit variance is shown to demonstrate their relation. The black dashed line represent the qudit variance obtained with the time-convolution less master equation with the effective spectral density. In these plots $\gamma_0 = 1$. The figures is reprinted from [175]. ©2021 American Physical Society.

The qudit occupation variance exhibits an initial increase. This initial increase is independent of the antiferromagnetic interaction and the system size. For long times we find an increase of Δ_Q^2, which is only observable for $g \neq 0$. Similarly to the dynamics of the spin glass order parameter the qualitative behavior of the occupation variance can be explained in the same way as in the weak coupling regime. We note, however, that the influence of the antiferromagnetic interaction can be seen on earlier times compared to the weak coupling regime. For $g = 0$, the dynamics of the occupation variance seem to be converged with respect to the system size. Since the results for $g \neq 0$ become independent of g in the thermodynamic limit, we expect that the results for non-vanishing antiferromagnetic interaction approach the results for $g = 0$ and $L = 96$ as $L \to \infty$. Furthermore, we find that the linear relation between q_{EA} and Δ_Q^2 seems to hold for $g = 0$, although it formally assumes a small coupling γ_0. From these two observations we conclude that in the thermodynamic limit the deviations of q_{EA} from one, i.e. $1 - q_{EA}$ scales with L^{-1} as $L \to \infty$ for $g \neq 0$. This demonstrates that in the thermodynamic limit the spin chain remains localized.

One notable difference to the weak coupling regime is that at long times ($\Omega t/(2\pi) \gtrsim 100$) the spin glass order parameter exhibits a slow decrease and the qudit variance exhibits a slow increase even for $g = 0$. This increase is not present in the perturbative solution obtained with the TCL2 master equation. As discussed previously, the weak hybridization between the qudit and its environment can be explained by the effective spectral density: the transition frequency of the qudit lies outside of the support of the spectral density. The coupling of the environment, however, induces a broadening of the transition frequency. Since this broadening is not included in the TCL2 master equation we assume that this broadening

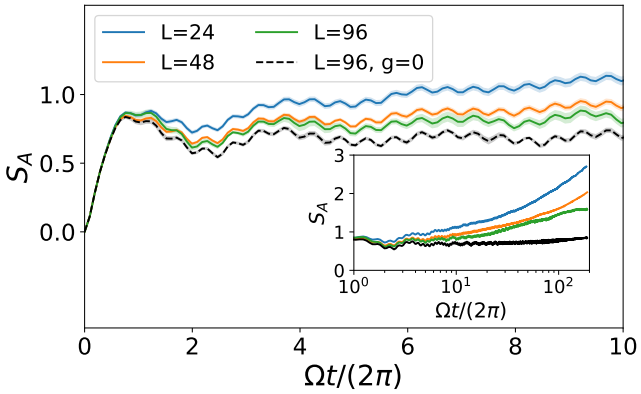

Figure 6.7: Half-chain entanglement entropy for intermediate coupling $\gamma_0 = 0.3$. The shaded area represents the error of the mean. The main plot shows the short times, the inset shows the long time behavior. The black dashed line represents the results for $g = 0$.

and the resulting hybridization of the qudit with its environment is the origin of the slow increase of Δ^2_{Q}, which we find for $g = 0$.

Last, we discuss the entanglement entropy S_A for the intermediate coupling $\gamma_0 = 1$, which is shown in Fig. 6.7. On short times the entanglement entropy exhibits an increase, which is independent of the system size and the anti ferromagnetic interaction. For $g \neq 0$ we find a second increase on a longer time scale. Similar to the weak coupling regime the increase becomes weaker as the system size increases. The reason for this is that the origin of this increase is the spin-spin interaction which can only influence the dynamics of the chain once the spins get entangled with the qudit. The influence of the antiferromagnetic interaction shifts to shorter times for increasing γ_0. Similarly to the dynamics of the spin glass parameter and the occupation variance, we find a slow increase of the entanglement entropy for $g = 0$ at long times ($\Omega t/(2\pi) \lesssim 50$).

We finish the discussion of the localized regime with some remarks. From the results presented here, we find that on the time scales accessible with ML-MCTDH the spin chain exhibits signatures of localization, i.e. the spins in the chain retains some information on these time scales. Furthermore, we find indications that for $\gamma_0 \lesssim 1$ the deviations of the spin glass parameter q_{EA} from one, which is a measure for the delocalization of the spins, vanishes as L^{-1} as $L \to \infty$.

6.3 Strong coupling regime: Thermalization induced by the qudit

In the previous section we discussed the weak and intermediate coupling regime. In these regimes, we find signatures of localization of the spins, i.e. for all times accessible with the ML-MCTDH approach and for all considered system sizes the spin glass parameter is

significantly larger than 0. Furthermore, we argued that for the scaled coupling γ the spin chain always approach localization in the thermodynamic limit $L \to \infty$. This originates from the fact that the initial state of the spin chain is a localized equilibrium state of the spin part of the Hamiltonian. In the thermodynamic limit, the influence of the qudit on the spin chain vanishes and the spins remain in their initial state.

According to the phase diagram, the system is expected to thermalize for a fixed system size L and sufficiently strong coupling between the qudit and the spin. This strong coupling regime, where the system is expected to thermalize, is analyzed in this section. Specifically, we consider the dynamics in the strong coupling regime of the system for fixed system size L. In thermalizing systems, the entanglement obeys an volume law, i.e. the entanglement entropy of a region in space tends to scale with the volume of the region. For the ML-MCTDH approach this implies that a large number of single-particle functions is required to accurately describe the wave function of the system (see discussion in Sec. 5.2). In order to obtain converged results in the strong coupling regime, we find numerically that we need to employ the full basis of the underlying Hilbert space. Thus, we are restricted to relatively small system sizes.

In the following, we discuss and analyze signatures of thermal behavior for a spin chain of length $L = 8$ and $L = 12$. To this end, we consider the spin glass parameter defined by Eq. (6.4), the local memory of a single spin, and the occupation of the qudit. To quantify the local memory of a single spin, we proceed in a similar way as in the previous chapter. We consider a single spin as an open system and calculate the corresponding dynamical map, i.e. we calculate the two quantities $\mathbf{M}(t)$ and $\mathbf{b}(t)$. As discussed in Sec. 2.5.3 the largest singular value of $\mathbf{M}(t)$ can be interpreted as the local memory of a subsystem. For a single disorder realization, the local memory is different for the different spins in the spin chain. The disorder averaged result describes the local memory of the considered spin averaged over different disorder realizations. Since the disorder average of the random local fields is uniform, the averaged local memory of a particular spin describes the average local memory of any spin.

We start our discussion with the dynamics of the spins. In Fig. 6.8 the spin glass parameter q_{EA} and the local memory is shown for $\gamma_0 = 3.5$. Initially, the spin glass order parameter is 1. For both system sizes q_{EA} exhibits a decay towards zero, which is an indication for the thermal behavior of the spins. For $L = 12$ the initial decay of q_{EA} is weaker than for $L = 8$. As discussed in the previous section, this initial decay is caused by the hybridization of the qudit with the spins whose strength is determined by γ. For $L = 12$ this coupling is smaller due to the scaling of the coupling, thus explaining the weaker initial decay. The asymptotic value of q_{EA} is zero for both system sizes, which is an indication for the thermal behavior of the system, i.e. the average correlation of a spin with its initial state is zero. At

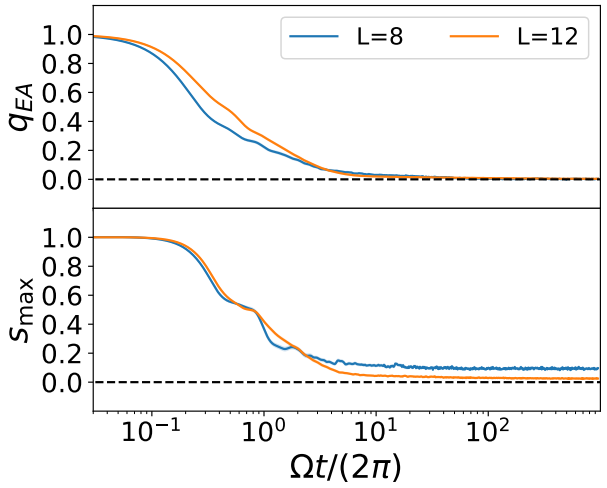

Figure 6.8: Spin glass parameter q_{EA} (upper plot) and the local memory of a single spin (lower plot) for $\gamma_0 = 3.5$. The shaded area represents the error of the mean. The qudit is initialized in the fourth state. Both quantities decay to zero, which is an indicator for the thermalization of the spins.

$t = 0$ the largest singular value of $s_{\max}$ is one. Similar to the overall decay of q_{EA} we find that $s_{\max}$ decays towards zero as $t \to \infty$. Compared to the initial decay of the spin glass parameter the initial decay of the largest singular value exhibits a delay. In the long time limit $s_{\max}$ decays to a value close to zero. In contrast to the asymptotic value of q_{EA} we find a dependence of the asymptotic value of $s_{\max}$ on the system size. For $L = 12$ the local memory is smaller compared to the asymptotic value of $L = 8$ as $t \to \infty$. For larger system sizes the local memory is smaller, which is the expected behavior for thermalizing systems. The results presented in Fig. 6.8 indicate that for fixed system size, the centrally coupled qudit is able to thermalize the spins for sufficiently strong coupling.

Next, we consider the dynamics of the qudit and investigate whether the qudit also thermalizes as $t \to \infty$. In order to discuss the asymptotic behavior of the qudit and to investigate the influence of the initial state of the qudit on its dynamics we show the qudit occupation for two different initial states of the qudit in Fig. 6.9. For both initial states of the qudit we find different time scales. The dynamics of the qudit on short time scales are similar for the two considered initial states: the occupation of the initial state n_i decreases and the occupation of the two neighboring states n_{i-1} and n_{i+1} increases. The initial dynamics are driven by the hybridization of the qudit and the spin chain. This interaction induces spin flips in the chain which are accompanied by a transition of the qudit from the level i to the levels $i - 1$ and $i + 1$. For intermediate times ($\Omega t/(2\pi) < 10^2$) the occupation of all levels increases and we find a rich dynamical behavior. On this time scale, the dynamics are different for the two different initial states. As $t \to \infty$ the occupation of the qudit saturates, i.e. the qudit relaxes to an equilibrium state. However, the asymptotic state of the qudit is different for the two different initial considered here. We conclude that the qudit equilibrates

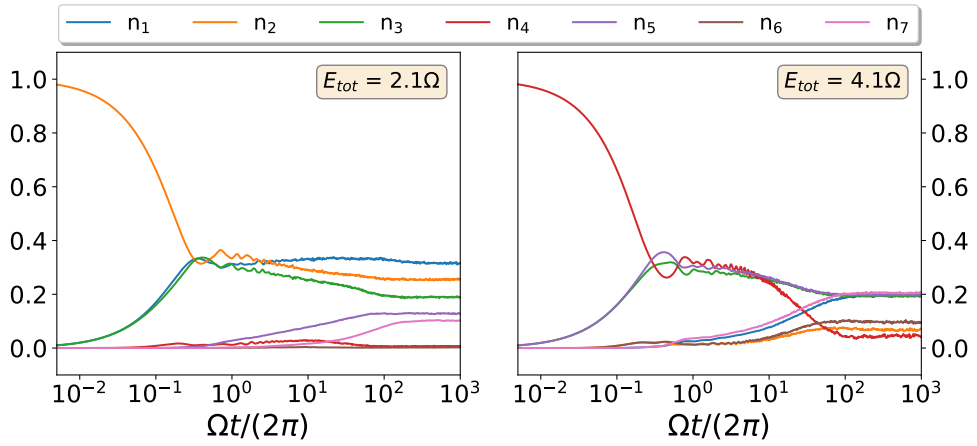

Figure 6.9: Occupation of the qudit levels n_i for different initial states of the qudit. The shaded area represents the error of the mean. In the left plot the qudit is initially in the second level, in the right plot the qudit is initially in the fourth level. In both situations the qudit occupation equilibrates, but the asymptotic occupation differs for the different initial situations.

but fails to thermalize as the equilibrium state violates the *subsystem state independence*.

We explain this violation of *subsystem state independence* by the dependence of the total energy on the qudit level spacing Ω. For the parameters considered here, Ω is the largest energy scale. One consequence of this is that the total energy depends significantly on the initial state of the qudit. For the two considered initial states, the total energy differs by a factor of 2 (see the boxes in Fig. 6.9). This implies that even if the system obeys the eigenstate thermalization hypothesis, i.e. expectation values of local operators are smooth functions of the energy of the system, the asymptotic state of the qudit can depend on its initial state as the total energy depends strongly on the initial state of the qudit. We note the qualitative behavior of the spins described above is independent of the initial state of the qudit, i.e. the two quantities q_{EA} and $s_{\max}$ decay to zero as $t \to \infty$ for both initial states of the qudit.

6.4 Summary

In this chapter we have investigated the stability of many-body localization with respect to long-range interactions mediated by a central degree of freedom. To this end we have analyzed the dynamics of a spin chain with random local fields and an antiferromagnetic nearest neighbor interaction in the presence of a centrally coupled d-level system, the qudit, in different parameter regimes.

In the weak and intermediate coupling regime we find numerical signatures of localization of the spins for all considered system sizes and times. Our analysis reveals that two mechanisms can lead to a delocalization of the spins. The first mechanism is the hybridization of the

spins with the qudit, the second one is the delocalization induced by the antiferromagnetic interaction. The second mechanism can only induce a delocalization if individual spins are entangled with the qudit. For the scaled spin-qudit coupling considered here, the second mechanism becomes weaker as the system size increases. Thus, in the thermodynamic limit the spins become localized for any γ_0, provided that the spin-qudit coupling is scaled as $L^{-1/2}$. Our analysis suggests that that the delocalization of the spins vanishes like L^{-1} in the thermodynamic limit.

For fixed system sizes and strong enough coupling γ_0 we find indications for the thermalization of the spins, i.e. the average autocorrelation of the spins at time t with its initial state vanishes and the local memory is small and decreases with the system size. For the qudit, on the other hand, we find non-thermal behavior. In particular we find a failure of *subsystem state independence*, which can be seen by the dependency of the asymptotic qudit occupation on the initial state of the qudit. This behavior is a consequence of the chosen parameters and is related to the large level spacing of the qudit: the total energy of the system depends significantly on the initial state of the qudit. Consequently, expectation values of local operators can depend on the initial state, even if the total system obeys the eigenstate thermalization hypothesis.

Here, we have considered the influence of a central degree of freedom on a phenomenological model of many-body localization. A possible next step is to investigate the influence of such a central degree of freedom on a system which is not trivially localized, such as the disordered XXZ Heisenberg spin chain discussed in the previous chapter.

7. Summary and Outlook

Thermalization describes the relaxation of a system, which is in a non-equilibrium state, to a thermal equilibrium state. Although a seemingly straightforward process, thermalization turns out to be a highly non-trivial phenomenon if investigated in terms of the basic dynamical laws of nature, prescribed by Newton's or Schrödinger's equation. In particular, the description of this problem within a fully quantum mechanical framework reveals a variety of interesting consequences, including an explanation of the statistical nature of thermalizing systems in terms of entanglement [5, 6, 13, 178] and a variety of non-thermal effects [22, 24, 42, 58]. In this thesis, we have contributed to different aspects of this highly topical field of research, by addressing several open questions. In Chap. 4 we investigated environment-induced effects and analyzed in which situations an environment can equilibrate or thermalize a system. In Chap. 5 we examined the local memory in thermal and non-thermal systems and the possibility to extract information about the dynamical behavior of the system from this. In Chap. 6 we investigated the stability of a many-body localization, with respect to long-range interactions. To address these questions and to focus on different aspects of thermalization separately, we considered the spin-boson model, the disordered XXZ Heisenberg spin chain, and a centrally coupled spin chain, respectively. Our analysis is based on a combination of analytic, numerical, and perturbative approaches. To calculate the time-dependent wave function and time-dependent expectation values, we employed exact diagonalization (ED) and the multilayer multiconfiguration time-dependent Hartree (ML-MCTDH) approach. The numerical results are supported with analytic results obtained from a perturbative treatment.

To discuss thermal and non-thermal behavior of the different systems, we considered the dynamics of subsystems, which is formally described by a linear, completely positive, trace preserving map, called the dynamical map. Based on properties of the dynamical map we have proposed a measure for the local memory in quantum systems (see Sec. 2.5.3), which can be used to detect thermal and non-thermal behavior. Using this measure a key feature of thermalizing systems can be investigated: As $t \to \infty$, no information about the initial state is stored in local observables, i.e. the reduced state of a subsystem becomes independent of its initial state. For certain parameters, all three models investigated exhibit this expected thermal behavior: In the weak coupling regime of the spin-boson, model the

spin relaxes to a unique stationary state (Sec. 4.2.1), in the thermal phase the local memory in the disordered XXZ Heisenberg spin chain decreases with L^{-1} (Sec. 5.3), and in the strong coupling regime of the centrally coupled spin chain, the spins lose their local memory (Sec. 6.3). On the other hand, the proposed measure can be used to detect two qualitatively different failures of thermalization: a violation of *subsystem state equilibration* and a violation of *subsystem state independence*. Both violations can be found if the remainder of the subsystem cannot act as a true environment for the subsystem. In the strong coupling regime of the spin-boson model with the gapped spectral density, discussed in Sec. 4.2.3, we have found a violation of *subsystem equilibration*. Examples for the violation of *subsystem state independence* are the localization of the spin-boson model discussed in Sec. 4.2.2, the many-body localization of the disordered XXZ Heisenberg spin chain discussed in Sec. 5.3, or the initial state dependence of the asymptotic state of the qudit in the centrally coupled spin chain in Sec. 6.3.

To understand thermalization it is crucial to understand environment-induced effects. In Chap. 4 we considered the spin-boson model as particularly simple model in which different environment-induced effects can be investigated. We focused on two effects: the ability to drive a subsystem towards a unique equilibrium state by inducing decoherence and dephasing (Sec. 4.2) and the ability to act as a memory for the subsystem thus leading to non-Markovian dynamics (Sec. 4.3). In the weak coupling regime of the spin-boson model we find clear indications that the environment thermalizes the spin, i.e. the asymptotic state becomes independent of the initial state of the spin. For strong spin-environment interaction different spectral densities give rise to different non-thermal behavior: A failure of *subsystem state independence* for the Ohmic spectral density and a failure of *Subsystem equilibration* for the gapped spectral density. Based on the measure for the local memory, the different asymptotic behaviors can be classified and investigated.

Another less well-understood effect of an environment is to act as a memory for a subsystem thus leading to non-Markovian dynamics. For the Ohmic spectral density and a particular initial state we analyzed memory effects in two different parameter regimes: a fast bath, i.e. $\omega_c \gg \Delta$, and the cross over regime $\omega_c \approx \Delta$. In the scaling limit, i.e. $\omega_c \gg \Delta$, we employed a perturbative analytic solution and the numerically exact ML-MCTDH approach to discuss memory effects and non-Markovian effects for a broad range of couplings strengths. Furthermore, we identified a non-analyticity of the non-Markovianity at $\alpha = 0$. The results show that the dynamics transition from non-Markov to Markovian as the decay of the spin changes from coherent to incoherent decay at $\alpha \approx 0.5$. Using our numerically exact results we tested the validity of an analytic solution and a perturbative master equation, and demonstrated certain limitations. For the particularly interesting cross over regime, $\omega_c \approx \Delta$, the analytic solution as well as the master equation are not valid and we have to use the

ML-MCTDH approach. In this regime we have found a complex, non-monotonic dependence of the non-Markovianity on the coupling strength.

In our analysis of Non-Markovian effects, we have focused on a particular pair of initial states. For future work, it is of interest to investigate the influence of the initial state on memory effects. For this, it might be beneficial to relate memory effects to the dynamical map itself. This would allow for a discussion of memory effects without analyzing the dynamics of the open system for particular initial states. Additionally, the influence of anharmonicities or interactions in the environment on the memory effects is an interesting continuation of this topic.

Many-body localization (MBL) is a known effect which prevents certain systems from reaching thermal equilibrium. In Chap. 5 we have analyzed local memory in thermalizing and many-body localized systems. To this end, we have considered the disordered XXZ-Heisenberg spin chain, a paradigmatic model which exhibits a transition from thermalizing to many-body localization as the disorder is increased. In the first part, 5.2, we have investigated the loss of local memory and have analyzed different delocalization mechanisms. On short and intermediate time scales the hybridization between the spins, induced by spin flips, lead to a loss of local memory. On longer time scales the antiferromagnetic interaction induces a slow decay of local memory, similar to the logarithmic time scale usually associated to many-body localization. Additionally, we have analyzed the local memory across the thermal to many-body localized transition. We have identified a slow decay of the local memory on a logarithmic time scale, similar to the logarithmic increase of the entanglement entropy, which is one of the indicators for many-body localization. For weak disorder strengths, $W \lesssim 2J$, the local memory distributes equally over the system size as $t \to \infty$, i.e. it scales approximately with L^{-1}. We have interpreted this as an indicator for thermal behavior. For stronger disorder, $2J - 3J \lesssim W$, the local memory scales slower than L^{-1} and it is not obvious how to classify this into either thermal or non-thermal behavior.

Our analysis was based on exact diagonalization, i.e. we have considered relatively small systems. It was recently pointed out that there is a regime in which thermalization in many-body localized systems can be induced by rare thermal regions. These regions are unlikely for small systems, but become more likely for increasing system sizes. For future works, it might be of interest to consider the effect of these rare thermal regions on the local memory. Similar to the discussion in [94], this can potentially be used to estimate the critical disorder strength of many-body localization for larger systems.

In the last chapter we have investigated the stability of many-body localization with respect to non-local interactions induced by a central degree of freedom. To this end, we have considered a disordered spin chain with nearest neighbor antiferromagnetic interaction and a centrally coupled degree of freedom. The central degree of freedom, the qudit

mediates long-range interactions. For weak qudit-spin coupling, we have found signatures of localization of the spin chain. In this regime, we have identified delocalization on short time scales induced by the qudit-spin coupling. The antiferromagnetic interaction in the spin chain lead to a further delocalization of the spins on a longer time scale. The hybridization between the spins and the qudit allows the antiferromagnetic interaction to delocalize the spins. As a consequence of the scaled qudit-spin coupling, signatures of delocalization of the spins vanish as L^{-1} as $L \to \infty$. Consequently, the spin chain remains localized in the limit $L \to \infty$, for any qudit-spin coupling strength. For fixed system size and large enough qudit-spin coupling we have found indications for the thermalization of the spins, i.e. the local memory decays towards zero as $t \to \infty$. The qudit state, on the other hand, equilibrates but violates the *subsystem state independence*. For the parameters considered here, the initial state of the qudit influences the total energy of system significantly, thus explaining the violation of *subsystem state independence*. Although the central degree of freedom drives the spins towards a unique equilibrium state, the spins fail to thermalize the qudit.

There are some unanswered questions, which need further investigations. First, we have identified a slow increase of the entanglement entropy. From the results presented here, we cannot decide if this is driven by the qudit-spin interaction or the delocalization induced by the antiferromagnetic interaction of the spins. Second, we have found a slow increase of the qudit variance, accompanied by a corresponding decay of the spin glass parameter for vanishing antiferromagnetic interaction. We have hypothesized that this is induced by a level broadening. To verify this, more sophisticated methods like the hierarchical equation of motion approach can be used [118–121]. Finally we note that the model we considered here is just a phenomenological model for many-body localization. An obvious continuation of this work is to investigate a centrally coupled XXZ Heisenberg spin chain, which exhibits a transition from thermal to many-body localized behavior.

Besides continuing the work in the different directions discussed above, there are other directions for further research. One possibility is to investigate memory effects for an environment which can be tuned from thermal to localized behavior, e.g. considering the disordered XXZ Heisenberg spin chain as an environment. Since memory effects can be investigated by the dynamics of the small system alone, this approach can potentially be used to classify systems into thermal or localized based on the induced non-Markovianity. Another interesting question is, whether it is possible to derive conditions for the dynamical map, which guarantee a unique stationary state. As was previously shown, non-degenerate energy gaps of the Hamiltonian guarantee *subsystem equilibration* and *bath state independence* [13]. It would be interesting to derive a similar condition which implies *subsystem state independence*.

Appendix

A Technical proofs

In this appendix we have collected the proofs for different equations we use to discuss physical aspects. The proofs presented in this section are purely technical and not necessary to understand the physical discussion.

A.1 Proof of the bound for $\delta_{1,2}(t;\hat{O})$

Here we prove the bound for the quantity $\delta_{1,2}(t;\hat{O})$ defined by Eq. (2.28) to quantify the influence of the initial state on the dynamics of an open system. The quantity for which we want to find an upper bound is denoted with $\delta_{1,2}(t;\hat{O})$ and is defined as

$$\delta_{1,2}(t;\hat{O}) = |\mathrm{tr}\{\hat{O}(\hat{\rho}^1(t) - \hat{\rho}^2(t))\}|, \tag{A.1}$$

where $\hat{O}$ is some observable of the open system, and $\hat{\rho}^{1/2}(t)$ denotes the time evolved density matrix corresponding to first/second initial state respectively . The difference between the two density matrices $\hat{\rho}^1(t)$ and $\hat{\rho}^2(t)$ can be written as

$$\hat{\rho}^1(t) - \hat{\rho}^2(t) = \frac{1}{2}\sum_{n=1}^{N^2-1}\Big(a_n^1(t) - a_n^2(t)\Big)T_n, \tag{A.2}$$

where $a_n^i(t) = \mathrm{tr}\{\hat{T}_n\rho^i\}$ and $\hat{T}_n$ are the generators of $\mathrm{SU}(N)$. We evaluate the trace in the eigenbasis of $\hat{O}$ yielding

$$\delta_{1,2}(t;\hat{O}) = \frac{1}{2}\Big|\sum_{n=1}^{N^2-1}\sum_{a=1}^{N}\Big(a_n^1(t) - a_n^2(t)\Big)o_a\,\langle o_a|\hat{T}_n|o_a\rangle\,\Big|. \tag{A.3}$$

Using the triangular inequality and rearranging the sums yields

$$\delta_{1,2}(t;O) \leq \frac{1}{2}\sum_{n=1}^{N^2-1}\Big|(a_n^1(t) - a_n^2(t))\Big|\sum_{a=1}^{N}|o_a|\,\Big|\,\langle o_a|T_n|o_a\rangle\,\Big| \tag{A.4}$$

Let $o_{\max}$ be the eigenvalue of $\hat{O}$ with the largest absolute value. The second sum is bounded by

$$\sum_{a=1}^{N} |o_a| \, \Big| \langle o_a|\hat{T}_n|o_a\rangle \Big| \leq |o_{\max}| \sum_{a=1}^{N} \Big| \langle o_a|\hat{T}_n|o_a\rangle \Big| \tag{A.5}$$

Similarly, it can be shown that the expectation value of $\hat{T}_n$ in an eigenstate of $\hat{O}$ is bounded by the eigenvalue of $\hat{T}_n$ with the largest eigenvalue, which in this case depends on n:

$$\Big| \langle o_a|\hat{T}_n|o_a\rangle \Big| \leq t_{n,\max} \tag{A.6}$$

From the definition of the generators of $\mathrm{SU}(N)$, see [46], it directly follows that $t_{n,\max}$ is bounded by $\sqrt{2}$. Using this, one obtains a bound for $\delta_{1,2}(t;\hat{O})$ reading

$$\delta_{1,2}(t;\hat{O}) \leq \frac{1}{2}|o_{\max}|\sqrt{2}N \sum_{n=1}^{N^2-1} |a_n^1(t) - a_n^2(t)| \tag{A.7}$$

where the factor N originates from the sum over the eigenbasis of $\hat{O}$. The remaining sum is the L^1 norm of the vector $\mathbf{a}^1(t) - \mathbf{a}^2(t)$, i.e.

$$\delta_{1,2}(t;\hat{O}) \leq \frac{1}{2}|o_{\max}|\sqrt{2}N \; ||\mathbf{a}^1(t) - \mathbf{a}^2(t)||_1. \tag{A.8}$$

To relate the distance between the time-dependent Bloch vectors to the initial distance we first employ that the sum norm of a vector $\vec{x}$ can be bounded by the Euclidean norm as $||\mathbf{x}||_1 \leq \sqrt{N}||\vec{x}||_2$. Using the singular value decomposition of $\mathbf{M}(t)$ one can write

$$||\mathbf{a}_n^1(t) - \mathbf{a}_n^2(t)||_2 = ||\mathbf{V}(t)\mathbf{S}(t)\mathbf{W}^T(t)\Big(\mathbf{a}^1(0) - \mathbf{a}^2(0)\Big)||_2. \tag{A.9}$$

Using the fact that $\mathbf{S}$ is a positive semidefinite diagonal matrix, it is easy to show that $||\mathbf{S}\mathbf{x}||_2 < s_{\max}||\mathbf{x}||_2$, where $s_{\max}$ is the largest diagonal element of $\mathbf{S}$. Using this, together with the fact that the Euclidean norm is invariant under orthogonal transformations one can write

$$\delta_{1,2}(t;\hat{O}) \leq \frac{N^{3/2}}{\sqrt{2}}|o_{\max}| \; s_{\max}(t) \; ||\mathbf{a}^1(0) - \mathbf{a}^2(0)||_2, \tag{A.10}$$

which finishes the proof of Eq. (2.29).

A.2 Weak coupling solution for the Bloch vector

Here, we present the analytic expression for the dynamical map for the Ohmic spectral density in the weak coupling and large ω_c limit. The two quantities $\mathbf{M}(t)$ and $\mathbf{b}(t)$ can be

derived from the analytic expression for the three components of the Bloch vector. They are given by

$$\langle\hat{\sigma}_x\rangle(t) = \mathrm{e}^{-\Gamma_{xx}t}\langle\hat{\sigma}_x\rangle(0) - \frac{\Gamma_x}{\Gamma_{xx}}(1-\mathrm{e}^{-\Gamma_{xx}t}) \tag{A.11}$$

$$\begin{aligned}\langle\hat{\sigma}_y\rangle(t) =& \mathrm{e}^{-\Gamma_{yy}/2t}\Bigg(\cos(\tilde{\Delta}t)\langle\hat{\sigma}_y\rangle(0) - \frac{\Gamma_{yy}}{2\tilde{\Delta}}\sin(\tilde{\Delta}t)\langle\hat{\sigma}_y\rangle(0) \\ &- \frac{2\Delta-\Gamma_{yz}}{\tilde{\Delta}}\sin(\tilde{\Delta}t)\langle\hat{\sigma}_z\rangle(0)\Bigg)\end{aligned} \tag{A.12}$$

$$\begin{aligned}\langle\hat{\sigma}_z\rangle(t) =& \mathrm{e}^{-\Gamma_{yy}/2t}\Bigg(\frac{2\Delta}{\tilde{\Delta}}\sin(\tilde{\Delta}t)\langle\hat{\sigma}_y\rangle(0) + \cos(\tilde{\Delta}t)\langle\hat{\sigma}_z\rangle(0) \\ &+ \frac{\Gamma_{yy}}{2\tilde{\Delta}}\sin(\tilde{\Delta}t)\langle\hat{\sigma}_z\rangle(0)\Bigg),\end{aligned} \tag{A.13}$$

where $\tilde{\Delta}$ denotes the renormalized frequency of the spin and is given by $\tilde{\Delta} = \frac{1}{2}\Big(8\Delta(2\Delta - \Gamma_{yz}) - \Gamma_{yy}^2\Big)^{1/2}$. These equations describe the time-evolution of the three components of the Bloch vector for weak coupling and large ω_c. The stationary rate approximation, leads to errors of the transient dynamics.

Using the analytic solution for the three components of the Bloch vector the action of the dynamical map, defined by the quantities $\mathbf{b}(t)$ and $\mathbf{M}(t)$ can be derived. The quantities $\mathbf{b}(t)$ and $\mathbf{M}(t)$ read

$$\mathbf{b}(t) = \Big(\tfrac{\Gamma_x}{\Gamma_{xx}}(1-\mathrm{e}^{-\Gamma_{xx}t}) \quad 0 \quad 0\Big)^T \tag{A.14}$$

$$\mathbf{M}(t) = \begin{pmatrix} \mathrm{e}^{-\Gamma_{xx}t} & 0 & 0 \\ 0 & \mathrm{e}^{-\Gamma_{yy}/2t}\Big(\cos(\tilde{\Delta}t) - \frac{\Gamma_{yy}}{2\tilde{\Delta}}\sin(\tilde{\Delta}t)\Big) & -\frac{2\Delta-\Gamma_{yz}}{\tilde{\Delta}}\mathrm{e}^{-\Gamma_{yy}/2t}\sin(\tilde{\Delta}t) \\ 0 & \frac{2\Delta}{\tilde{\Delta}}\mathrm{e}^{-\Gamma_{yy}/2t}\sin(\tilde{\Delta}t) & \mathrm{e}^{-\Gamma_{yy}/2t}\Big(\cos(\tilde{\Delta}t) + \frac{\Gamma_{yy}}{2\tilde{\Delta}}\sin(\tilde{\Delta}t)\Big) \end{pmatrix}. \tag{A.15}$$

Note that in this perturbative treatment, the time-evolution of $\langle\hat{\sigma}_y\rangle(t)$ and $\langle\hat{\sigma}_z\rangle(t)$ is independent of $\langle\hat{\sigma}_x\rangle(t)$, and thus $\mathbf{M}(t)$ is block diagonal. The singular values of $\mathbf{M}(t)$ are given by the square root of the eigenvalues of $\mathbf{M}^T(t)\mathbf{M}(t)$. Thus, the singular value which is associated to the dynamics of $\langle\hat{\sigma}_x\rangle$ is given by $\mathrm{e}^{-\Gamma_{xx}t}$. The other two singular values are obtained by diagonalizing the 2×2 block associated to the dynamics of $\langle\hat{\sigma}_y\rangle$ and $\langle\hat{\sigma}_z\rangle$. The two singular values $s_\pm(t)$ are given by

$$s_\pm(t) = \frac{\mathrm{e}^{-\Gamma_{yy}/2t}}{2}\Bigg(A(t) \pm \sqrt{A^2(t) - 4\,B(t)}\Bigg), \tag{A.16}$$

where we defined

$$A(t) = \left(\frac{\Gamma_{yy}^2}{2\tilde{\Delta}^2} + \frac{4\Delta^2}{\tilde{\Delta}^2} - \frac{(2\Delta - \Gamma_{yz})^2}{\tilde{\Delta}^2}\right)\sin^2(\tilde{\Delta}t) + 2\cos^2(\tilde{\Delta}t)$$

$$B(t) = \frac{\Gamma_{yy}^4}{8\tilde{\Delta}^4}\sin^4(\tilde{\Delta}t) - 2\frac{\Gamma_{yy}^2}{4\tilde{\Delta}^2}\sin^2(\tilde{\Delta}t)\cos^2(\tilde{\Delta}t) - \frac{4\Delta^2}{\tilde{\Delta}^2}\frac{(2\Delta - \Gamma_{yz})^2}{\tilde{\Delta}^2}\sin^4(\tilde{\Delta}t) + \cos^4(\tilde{\Delta}t)$$

Since $A(t)$ and $B(t)$ are periodic with period $2\tilde{\Delta}$, it follows that $s_{\pm}(t)$ are described by damped oscillations, where the damping is given by $\mathrm{e}^{-\Gamma_{yy}/2t}$ and the period of the oscillation is $2\tilde{\Delta}$. These two singular values describe the coherent decay of $\langle\hat{\sigma}_y\rangle(t)$ and $\langle\hat{\sigma}_z\rangle(t)$.

A.3 Symmetry of the spin-boson model and relation between different initial states

In this section we discuss how a symmetry of the spin-boson model can be employed to relate the dynamics of the spin for different initial states. To prove this, we first note that $\sigma_x^2 = \mathbf{1}$ and $\sigma_x^\dagger = \sigma_x$ holds, and thus the transformation $\hat{\tilde{O}} = \sigma_x \hat{O} \sigma_x$ is unitary. Expectation values are invariant under unitary transformations:

$$\begin{aligned}\langle\hat{\sigma}_i\rangle &= \mathrm{tr}\{\hat{\sigma}_x\hat{\sigma}_i\hat{\sigma}_x\hat{\sigma}_x\mathrm{e}^{-i\hat{H}t}\hat{\sigma}_x\hat{\sigma}_x\hat{\rho}(0)\hat{\sigma}_x\hat{\sigma}_x\mathrm{e}^{i\hat{H}t}\hat{\sigma}_x\} \\ &= \mathrm{tr}\{\hat{\tilde{\sigma}}_i\mathrm{e}^{-i\hat{\tilde{H}}t}\hat{\tilde{\rho}}(0)\mathrm{e}^{i\hat{\tilde{H}}t}\}.\end{aligned} \tag{A.17}$$

This transformation only acts on the Hilbert space of the spin, and thus, transforms only the spin operators. The transformed operators read

$$\hat{\sigma}_x^\dagger\hat{\sigma}_x\hat{\sigma}_x = \hat{\sigma}_x, \tag{A.18}$$

$$\hat{\sigma}_x^\dagger\hat{\sigma}_y\hat{\sigma}_x = -\hat{\sigma}_y, \tag{A.19}$$

$$\hat{\sigma}_x^\dagger\hat{\sigma}_z\hat{\sigma}_x = -\hat{\sigma}_z. \tag{A.20}$$

Using the relations (A.18), (A.19), and (A.20) the transformed Hamiltonian can be calculated yielding

$$\hat{\tilde{H}} = \hat{\sigma}_x^\dagger\hat{H}\hat{\sigma}_x = \Delta\hat{\sigma}_x + \hat{H}_B + \hat{\sigma}_z\sum_n(-c_n)\hat{q}_n, \tag{A.21}$$

where $\hat{H}_B$ denotes the Hamiltonian of the harmonic environment. The transformation only changes the sign of the couplings c_n. The properties of the environment which influences the dynamics of the spin are fully characterized by the spectral density [125, 126], which is

defined as

$$J(\omega) = \frac{\pi}{2} \sum_n \frac{c_n^2}{\omega_n} \delta(\omega - \omega_n). \tag{A.22}$$

Since the spectral density depends on the squared couplings, the two Hamiltonians $\hat{H}$ and $\hat{\tilde{H}}$ give rise to the same spectral density. Consequently, the reduced spin dynamics induced by $\hat{H}$ and $\hat{\tilde{H}}$ are equal.

Last, we discuss the action of the unitary transformation on the initial state. Any pair of initial states $\hat{\rho}_1$ and $\hat{\rho}_2$ which are represented by antipodal points on the great circle on the Bloch sphere through the north pole and the point $(1\ 0\ 0)^T$, are transformed into each other by the unitary transformation mediated by $\hat{\sigma}_x$. Thus, we conclude that for these pairs of initial states $\hat{\rho}_1$ and $\hat{\rho}_2$ the following holds for all times

$$\langle \hat{\sigma}_x \rangle_2 (t) = \langle \hat{\sigma}_x \rangle_1 (t) \tag{A.23}$$

$$\langle \hat{\sigma}_y \rangle_2 (t) = - \langle \hat{\sigma}_y \rangle_1 (t) \tag{A.24}$$

$$\langle \hat{\sigma}_z \rangle_2 (t) = - \langle \hat{\sigma}_z \rangle_1 (t). \tag{A.25}$$

In this case the trace distance can be written as

$$\mathcal{D}(t) = \sqrt{\langle \hat{\sigma}_z \rangle_1^2 + \langle \hat{\sigma}_y \rangle_1^2}. \tag{A.26}$$

A.4 Asymptotic behavior of the non-Markovianity in the spin-boson model

Here, we prove Eq. (4.20) which we use to analyze the asymptotic behavior of the summed non-Markovianity for the spin-boson model as $\alpha \to 0$. The starting point of the derivation is the analytic solution for the trace distance given by Eq. (4.17) and the property

$$\mathcal{D}(t + \frac{\pi}{\tilde{\Delta}}) = \mathrm{e}^{-\frac{\pi\gamma}{\tilde{\Delta}}} \mathcal{D}(t) \tag{A.27}$$

Since this holds for all times t, the same holds for the derivative of the trace distance $\sigma(t) = \partial_t \mathcal{D}(t)$. Assuming that the non-Markovianity $\mathcal{N}$ is finite, which is true for all parameters considered here, the defining integral of $\mathcal{N}$ can be partitioned as

$$\mathcal{N} = \sum_{n=0}^{\infty} \int_{\substack{0 \\ \sigma>0}}^{\pi/\tilde{\Delta}} \mathrm{d}t\ \sigma\Big(n\frac{\pi}{\tilde{\Delta}} + t\Big). \tag{A.28}$$

Employing property (A.27), this can be written as

$$\mathcal{N} = \sum_{n=0}^{\infty} \mathrm{e}^{-n\pi\gamma/\tilde{\Delta}} \int_{\substack{0 \\ \sigma>0}}^{\pi/\tilde{\Delta}} \mathrm{d}t\ \sigma(t), \tag{A.29}$$

where the integral measures the information back flow during the first period of the time evolution. Let $I \subset [t, t+\pi/\tilde{\Delta}]$ denote the times at which $\sigma(t) > 0$. For simplicity, we assume that I consists of a single, connected interval. This is true for the analytic solution given by Eq. (4.17). In the following we denote with $t_{\min}$ and $t_{\max}$ the lower and upper end of the interval I, respectively. From the fundamental theorem of calculus it then follows that

$$\mathcal{N} = \sum_{n=0}^{\infty} \mathrm{e}^{-n\pi\gamma/\tilde{\Delta}} \underbrace{\Big(\mathcal{D}(t_{\max}) - \mathcal{D}(t_{\min})\Big)}_{\mathcal{N}_1}. \tag{A.30}$$

Since $\pi\gamma/\tilde{\Delta} > 0$ the geometric series can be resumed resulting in

$$\mathcal{N} = \frac{\mathcal{N}_1}{1 - \mathrm{e}^{-\pi\gamma/\tilde{\Delta}}}, \tag{A.31}$$

which represents the resumed expression for the non-Markovianity used in Sec. 4.3.

B Experimental realization of the spin-boson model

The gapped spectral density considered in Sec. 4.2.3 originates from an experimental realization of the spin-boson model using trapped ions [131]. Using a linear Paul trap a spin-boson model with up to five bosonic degrees of freedom was realized. The distinct feature of the experiment is that the smallest frequency of the bosonic environment is determined by the frequency of the trap, and is thus always larger than zero. We consider the the continuum limit of the experimental spectral density which is derived as follows. The spectral density of the five ion model is given by

$$J_5(\omega) = \frac{\pi}{4}\alpha \sum_{n=1}^{5} \omega_n \mathcal{M}_n^2 \delta(\omega - \omega_n), \tag{B.1}$$

where ω_n and $\mathcal{M}_n$ are determined from experimental parameters and the geometry of the trap [129–131]. α denotes the coupling strength between the spin and the environment. To study the dynamics for different coupling strengths α, we fit the experimental parameters for $J_5(\omega)/\alpha$ with the function

$$J_{\mathrm{fit}}(\omega) = \frac{\pi}{4} a(\omega - b)\mathrm{e}^{-\left(\frac{\omega-b}{c}\right)^3}, \tag{B.2}$$

where a, b and c are fitting parameters. The gapped spectral density we consider is thus given by

$$J_G(\omega/\omega_1) = \alpha\frac{\pi}{4}a(\omega - b)\mathrm{e}^{-\left(\frac{\omega-b}{c}\right)^3}, \tag{B.3}$$

where α denotes the coupling strength, and $(a, b, c) = (0.677, 0.541, 1.280)$.

Bibliography

[1] V. I. Arnold and A. Avez, *Ergodic problems of classical mechanics*, New York, Benjamin, 1968.

[2] J. L. Lebowitz and O. Penrose, *Physics today* **26**, 23 (1973).

[3] L. Reichl, *A Modern Course in Statistical Physics*, John Wiley & Sons, 2nd edition, 1997.

[4] N. Simányi, *Ergod. Theory Dyn. Syst.* **19**, 741–766 (1999).

[5] J. M. Deutsch, *Phys. Rev. A* **43**, 2046 (1991).

[6] M. Srednicki, *Phys. Rev. E* **50**, 888 (1994).

[7] J. M. Deutsch, *Rep. Prog. Phys.* **81**, 082001 (2018).

[8] M. Rigol, V. Dunjko, and M. Olshanii, *Nature* **452**, 854 (2008).

[9] R. Steinigeweg, A. Khodja, H. Niemeyer, C. Gogolin, and J. Gemmer, *Phys. Rev. Lett.* **112**, 130403 (2014).

[10] W. Beugeling, R. Moessner, and M. Haque, *Phys. Rev. E* **89**, 042112 (2014).

[11] H. Kim, T. N. Ikeda, and D. A. Huse, *Phys. Rev. E* **90**, 052105 (2014).

[12] R. Mondaini, K. R. Fratus, M. Srednicki, and M. Rigol, *Phys. Rev. E* **93**, 032104 (2016).

[13] N. Linden, S. Popescu, A. J. Short, and A. Winter, *Phys. Rev. E* **79**, 061103 (2009).

[14] C. Gogolin and J. Eisert, *Rep. Prog. Phys.* **79**, 056001 (2016).

[15] P. Reimann, *Phys. Rev. Lett.* **101**, 190403 (2008).

[16] M. Cramer and J. Eisert, *New J. Phys.* **12**, 055020 (2010).

[17] A. J. Short and T. C. Farrelly, *New J. Phys.* **14**, 013063 (2012).

[18] P. Reimann and M. Kastner, *New J. Phys.* **14**, 043020 (2012).

[19] M. Rigol, A. Muramatsu, and M. Olshanii, *Phys. Rev. A* **74**, 053616 (2006).

[20] M. A. Cazalilla, *Phys. Rev. Lett.* **97**, 156403 (2006).

[21] M. Kollar and M. Eckstein, *Phys. Rev. A* **78**, 013626 (2008).

[22] P. W. Anderson, *Phys. Rev.* **109**, 1492 (1958).

[23] I. V. Gornyi, A. D. Mirlin, and D. G. Polyakov, *Phys. Rev. Lett.* **95**, 206603 (2005).

[24] D. Basko, I. Aleiner, and B. Altshuler, *Annals of Physics* **321**, 1126 (2006).

[25] M. Serbyn, Z. Papić, and D. A. Abanin, *Phys. Rev. Lett.* **111**, 127201 (2013).

[26] D. A. Huse, R. Nandkishore, and V. Oganesyan, *Phys. Rev. B* **90**, 174202 (2014).

[27] J. Z. Imbrie, *J. Stat. Phys.* **163**, 998 (2016).

[28] M. Schreiber, S. S. Hodgman, P. Bordia, H. P. Lüschen, M. H. Fischer, R. Vosk, E. Altman, U. Schneider, and I. Bloch, *Science* **349**, 842 (2015).

[29] J.-y. Choi, S. Hild, J. Zeiher, P. Schauß, A. Rubio-Abadal, T. Yefsah, V. Khemani, D. A. Huse, I. Bloch, and C. Gross, *Science* **352**, 1547 (2016).

[30] M. Schulz, R. Hooley, C. A. ad Moesser, and F. Pollmann, *Phys. Rev. Lett.* **122**, 040606 (2019).

[31] S. Iyer, V. Oganesyan, G. Refael, and D. A. Huse, *Phys. Rev. B* **87**, 134202 (2013).

[32] M. Thoss, H. Wang, and W. H. Miller, *J. Chem. Phys.* **115**, 2991 (2001).

[33] H. Wang and M. Thoss, *J. Phys. Chem. A* **111**, 10369 (2007).

[34] H. Wang and M. Thoss, *New J. Phys.* **10**, 115005 (2008).

[35] H. Wang and J. Shao, *J. Chem. Phys.* **137**, 22A504 (2012).

[36] H. Wang and J. Shao, *J. Phys. Chem. A* **123**, 1882 (2019).

[37] E. Davies, *Quantum Theory of Open Systems*, Academic Press, London, 1976.

[38] R. Alicki and K. Lendi, *Quantum Dynamical Semigroups and Applications*, Lecture Notes in Physics, Springer Berlin Heidelberg, 2007.

[39] H.-P. Breuer and F. Petruccione, *The Theory of Open Quantum Systems*, Oxford University Press, Oxford, 2007.

[40] H. Spohn, *Rept. Math. Phys.* **10**, 189 (1976).

[41] H. Spohn, *Lett Math Phys* **2**, 33 (1977).

[42] D. A. Lidar, I. L. Chuang, and K. B. Whaley, *Phys. Rev. Lett.* **81**, 2594 (1998).

[43] F. Bloch, *Phys. Rev.* **70**, 460 (1946).

[44] F. T. Hioe and J. H. Eberly, *Phys. Rev. Lett.* **47**, 838 (1981).

[45] K. Lendi, *Phys. Rev. A* **34**, 662 (1986).

[46] G. Kimura, *Physics Letters A* **314**, 339 (2003).

[47] G. Kimura and A. Kossakowski, *Open Syst. Inf. Dyn.* **12**, 207 (2005).

[48] L. Jakóbczyk and M. Siennicki, *Phys. Lett. A* **286**, 383 (2001).

[49] M. S. Byrd and N. Khaneja, *Phys. Rev. A* **68**, 062322 (2003).

[50] K. Kraus, A. Böhm, J. Dollard, and W. Wootters, *States, Effects, and Operations: Fundamental Notions of Quantum Theory*, Lecture Notes in Physics, Vol. 190 (Springer, Berlin), 1983.

[51] M. A. Nielsen and I. L. Chuang, *Quantum Computation and Quantum Information*, Cambridge University Press, Cambridge,England, 2000.

[52] L. F. Santos and M. Rigol, *Phys. Rev. E* **81**, 036206 (2010).

[53] M. Rigol and L. F. Santos, *Phys. Rev. A* **82**, 011604 (2010).

[54] L. D'Alessio, Y. Kafri, A. Polkovnikov, and M. Rigol, *Adv. Phys.* **65**, 239 (2016).

[55] R. Nandkishore and D. A. Huse, *Annu. Rev. Condens. Matter Phys.* **6**, 15 (2015).

[56] M. C. Bañuls, J. I. Cirac, and M. B. Hastings, *Phys. Rev. Lett.* **106**, 050405 (2011).

[57] S. Chakravarty, *Phys. Rev. Lett.* **49**, 681 (1982).

[58] A. J. Bray and M. A. Moore, *Phys. Rev. Lett.* **49**, 1545 (1982).

[59] T. J. G. Apollaro, C. Di Franco, F. Plastina, and M. Paternostro, *Phys. Rev. A* **83**, 032103 (2011).

[60] E. Y. Wilner, H. Wang, G. Cohen, M. Thoss, and E. Rabani, *Phys. Rev. B* **88**, 045137 (2013).

[61] E. T. Jaynes, *Phys. Rev.* **106**, 620 (1957).

[62] E. T. Jaynes, *Phys. Rev.* **108**, 171 (1957).

[63] J.-S. Caux and J. Mossel, *J. Stat. Mech.* **2011**, P02023 (2011).

[64] M. Rigol, V. Dunjko, V. Yurovsky, and M. Olshanii, *Phys. Rev. Lett.* **98**, 050405 (2007).

[65] T. Langen, S. Erne, R. Geiger, B. Rauer, T. Schweigler, M. Kuhnert, W. Rohringer, I. E. Mazets, T. Gasenzer, and J. Schmiedmayer, *Science* **348**, 207 (2015).

[66] J. Z. Imbrie, V. Ros, and A. Scardicchio, *Ann. Phys.* **529**, 1600278 (2017).

[67] A. Chandran, I. H. Kim, G. Vidal, and D. A. Abanin, *Phys. Rev. B* **91**, 085425 (2015).

[68] J. H. Bardarson, F. Pollmann, and J. E. Moore, *Phys. Rev. Lett.* **109**, 017202 (2012).

[69] D. A. Abanin, E. Altman, I. Bloch, and M. Serbyn, *Rev. Mod. Phys.* **91**, 021001 (2019).

[70] B. Sutherland, *Beautiful Models: 70 Years of Exactly Solved Quantum Many-body Problems*, World Scientific, 2004.

[71] T. Guhr, A. Müller–Groeling, and H. A. Weidenmüller, *Phys. Rep.* **299**, 189 (1998).

[72] A. A. Abul-Magd and A. Y. Abul-Magd, *Physica A* **396**, 185 (2014).

[73] E. P. Wigner, *Ann. Math.* **62**, 548 (1955).

[74] E. P. Wigner, *Ann. Math.* **65**, 203 (1957).

[75] E. P. Wigner, *Ann. Math.* **67**, 325 (1958).

[76] F. J. Dyson, *J. Math. Phys.* **3**, 140 (1962).

[77] M. V. Berry, M. Tabor, and J. M. Ziman, *Proc. R. Soc. Lond.* **356**, 375 (1977).

[78] O. Bohigas, M. J. Giannoni, and C. Schmit, *Phys. Rev. Lett.* **52**, 1 (1984).

[79] D. Wintgen and H. Friedrich, *Phys. Rev. A* **35**, 1464 (1987).

[80] A. R. Kolovsky and A. Buchleitner, *EPL* **68**, 632 (2004).

[81] Y. Y. Atas, E. Bogomolny, O. Giraud, and G. Roux, *Phys. Rev. Lett.* **110**, 084101 (2013).

[82] V. Oganesyan and D. A. Huse, *Phys. Rev. B* **75**, 155111 (2007).

[83] M. Serbyn and J. E. Moore, *Phys. Rev. B* **93**, 041424 (2016).

[84] P. Sierant and J. Zakrzewski, *Phys. Rev. B* **99**, 104205 (2019).

[85] B. Eckhardt, *Phys. Rep.* **163**, 205 (1988).

[86] M. Rigol, *Phys. Rev. Lett.* **103**, 100403 (2009).

[87] B. Bauer and C. Nayak, *J. Stat. Mech.* **2013**, P09005 (2013).

[88] A. Pal and D. A. Huse, *Phys. Rev. B* **82**, 174411 (2010).

[89] G. De Tomasi, S. Bera, J. H. Bardarson, and F. Pollmann, *Phys. Rev. Lett.* **118**, 016804 (2017).

[90] D. J. Luitz, F. m. c. Huveneers, and W. De Roeck, *Phys. Rev. Lett.* **119**, 150602 (2017).

[91] P. Ponte, C. R. Laumann, D. A. Huse, and A. Chandran, *Phil. Trans. R. Soc. A* **375**, 20160428 (2017).

[92] W. De Roeck and F. Huveneers, *Phys. Rev. B* **95**, 155129 (2017).

[93] T. Thiery, F. Huveneers, M. Müller, and W. De Roeck, *Phys. Rev. Lett.* **121**, 140601 (2018).

[94] A. Morningstar, L. Colmenarez, V. Khemani, D. J. Luitz, and D. A. Huse, *Phys. Rev. B* **105**, 174205 (2022).

[95] S. Edwards and P. Anderson, *J. Phys. Condens. Matter* **5**, 965 (1975).

[96] H. Kim and D. A. Huse, *Phys. Rev. Lett.* **111**, 127205 (2013).

[97] R. Vosk, D. A. Huse, and E. Altman, *Phys. Rev. X* **5**, 031032 (2015).

[98] M. Žnidarič, T. Prosen, and P. Prelovšek, *Phys. Rev. B* **77**, 064426 (2008).

[99] A. Smirne, E.-M. Laine, H.-P. Breuer, J. Piilo, and B. Vacchini, *New J. Phys.* **14**, 113034 (2012).

[100] A. Kossakowski, *Open Syst. Inf. Dyn.* **10**, 213 (2003).

[101] N. Makri, *J. Phys. Chem. B* **103**, 2823 (1999).

[102] D. N. Page, *Phys. Rev. Lett.* **71**, 1291 (1993).

[103] R. Orus, *Annals of Physics* **349**, 117 (2014).

[104] G. Vidal, *Phys. Rev. Lett.* **91**, 147902 (2003).

[105] G. Vidal, *Phys. Rev. Lett.* **93**, 040502 (2004).

[106] D. Gobert, C. Kollath, U. Schollwöck, and G. Schütz, *Phys. Rev. E* **71**, 036102 (2005).

[107] S. Paeckel, T. Köhler, A. Swoboda, S. R. Manmana, U. Schollwöck, and C. Hubig, *Ann. Phys.* **411**, 167998 (2019).

[108] H. Wang and M. Thoss, *J. Chem. Phys.* **119**, 1289 (2003).

[109] U. Manthe, *J. Chem. Phys.* **128**, 164116 (2008).

[110] O. Vendrell and H.-D. Meyer, *J. Chem. Phys.* **134**, 044135 (2011).

[111] H. Wang, *J. Phys. Chem. A* **119**, 7951 (2015).

[112] J. Frenkel, *Wave Mechanics*, Oxford: Clarendon, 1934.

[113] S. Nakajima, *Prog. Theor. Phys.* **20**, 948 (1958).

[114] R. Zwanzig, *J. Chem. Phys.* **33**, 1338 (1960).

[115] H. Mori, *Prog. Theor. Phys.* **33**, 423 (1965).

[116] F. Shibata, Y. Takahashi, and N. Hashitsume, *J. Stat. Phys.* **17**, 171 (1977).

[117] S. Chaturvedi and F. Shibata, *Z. Phys. B* **35**, 297 (1979).

[118] Y. Tanimura and R. Kubo, *J. Phys. Soc. Jpn.* **58**, 101 (1989).

[119] Y. Tanimura, *Phys. Rev. A* **41**, 6676 (1990).

[120] J. Jin, X. Zheng, and Y. Yan, *J. Chem. Phys.* **128**, 234703 (2008).

[121] Y. Ke, R. Borrelli, and M. Thoss, *J. Chem. Phys.* **156**, 194102 (2022).

[122] R. Feynman and F. Vernon, *Ann. Phys.* **24**, 118 (1963).

[123] J. Shao and P. Hänggi, *Phys. Rev. Lett.* **81**, 5710 (1998).

[124] J. Okamoto, L. Mathey, and R. Härtle, *Phys. Rev. B* **94**, 235411 (2016).

[125] A. J. Leggett, S. Chakravarty, A. T. Dorsey, M. P. Fisher, A. Garg, and W. Zwerger, *Rev. Mod. Phys.* **59**, 1 (1987).

[126] U. Weiss, *Quantum Dissipative Systems*, World Scientific, Singapore, 2nd edition, 1999.

[127] R. A. Marcus and N. Sutin, *Biochim. Biophys. Acta* **811**, 265 (1985).

[128] U. Weiss, H. Grabert, and S. Linkwitz, *J. Low Temp. Phys.* **68**, 213 (1987).

[129] D. Porras and J. I. Cirac, *Phys. Rev. Lett.* **92**, 207901 (2004).

[130] D. Porras, F. Marquardt, J. von Delft, and J. I. Cirac, *Phys. Rev. A* **78**, 010101 (2008).

[131] G. Clos, D. Porras, U. Warring, and T. Schaetz, *Phys. Rev. Lett.* **117**, 170401 (2016).

[132] H. Spohn, *Commun.Math. Phys.* **123**, 277 (1989).

[133] R. A. Harris and R. Silbey, *J. Chem. Phys.* **78**, 7330 (1983).

[134] I. de Vega, U. Schollwöck, and F. A. Wolf, *Phys. Rev. B* **92**, 155126 (2015).

[135] H. Wang and M. Thoss, *Chem. Phys.* **370**, 78 (2010).

[136] R. Silbey and R. A. Harris, *J. Chem. Phys.* **80**, 2615 (1984).

[137] R. A. Harris and R. Silbey, *J. Chem. Phys.* **83**, 1069 (1985).

[138] S. V. Tyablikov, *Methods in the Quantum Theory of Magnetism*, Springer New York, NY, 1967.

[139] A. L. Kuzemsky, *Int. J. Mod. Phys. B* **29**, 1530010 (2015).

[140] S. Wenderoth, H.-P. Breuer, and M. Thoss, *Phys. Rev. A* **104**, 012213 (2021).

[141] G. Clos and H.-P. Breuer, *Phys. Rev. A* **86**, 012115 (2012).

[142] L. Kidon, H. Wang, M. Thoss, and E. Rabani, *J. Chem. Phys.* **149**, 104105 (2018).

[143] M. M. Wolf, J. Eisert, T. S. Cubitt, and J. I. Cirac, *Phys. Rev. Lett.* **101**, 150402 (2008).

[144] A. Rivas, S. F. Huelga, and M. B. Plenio, *Phys. Rev. Lett.* **105**, 050403 (2010).

[145] D. Chruściński, A. Kossakowski, and A. Rivas, *Phys. Rev. A* **83**, 052128 (2011).

[146] S. Luo, S. Fu, and H. Song, *Phys. Rev. A* **86**, 044101 (2012).

[147] A. Rivas, S. F. Huelga, and M. B. Plenio, *Rep. Prog. Phys.* **77**, 094001 (2014).

[148] H.-P. Breuer, E.-M. Laine, J. Piilo, and B. Vacchini, *Rev. Mod. Phys.* **88**, 021002 (2016).

[149] I. de Vega and D. Alonso, *Rev. Mod. Phys.* **89**, 015001 (2017).

[150] H.-P. Breuer, E.-M. Laine, and J. Piilo, *Phys. Rev. Lett.* **103**, 210401 (2009).

[151] E.-M. Laine, J. Piilo, and H.-P. Breuer, *Phys. Rev. A* **81**, 062115 (2010).

[152] L. Li, M. J. W. Hall, and H. M. Wiseman, *Phys. Rep.* **759**, 1 (2018).

[153] C. A. Fuchs and J. van de Graaf, *IEEE Trans. Inf. Theory* **45**, 1216 (1999).

[154] M. B. Ruskai, *Rev. Math. Phys.* **06**, 1147 (1994).

[155] S. Wißmann, A. Karlsson, E.-M. Laine, J. Piilo, and H.-P. Breuer, *Phys. Rev. A* **86**, 062108 (2012).

[156] J. Smith, A. Lee, P. Richerme, B. Neyenhuis, P. W. Hess, P. Hauke, M. Heyl, D. A. Huse, and C. Monroe, *Nat. Phys.* **12**, 907 (2016).

[157] S. S. Roy, U. Mishra, and D. Rakshit, *EPL* **129**, 30005 (2020).

[158] A. Nico-Katz, A. Bayat, and S. Bose, *Phys. Rev. B* **105**, 205133 (2022).

[159] P. Jordan and E. Wigner, *Z. Phys.* **47**, 631 (1928).

[160] P. Hauke and M. Heyl, *Phys. Rev. B* **92**, 134204 (2015).

[161] D. J. Luitz, N. Laflorencie, and F. Alet, *Phys. Rev. B* **91**, 081103 (2015).

[162] E. H. Lieb and D. W. Robinson, *Comm. Math. Phys.* **28**, 251 (1972).

[163] E.-M. Laine, J. Piilo, and H.-P. Breuer, *Europhys. Lett.* **92**, 60010 (2010).

[164] J. Sous and E. Grant, *Phys. Rev. Lett.* **120**, 110601 (2018).

[165] W. Morong, F. Liu, P. Becker, K. S. Collins, L. Feng, A. Kyprianidis, G. Pagano, T. You, A. V. Gorshkov, and C. Monroe, *Nature* **599**, 393 (2021).

[166] A. D. Luca and A. Scardicchio, *EPL* **101**, 37003 (2013).

[167] K. Agarwal, S. Gopalakrishnan, M. Knap, M. Müller, and E. Demler, *Phys. Rev. Lett.* **114**, 160401 (2015).

[168] P. Ponte, Z. Papić, F. Huveneers, and D. A. Abanin, *Phys. Rev. Lett.* **114**, 140401 (2015).

[169] N. Y. Yao, C. R. Laumann, S. Gopalakrishnan, M. Knap, M. Müller, E. A. Demler, and M. D. Lukin, *Phys. Rev. Lett.* **113**, 243002 (2014).

[170] A. O. Maksymov and A. L. Burin, *Phys. Rev. B* **101**, 024201 (2020).

[171] R. M. Nandkishore and S. L. Sondhi, *Phys. Rev. X* **7**, 041021 (2017).

[172] S. Nag and A. Garg, *Phys. Rev. B* **99**, 224203 (2019).

[173] R. Nandkishore, S. Gopalakrishnan, and D. A. Huse, *Phys. Rev. B* **90**, 064203 (2014).

[174] D. Hetterich, N. Y. Yao, M. Serbyn, F. Pollmann, and B. Trauzettel, *Phys. Rev. B* **98**, 161122 (2018).

[175] N. Ng, S. Wenderoth, R. R. Seelam, E. Rabani, H.-D. Meyer, M. Thoss, and M. Kolodrubetz, *Phys. Rev. B* **103**, 134201 (2021).

[176] N. Ng and M. Kolodrubetz, *Phys. Rev. Lett.* **122**, 240402 (2019).

[177] L. Zhang, V. Khemani, and D. A. Huse, *Phys. Rev. B* **94**, 224202 (2016).

[178] J. von Neumann, *Z. Phys.* **57**, 30 (1929).